THULIUM DOPED FIBER BASED LASERS AND AMPLIFIERS

By

SHAOXIANG CHEN

School of Electrical and Electronics Engineering

A thesis submitted to the Nanyang Technological University
in partial fulfilment of the requirement for the degree of
Doctor of Philosophy

2019

Statement of Originality

I hereby certify that the work embodied in this thesis is the result of original research, is free of plagiarised materials, and has not been submitted for a higher degree to any other University or Institution.

09/04/2019
. . . . . .
Date

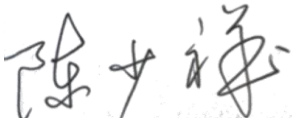
. . . . . .
Shaoxiang Chen

Supervisor Declaration Statement

I have reviewed the content and presentation style of this thesis and declare it is free of plagiarism and of sufficient grammatical clarity to be examined. To the best of my knowledge, the research and writing are those of the candidate except as acknowledged in the Author Attribution Statement. I confirm that the investigations were conducted in accord with the ethics policies and integrity standards of Nanyang Technological University and that the research data are presented honestly and without prejudice.

09/04/2019

. . . . . .

Date

. . . . . .

Yoo Seongwoo

Authorship Attribution Statement

This thesis mainly contains material from 4 paper(s) published in the following peer-reviewed journal(s) / from papers accepted at conferences in which I am listed as an author.

Chapter 4 is published as

1. **Shaoxiang Chen,** Yongmin Jung, Shaiful Alam, Raghuraman Sidharthan, Daryl Ho, Seongwoo Yoo, David J. Richardson *et al*., "Ultra-wideband Operation of a Tunable Thulium Fibre Laser offering Tunability from 1679–1992 nm," *2017 European Conference on Optical Communication (ECOC)*, Gothenburg, 2017, pp. 1-3. (**Finalist for Best Student Paper Award**).
   The contributions of the co-authors are as follows:
   - Prof David J. Richardson, Asst/Prof Seongwoo Yoo and Dr Shaiful Alam provided the initial project direction. And many thanks for their strong support for this project under the EPSRC funded Hollow Core Fiber Photonics Programme Grant, and by the Academic Research Fund Tier 1, Ministry of Education (Singapore).
   - Dr Raghuraman Sidharthan and Mr Daryl Ho helped to fabricate the Tm/Ge co-doped fiber under the guidance and suggestion of Asst/Prof Seongwoo Yoo.
   - Regarding to the fiber parameters of Tm/Ge co-doped fiber, I have made discussions with Asst/Prof Seongwoo Yoo.
   - I mainly conducted all the experiments for the works including the fiber characterization, fiber laser setup design with helpful assists from Dr Yongmin Jung, Dr Yongmin Jung has given me many hands-on practice during experiment.
   - And I appreciate the daily approachable suggestions from Dr Shaiful Alam.
   - I measured the experimental data and post-processing. I prepared the manuscript draft. The manuscripts were elaborately revised by Dr Yongmin Jung, Dr Shaiful Alam and Prof David J. Richardson.

2. Shaoxiang Chen, Yongmin Jung, Shaiful Alam, Saurabh Jain, Morten Ibsen, Raghuraman Sidharthan, Daryl Ho, Seongwoo Yoo, and David J. Richardson, "Ultra-short wavelength operation of a thulium doped fiber laser in the 1620-1660nm wavelength band," in Optical Fiber Communication Conference, OSA

Technical Digest (online) (Optical Society of America, 2018), paper M2J.4.
(Finalist for Corning Outstanding Student Paper Competition)
The contributions of the co-authors are as follows:

- Prof David J. Richardson, Asst/Prof Seongwoo Yoo and Dr Shaiful Alam have supervised my work in the published conference paper.
- I have mainly conducted the experimental works including the fiber length optimization, splicing optimization, laser performance characterization. And I have received good suggestions from Dr Yongmin Jung during experiment.
- Dr Saurabh Jain has advised me in the part of fluorescence lifetime measurement for Tm/Ge co-doped fiber.
- Associate Prof Morten Ibsen has helped to mount the tunable fiber Bragg grating used in chapter 4 and the above published paper.
- Under the guidance of Asst/Prof Seongwoo Yoo, Dr Raghuraman Sidharthan and Mr Daryl Ho have fabricated the Tm/Ge co-doped fiber, and they also have prepared the preform by MCVD.
- I have prepared the figures from experimental data and manuscript draft. Thanks a lot for Prof David J. Richardson, Dr Shaiful Alam and Dr Yongmin Jung's contribution to polish the manuscript.

3. Shaoxiang Chen , Yongmin Jung, Shaiful Alam, Raghuraman Sidharthan, Daryl Ho, Seongwoo Yoo, David J. Richardson, Jae M. Daniel, "Ultra-short Wavelength Operation of Thulium-doped Fibre Amplifier in the 1628-1655nm Waveband", 2018 European Conference on Optical Communication (ECOC), Rome, 2018, Mo3E.1.

   The contributions of the co-authors are as follows:

   - Firstly, Prof David J. Richardson, Asst/Prof Seongwoo Yoo and Dr Shaiful Alam have supervised the work to achieve the good result.
   - Dr Raghuraman Sidharthan and Mr Daryl Ho have prepared the Tm/Ge co-doped fiber, which is used as gain fiber in the work of Tm-doped fiber amplifier. In addition, Asst/Prof Seongwoo Yoo has provided many suggestions for the fiber parameters of Tm/Ge co-doped fiber, such as doping concentration, fiber core size.
   - I have mainly conducted all the experiments for the works including the tunable laser source characterization, fiber length optimization of Tm/Ge

co-doped fiber, the characterization of tunable fibre Bragg grating, with helpful assists from Dr Yongmin Jung, and with daily approachable suggestions from Dr Shaiful Alam.

- Special thanks to Dr Jae M. Daniel for his good suggestion at the beginning of the project, i.e. the co-dopant of germanium in silica-based Tm-doped fiber is beneficial for blue-shifted emission- and absorption cross-section.
- After I prepared the manuscript draft, Dr Yongmin Jung, Dr Shaiful Alam and Prof David J. Richardson have revised the draft to present the result better.

Chapter 5 is published as

4. Fedia Ben Slimen, **Shaoxiang Chen**, Joris Lousteau, Yongmin Jung, Shaiful Alam, Nicholas White, David J. Richardson, and Francesco Poletti, "Tm^{3+}-doped Germanate Large Mode Area Single Mode Fiber for 2μm Lasers and Amplifiers," in Advanced Photonics 2018 (BGPP, IPR, NP, NOMA, Sensors, Networks, SPPCom, SOF), OSA Technical Digest (online) (Optical Society of America, 2018), paper SoTu4H.2.

   The contributions of the co-authors are as follows:

   - Prof Francesco Poletti, Prof David J. Richardson and Dr Shaiful Alam have provided the idea to initial the project of Tm^{3+}-doped germanate glass fiber and its application in fiber lasers and amplifiers. And thanks a lot for their strong support for this project under the funding of Future Photonics Hub by U.K engineering and Physical Science Research Council, and by the ERC LightPipe project.
   - Dr Fedia Ben Slimen has developed the multi-oxide component germanate glass for core and cladding glass of Tm^{3+}-doped germanate glass fiber.
   - Dr Fedia Ben Slimen, and me have together measured the transition temperature and crystallization temperature under the guidance of Dr Joris Lousteau.
   - Special thanks to Mr Nicholas White and Dr Fedia Ben Slimen for their help for the fabrications of single cladding and D-shape double cladding Tm^{3+}-doped germanate glass fiber.

- Dr Yongmin Jung has advised me a lot on fiber characterization. I have conducted the fiber characterization including the absorption, lifetime, absorption- and emission cross-section, gain coefficient.
- I also have conducted all the lasing and amplifier experiments shown in the paper above and other experiments in Chapter 5

09/04/2019
. . . . . .
Date

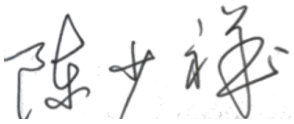
. . . . . .
Shaoxiang Chen

Abstract

In general, the work in this thesis could be divided into two parts, but more work is focused on the first part.

Compared with aluminosilicate based Thulium-doped fibers (TDF), germanosilicate based TDFs have a blue-shifted absorption and emission cross-section in the transition from level $^3F_4$ to level $^3H_6$. Due to the quasi-three-level nature and broad fluorescence emission from level $^3F_4$ to level $^3H_6$, the germanosilicate based TDFs is envisaged to provide much higher gain at short wavelength below 1700nm. Combination of aluminosilicate based TDF and germanosilicate based TDF will provide a broadened emission window in the transition from level $^3F_4$ to level $^3H_6$. Literately, aluminosilicate based Thulium-doped fiber amplifiers (TDFAs) have been demonstrated from 1660nm to 2050nm. This broadband TDFAs combined with hollow-core photonic bandgap fiber provide a solution to the next generation fiber communication. Considering the long wavelength edge of extended L-band EDFA at 1620nm, there is an obvious gap between L-band EDFA and state-of-the-art TDFAs. In order to seamlessly fill the gap, the short wavelength gain of a new germanosilicate based TDF (Tm/Ge co-doped fiber) is exploited by low-loss cavity management, long wavelength amplified spontaneous emission (ASE) suppression, thus realizing continuous wavelength lasing at short wavelength. Particularly wavelength tuning in the 1620-1660nm is realized by a compressively tunable fiber Bragg grating. When a band-pass filter is employed, ultrafast fiber lasers at 1650nm waveband is realized, which potentially unleash the application of thulium-doped fiber laser in the wavelength region below 1700nm.

Intriguingly, for the germanate glass (multi-component glass mainly GeO_2, but without SiO_2), it provides a distinct environment for Tm^{3+} ions, in particular, the germanate glass host provide a much higher Tm-doping concentration capacity and longer fluorescence lifetime compared with silica glass. In the second part of the thesis, all the work are based on Tm-doped germanate glass fiber, which includes three main topics. The first topic focuses on the characterization of an in-house fabricated large mode area (LMA) Tm^{3+}-doped germanate glass fiber (TGF). Secondly, based on the in-band core-pumping scheme, a single-mode fiber laser at 1950nm incorporating short length TGF is demonstrated with very high slope efficiency. Finally, with the short length of double-clad TGF, a compact TDFA with attractive gain is built operating in the 1880-2000nm waveband. Moreover, the double-clad TGF is incorporated as power amplifier in a master oscillator power amplifier (MOPA) system seeded by dissipative solitons, showing promise as a candidate for high-power pulse fiber laser with mitigated nonlinearity.

Acknowledgements

Over the past four years, I have experienced a wonderful journey as a joint PhD student between Nanyang Technological University and University of Southampton, ORC, and I feel so lucky that I have had the opportunity to work with so many talented people. I am so grateful for their support, considerate advice and friendship, otherwise my journey will be struggling.

I would like to thank my supervisor Professor Seongwoo Yoo for his full supports to my research work, for his considerate advice for each project I have been involved in, for providing me the freedom and guidance to participate in the interesting projects full of challenges.

I really thank Professor David. Richardson as my supervisor in ORC for his insightful advice. For my projects, Dave always shows me a big picture, which motivate me to achieve the promising results. Dave has taught me a lot about how to think in multi perspective and how to solve problem efficiently. Moreover, I really thank him for his comments and guidance to the preliminary results during each group meeting. I have learnt a lot from Dave far beyond research and study.

I would like to give many thanks to Dr. Shaiful Alam for his unselfish and patient guidance to my projects. I really miss his everyday visit to lab for his valuable suggestions about experiment. Shaiful is always approachable in his office when I face difficulty, and I really appreciate it. Thanks a lot for Shaiful's sharing about how to do experiment, how to prepare in advance and how to be a young researcher.

I would like to express my great thanks to Dr. Yongmin Jung for his dedicated help to my PhD projects. As an expert in the field of fiber devices, Yongmin could always simplify the difficulty. Yongmin is always there to give me a hand when I am in trouble, and I learnt a lot from his efforts and attitude to research.

I would like to thank Dr. Saurabh Jain for his encouragement and good advice for my projects, from which I benefit a lot. I really thanks Dr. Molten Ibsen for his help to mount the compressive fiber Bragg grating. I also thank Dr. Raghuraman Sidharthan and Mr. Daryl Ho for their efforts for Tm/Ge co-doped fiber fabrication. I would like to thank Dr. Fedia Ben Slimen for her contribution to the development of Tm germanate glass and the corresponding

fiber fabrication. I also would like to Mr. Zhengqi Ren for his assists with the work of master-oscillator power amplifier system at 2μm. I also thank Dr. Jonathon Price, Dr. Yu Xia, Dr. Di Lin, Dr. Lin Xu, Dr. Qiongyue Kang, Mr. Qiang Fu and Miss Sijing Liang for their great assists during my PhD study. Also, I give my special thanks to Prof. Perry Shum Ping for his recommendation and encouragement.

I would like to proudly thank the unselfish supports of my parents and my two brothers. With their love, encouragement and understanding, I could get through the eventful four-year journey with confidence. In the end, I proudly thank my lovely wife for her endless love.

Contributions

Firstly, the author is responsible for all the work in this thesis.

Secondly, for the work presented in Chapter 3, the Tm/Ge co-doped fiber is fabricated by Dr. Raghuraman Sidharthan and Mr. Daryl Ho under the supervision of Asst. Prof Seongwoo Yoo at COFT, NTU. For the characterization part of the Tm/Ge co-doped fiber, the corresponding work is all done by the author, i.e. the fluorescence characterization, absorption measurement by supercontinuum source, cross-section and gain coefficient calculation, as well as the lasing efficiency test. For the work in Chapter 4, the tunable source is first rebuilt with the assist of Dr. Yongmin Jung. In the following part, the ultra-wideband operation of TDFLs are conducted by the author. In order to further push the operating wavelength, the author proposed to use the all fiber low-loss laser cavity by incorporating two highly reflective tunable FBG. And the tunable FBG is mounted with the help of Assoc. Prof Morten Ibsen. To achieve amplification at short wavelength below 1660nm, the author has conducted the work of TDFA in a double pass configuration, where the tunable FBG with operating wavelength matched with signal is employed to filtering ASE noise. To explore the possibility of achieving ultrafast mode-locked fiber laser by using the Tm/Ge co-doped fiber, the author conducted the work in Chapter 4.6 with the assists of Mr. Zhengqi Ren, where a FBG with bandwidth of 20nm spanning from 1640-1660nm is employed. A lot of discussions with Dr. Jonathon Price are conducted to the result of mode-locked fiber laser at 165nm waveband.

In addition, for the work presented in chapter 5, the Tm^{3+}-doped germanate glass is developed by Dr. Fedia Ben Slimen and Dr. Joris Lousteau under the supervision of Prof. Francesco Poletti. By using the developed Tm^{3+}-doped germanate glass, large mode area (20μm) Tm^{3+}-doped germanate glass fiber is fabricated by Dr. Fedia Ben Slimen. In the following sections, the characterizations of glass and fiber are conducted by the author. In addition, the author has also conducted all the related experiments including fiber laser performance, double-clad

Tm^{3+}-doped germanate glass based amplifier and master-oscillator power amplifier system. In order to optimize the experimental result in Tm germanate glass fiber (TGF), the author has also conducted the related simulation work for lasing efficiency calculation and optimal TGF length.

Finally, all the work included in this thesis has been conducted under the supervision of Prof David J. Richardson, Dr. Shaiful Alam and Asst. Prof Seongwoo Yoo.

Table of Contents

List of figures

Acronym

ASE	amplified spontaneous emission
BW	bandwidth
CPS	cladding pump stripper
CTE	coefficient of thermal expansion
CW	continuous wave
CR	cross-relaxation
DWDM	dense wavelength division multiplexing
DM	dichroic mirror
DTA	differential thermal analysis
DCF	dispersion compensating fiber
EPMA	electron probe micro analysis
Er	Erbium
EDF	Er^{3+}-doped fiber
EDFA	Er^{3+}-doped fiber amplifier
EDTMF	erbium-doped tellurite microstructure fiber
EYDFL	Er: Yb co-doped fiber lasers
ESA	excited state absorption
FBG	fiber Bragg grating
FUT	fiber under test
FWHM	full width half maximum
G	gain
Ge	germanium
HR	high reflection
HC-PBGF	hollow-core photonic-bandgap fiber
LMA	large mode area
LD	laser diodes
LHS	left hand side
LPFG	long period fiber grating
MOPA	master oscillator power amplifier
MFD	mode field diameter
MCVD	modified chemical vapor deposition
MM	multimode
NIR	near-infrared
NAD	net-anomalous dispersion
NND	net-normal dispersion
NF	noise figure
NL	noise-like
NOLM	nonlinear optical loop mirror
NPR	nonlinear polarization rotation
NA	numerical aperture
OCT	optical coherence tomography
OSNR	optical signal to noise ratio
PCF	photonics crystal fibers
PC	polarization controllers
RI	refractive index
RHS	right hand side
SA	saturable absorber

SESAM	semiconductor saturable absorber mirror
SNR	signal to noise ratio
SMF	single-mode fiber
SDM	space division multiplexing
SC	supercontinuum (SC)
SLD	superluminescent diode (SLD)
TEC	temperature controller (TEC)
Tm	thulium (Tm)
TDFA	thulium-doped fiber amplifier (TDFA)
TBP	time-bandwidth time (TBP)
TDFL	Tm-doped fiber laser
TGF	Tm^{3+}-doped germanate glass fiber (TGF)
WDM	wavelength division multiplexing or wavelength division multiplexer
YDF	Yb^{3+}-doped fiber
Yb	Ytterbium
ZDW	zero-material dispersion wavelength

Chapter 1 Introduction

Fiber waveguide offers many prominent advantages that accelerate its wide applications in terms of amplifiers and lasers. Firstly, fiber waveguide enables the implementation of the low-loss all fiber system by replacing bulky optical elements with low-loss fiberized components. Moreover, the all-fiber system helps avoid the complexity of alignment in free space optics, exhibiting the resilience of mechanical disturbance and reducing footprint by its flexibility. Due to the large surface area to volume ratio of fiber waveguide, efficient cooling is achievable, which endows direct contact between fiber and a cooling medium, allowing efficient heat extraction from a fiber core. Another advantage of fiber waveguide lies in its small core diameter; therefore, it is capable of obtaining single mode operation, providing a high beam quality. In addition to the aforementioned advantages of fiber waveguide, the success of rare-earth doped fiber could also attribute to high gain extractible from fiber per optical pass as compared to solid-state lasers, adoption of high power laser diode as a pump source and high optical-to-optical conversion efficiency. With the low loss Neodymium (Nd)-doped fiber fabricated in 1985, researchers subsequently have started to focus on using rare-earth doped fiber as gain medium for optical amplifiers and lasers. Particularly, the invention of Erbium-doped fiber amplifier (EDFA) have sparked the revolution of telecommunication, making all-optical long-haul communication system possible. Up to now, drastic progress has been achieved in various configurations of lasers and amplifiers by employing different rare-earth doped fibers (Nd^{3+}, Yb^{3+}, Er^{3+}, Tm^{3+}, Ho^{3+},etc). In this thesis, I will focus on the study of Tm^{3+}-doped fiber (TDF) based laser and amplifier.

1.1 Motivation

Over the past 30 years, research and development in long-haul telecommunication optical fibers has focused on the 1.55 μm wavelength region, where the lowest loss of silica-based fiber overlaps with the bandwidth (BW) of EDFA. Today's telecomm networks are rapidly being driven towards their capacity crunch as a result of the exponentially increasing volume of internet traffic. With silica-based fiber as a transmission medium, EDFA-based optical communication technologies such as wavelength division multiplexing (WDM), space division multiplexing (SDM), have increased impressive data transmission capacity. Based on the combined C- and extended L-band EDFAs, an aggregate capacity above Pbit s^{-1} has been achieved in WDM system over a multicore fiber[1] Based on the silica-based EDF, the operating wavelength range of EDFA backed telecomm ranges from 1480 to 1620 nm. In order

to exploit the broad low-loss range (<0.3 dB /km) of conventional silica fiber in the waveband from 1450 to 1700nm as shown in Fig 1. 1 , silica-based Tm^{3+}-doped fiber amplifiers (TDFAs) in the waveband of 1450 to 1500 nm, have been proposed as a promising candidate to complement the combined C- and L-band EDFA in WDM optical communication system[2][3][4][5]. On the other hand, the long edge of silica-based L-band EDFA could reach up to 1620nm, with optical bandwidth of 80 nm remained. Ove the past few years, based on the transition from $^3F_4$ to $^3H_6$, of Tm^{3+}, broadband TDFAs spanning from 1650 to 2050 nm have been widely reported. Currently, there is still unbridged spectral gap of 30 nm to offer seamless transmission window encompassing S to U-band. Additionally, the TDFA based data transmission utilizing a low-loss wide bandwidth hollow core photonics bandgap fiber is successfully demonstrated at 2 μm[6]. Therefore, it is an immediate requirement to bridge the gap between L-band EDFA and TDFA, to enhance the capacity of conventional silica fiber based WDM communication system. If so, the combination of EDFA and TDFA could operate in a seamless waveband from 1450nm to 2050, which is promising for next generation fiber communication.

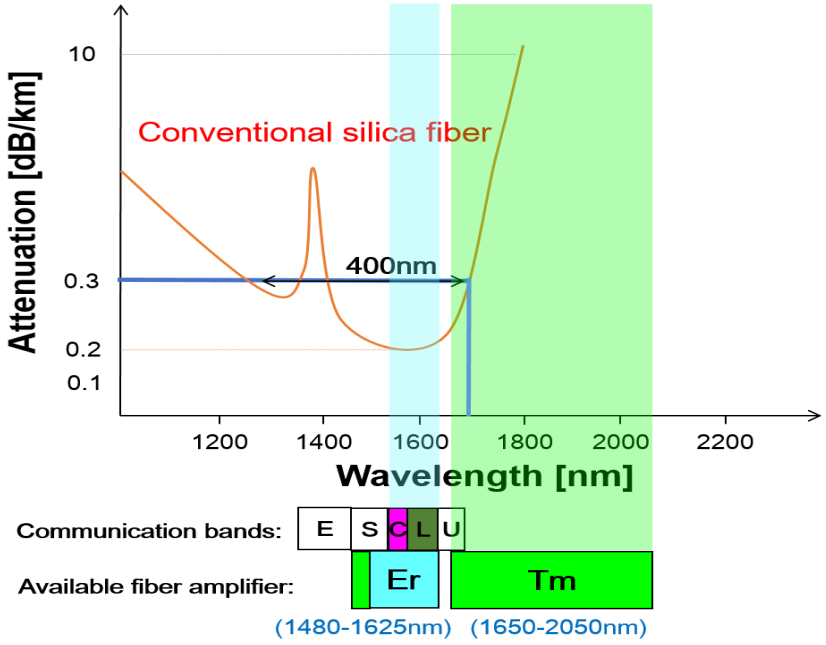

Figure 1.1 (Top) the attenuation of conventional silica in the wavelength region from 1μm to 1.8μm. (Bottom) the wavelength coverage of EDFA and TDFA for different communication bands from S band to U band and beyond.

On the other hand, laser radiation in the short wavelength region below 1720 nm has drawn attentions of bio photonics community due to the lower scattering coefficient and moderate water absorption loss in the spectral range of 1620-1720 nm. Absorption by fat exceeding the absorption caused by water at 1720 nm, thus allowing selective targeting of tissues containing lipids in different skin treatments. In addition, due to the reduced absorption of water in spectral region of 1600-1720 nm, lasers in this region provide higher penetration in biological tissues[7]. In addition, the advantage of high penetration is implemented in many applications, such as in optical coherent tomography by the 1675nm fiber laser and three-photon imaging by the 1650 nm fiber laser[8][9]. Owing to the broad emission bandwidth of TDFs from 1600 to 2200 nm, TDFs have been employed to implement the aforementioned applications. However, the peak wavelength of fluorescence emission is around 1850 nm or beyond. In order to achieve TDFs based lasing and amplifier at short wavelength, artificial spectral filtering is proposed to suppress the amplified spontaneous emission (ASE) at long wavelength region in various configurations, such as Holmium-doped fiber with apparent absorption at above 1800nm. Another example is photonic crystal fibers (PCFs) by exploiting the low-pass transmission properties based on confinement loss evaluation [10]. By controlling the geometrical structure of a particular PCF design, the long cut-off wavelength (such as 1800nm, 1750nm) could be implemented with long cut-off wavelength above 1750 nm. The abovementioned discrete long-wavelength ASE filters contribute to demonstration of lasers and amplifiers at 1700 nm[11][12]. However, the ASE filters will also introduce additional loss at wavelength below 1800 nm, which hampers building up of optical gain and lasing efficiency at the short wavelength. Due to the quasi three-level in the transition from $^3F_4$ to $^3H_6$ accompanied by reabsorption at short wavelength, lasing or amplification at wavelength below 1700 nm has been recognized as a challenging wavelength.

Emission from Tm^{3+} ions covers 1600-2200 nm in silica host. Therefore, Tm^{3+} ions is promising to access the short wavelength region from 1720 nm down to 1620 nm. Additionally, glass compositions affect emission properties. For example, in order to extend L-band gain of EDFA to longer wavelength, different glass hosts such as tellurite, antimony and Bi_2O_3-based EDF were widely investigated [13][14][15]. Furthermore, the emission can be modified via a co-doping scheme. For TDFs, holmium is co-doped to extend the emission to longer wavelength[16][17]. In order to achieve short wavelength emission for TDF, Tb^{3+} ions are co-doped in the cladding of TDF to suppress the emission of 1700-2000 nm by the absorption of Tb^{3+} ions. Due to the distribute ASE filtering by Tb^{3+} ions, the ASE peak at 1720nm is achieved.

Actually, the intrinsic emission window of TDF is not blue shifted but suppressed in long wavelength region[18][19]. On the other hand, Barnes et al have proposed that the germanosilicate glass as a host for Tm^{3+} ions be able to realize short wavelength lasing, which is in contrast to the conventional aluminosilicate glass, [20] [21]. In addition, low Tm^{3+}-doping concentration is advantageous for lasing at short wavelength edge of the transition $^3F_4$-$^3H_6$ because a high excitation fraction is attainable by core pumping[22]. In this context, I take the stimulation in Chapter 4 to exploit a low Tm^{3+}-doped germane-silicate glass fiber (or namely Tm/Ge co-doped fiber) as gain medium operating in the spectral region from 1620 to 1720nm.

On the other hand, the 2μm wavelength sources have become attractive due to the applications such as LIDAR, range finding, remote sensing. In addition, there is prominent atmospheric water absorption in the wavelength region from 1800 to 1950 nm, which is attractive for medical applications. And the direct absorption in 2 μm waveband in materials such as polymers and plastics have unlocked the application of 2μm lasers in material processing and welding[23]. Due to the high absorption in the 2μm waveband in eye's cornea [24], the 2μm lasers hold the advantage of eye-safe feature over 1μm fiber laser. Meanwhile, TDFLs could offer as an alternative source in the 2μm waveband, outperforming its rival solid-state lasers. Despite the progress achieved in different TDFL architectures, TDFLs in the 2μm waveband have not been fully exploited in the high-power regime. Compared with Ytterbium-doped fiber laser at 1μm, TDFLs operating at 2 μm could have larger core size for single mode operation, allowing a 4-fold increase of the saturation energy and the threshold of nonlinear effect. In the perspective of high power 2μm fiber laser, high Tm^{3+}-doping is intrinsic preferred. When Tm^{3+}-doping is sufficiently high, cross-relaxation process is involved, thus exhibiting a high slope efficiency. In addition, high Tm^{3+}-doping is conducive to mitigate the nonlinear effect by employing short fiber length. However, for the state-of-art silica-based TDFs, Tm^{3+}-doping concentration encounters its bottleneck owing to the ion clustering effect for the defined waveguide structure in silica glass.

Compared with silica glass host, multi-component glasses (e.g. germanate glass, silicate glass, tellurite glass) are better Tm^{3+} glass host due to their higher Tm^{3+} solubility. Amongst the multi-component glass, germanate glass has the combined attributes of high Tm^{3+}-doping capability, comparatively low phonon energy (~900 cm^{-1}), long fluorescence lifetime, IR transmission up to 6 μm. Lower phonon energy could enhance the luminescence quantum efficiency. Furthermore, the heavily Tm^{3+} doped (typically up to 10^{21} ions/cm^3) germanate glass fiber enables large pump absorption and high gain per unit length of the fiber, which

could mitigate the nonlinear effect in a short fiber length. Despite the twofold higher nonlinear index of germanate glass than that of silica fiber, the nonlinear threshold could be dominated by the high Tm^{3+}-doping concentration[25]. Moreover, the concept of large mode area (LMA) and low numerical aperture (NA) could also be introduced in Tm germanate glass fiber (TGF) to enhance laser output power further by decreasing the laser intensity, which is particularly employed in the configurations of cladding-pumped fiber laser and mater-oscillator power-amplifier (MOPA)[26][27][28]. Particularly, for the MOPA system in [27], the gain fibers employed in seed, preamplifier and power amplifier are all short length TGFs, promising to achieve compact fiber devices. To my best knowledge, the TGF based laser works remain in the continuous wave (CW) regime[26] [27][29][30]. In this context, researchers from our group have focused on optimizing the composition of germanate glass for lasing and amplification. Based on the in-house fabricated LMA Tm^{3+}-doped germanate glass fiber (TGF), it is anticipated to achieve high power TDFL with high beam quality, and short fiber length TDFA, and specifically high power pulsed MOPA system in the 2μm waveband.

1.2 Thesis outline

This thesis comprises six chapters focusing on the topic of TDF based lasers and amplifiers. Chapter 1 discusses the motivation of this thesis in the context of anticipated growing applications of TDF in optical fiber communication and fiber lasers. Moreover, the thesis structure is briefed.

Chapter 2 introduces the fundamentals and background of my thesis with key subjects included, such as fiber waveguide, the development of rare-earth (mainly Yb^{3+}, Er^{3+}, and Tm^{3+}) doped fiber lasers from 1μm to 2μm in the near infrared region and thulium spectroscopy. Besides the thulium spectroscopy, details including cross-relaxation process, pump schemes are discussed. The effect of glass composition including Tm^{3+}-doping concertation on the fluorescence emission window and lasing efficiency are detailed. Tunable TDFLs implemented in different laser configurations and the applications of TDFL at short wavelength below 1700 nm are reviewed. In addition, the state-of-the-art TDFAs in many different configurations covering from 1650nm to 2050nm are summarized, and in the last section, a theoretical description of an accurate TDFA model is provided.

Chapter 3 mainly focuses on the characterization of Tm/Ge co-doped fiber by preliminary experimental setup. Firstly, an 1565nm Er/Yb co-doped fiber laser is built and characterized as pump source for the experiments in the subsequent chapters. Absorption and emission of

Tm/Ge co-doped fibers are studied. Their corresponding cross-sections and gain coefficient are obtained. Moreover, free-running laser is tested for the Tm/Ge co-doped fiber. Due to the non-negligible splicing loss between Tm/Ge co-doped fiber and single-mode fiber (SMF), splicing optimization is undertaken to ensure all-fiber configuration for fiber lasers and fiber amplifier in the following chapters.

In Chapter 4, in the laser configuration with external laser cavity, an ultra-wide tunable TDFL is demonstrated in the wavelength from 1679 nm to 1992 nm using the combination of Tm/Ge co-doped fiber and commercial TDF as gain fiber, where the lasing wavelength is selected by diffraction grating. In addition, with a home-made ASE filter to suppress long wavelength emission, being placed between two segments of Tm/Ge co-doped fiber, a tunable TDFL is reported with the wavelength tunability from 1650nm to 2000nm. In order to access the short wavelength region below 1650 nm, a pair of tunable high reflective FBGs operating from 1660nm to 1610nm are employed as retroreflector of laser cavity. Therefore, with the optimized 4.5m Tm/Ge co-doped fiber as gain fiber, I have achieved an ultrashort wavelength operation of TDFL in the 1620-1660nm band in an all-fiber linear laser cavity, particularly, the lasing efficiency is 6.24% at 1660nm. With the shortest lasing wavelength of TDFL reaching the edge of silica-based L-band EDFA, I have explored the possibility of TDFA to fill the gap between silica-based EDFA and TDFA. In a forward pump configuration pumped by 1565nm fiber laser, a double-pass Tm/Ge co-doped fiber based amplifier is constructed, operating in the wavelength region from 1628 nm to 1655 nm, with a gain bandwidth of ~2THz extended when compared to the previous best report. Up to 19 dB small signal gain (external) and a NF as low as 4.4 dB were achieved at 1655nm with >30dB in-band OSNR. In addition to the abovementioned tunable TDFLs in CW regime and TDFA by incorporating the Tm/Ge co-doped fiber, I have demonstrated a self-starting all-fiber passively ultra-short wavelength mode-locked thulium doped fiber laser (TDFL) based on nonlinear optical loop mirror (NOLM) in both soliton and noise-like (NL) pulse regimes, by far, the shortest wavelength operation of a mode-locked thulium-doped fiber laser. Stable soliton pulses centered at 1656.1nm with 0.55nm FWHM is achieved with a repetition rate of 1.28MHz, pulse duration of 0.32ps and pulse energy of 109pJ. With pump power increased, the oscillator could operate in NL regime. Stable NL pulses with coherence spike width of 890fs and pulse energy of up to 20nJ are achieved with a central wavelength of 1656.2nm with 4.51nm FWHM.

In Chapter 5, based on a novel multi-oxide germanate glass ($61GeO_2$-$15PbO$-$10ZnO$-$3ZnF_2$-$6Na_2O$-$4Nb_2O_5$-$1GdF_2$), progress achieved by utilizing the in-house fabricated LMA (20μm)

Tm^{3+}-doped germanate glass fiber (TGF) is presented. After preliminary fiber characterisation of in-house fabricated LMA TGF, a CW TDFL at 1952nm with maximum power of 1.5 W is demonstrated when core-pumped at 1565nm. A high slope efficiency of 55.9% with respect to absorbed pump power and nearly diffraction-limited beam quality are achieved. Based on this attractive laser performance of LMA TGF, a D-shape double-clad LMA TGF is proposed to explore the capability of high power pulse fiber laser at 2μm. In addition, a TGF based amplifier spanning from 1880nm to 2000nm was demonstrated with peak gain of 13dB and 10dB at 1930nm for small signal and saturated signal respectively. Finally, a pulse-MOPA fiber system incorporating double-clad LMA TGF as main amplifier was demonstrated with output power of 3.7W, corresponding to an energy of 0.27μJ with pulse duration 57ps.

Chapter 6 concludes the works in thesis and discusses future work. For future works, a Tm/Ge co-doped fiber with W-type index profile is proposed to achieve efficient lasing and amplification below 1700 nm. And the short wavelength limit of this W-type Tm/Ge co-doped fiber as amplifier will be investigated. Moreover, given that the zero-material dispersion wavelength of pure germanate glass is around 1734nm, the dispersion property of TGF will be measured. As to the pulse energy and pulse duration at 2 μm limited by anomalous dispersion of silica fiber, a novel silica-based LMA TDF with normal dispersion in the 2μm waveband is proposed.

Chapter 2 Background and theory

2.1 Optical fiber waveguide

Optical fiber waveguides, generally comprising a cylindrical core, cladding and polymer buffer layers, provide an attractive approach for light propagation. The number of guided modes in an optical fiber is determined by the V-number. In a circular step-index waveguide with core RI of n_{core} and cladding RI of n_{clad}, the V-number can be defined as:

$$V = \frac{2\pi a}{\lambda}\sqrt{n^2_{core} - n^2_{clad}} \quad \ldots 2.1$$

$$M \approx \frac{V^2}{2} \quad \ldots 2.2$$

where α is the core radius, λ is light wavelength in vacuum. The optical fiber only supports fundamental mode when V<2.405. For V>2.405, the optical fiber could be multi-modes, and the number of guided modes, *M*, is approximately as equation 2.2.

Due to the mechanism of total internal reflection between high refractive index (RI) core and low-RI cladding, an optical fiber is capable of confining light very well in the core. With techniques of fiber fabrication rapidly developed, optical fibers with very low scattering loss and low impurity loss are achieved. Owing to its well guiding in core and high transmission capacity at the optical frequency, optical fibers are initially implemented as a low-attenuation, high capacity channel for telecommunication, which have replaced the conventional cables. Instead of only focusing on the telecommunication field, some researchers recognized the excellent properties of fiber waveguides as a gain medium by doping with rare-earth elements such as Neodymium (Nd), Ytterbium (Yb), Erbium (Er) and Thulium (Tm). Compared with bulk solid gain medium, optical fibers doped with rare-earth cations exhibit many advantages. Firstly, the large surface-area-to-volume ratio of optical fiber allows efficient heat dissipation, enabling thermal management for power scaling. Secondly, significantly enhanced beam quality results from the well confinement of light in fiber waveguide structure. Thirdly, the complicated alignment of optical components in free-space could be avoided by all-fiberized architecture, thus achieving compactness fiber devices. The aforementioned characteristics of optical fibers boost their wide applications as a gain medium in lasers and amplifiers.

2.2 Rare-earth dopants for near-infrared emission

Due to the aforementioned advantages of fiber waveguides, researchers around the world have contributed to improve the performances of fiber-based devices. Particularly, the fiber devices in the near-infrared (NIR) region from 0.8 μm to 2 μm, have attracted growing attentions owing to their wide applications such as optical communication, micromachining, medicine and remote sensing. The NIR emission in fiber devices could be realized by doping with rare-earth elements. Among the rare-earth dopants in active fibers, Yb, Er and Tm are the most successful ones incorporated in optical fibers in the NIR region. Despite additional Rayleigh scattering caused by the rare-earth dopants, the high gain in the fiber easily overcome the loss.

Regarding power scalability of fiber laser, the Yb^{3+} amongst rare-earth dopants has been a choice of gain dopants for output power and highest slope efficiency at 1μm in a form of Yb^{3+}-doped fibers (YDFs). There are a few reasons behind this success. Firstly, the quantum efficiency of YDF laser is close to 100% due to very low energy difference between pump photon and laser photon. Secondly, due to the simple level structure of the Yb^{3+} ions between $^2F_{7/2}$ to $^2F_{5/2}$ and lacking of higher lying energy states, the possibility of any energy transfer, quenching process and excited state absorption processes are reduced, therefore, the doping concentration of Yb^{3+} ions could be high in YDFs. Moreover, Yb^{3+} possess a broadband absorption spectrum spanning from ~850nm to ~1080 nm, specifically, the absorption cross section in the 915-975nm is very high. Also, high-brightness pump sources are available at 915-975 nm. Therefore, the high quantum efficiency in conjunction with the available pump sources enables YDF laser power level above multi-kW with near-diffraction-limited beam quality.

Er^{3+}-doped fibers (EDFs) have an emission waveband spanning in 1480-1620 nm which is located in both 'eye-safety' region and atmospheric transparency window. However, EDF owns a narrow absorption band in commercially available pump sources. In addition, the doping concentration of Er^{3+} in EDF is limited due to clustering effect. Moreover, the power of multimode pump diodes at 1.5 μm lag behind their counterparts at 0.9-1.0 μm. Compared with YDFL, the power of EDFL is limited by small absorption cross-section and Er^{3+}-doping concentration. To overcome this issue, Yb is often co-doped with Er as an alternative. To date, the highest power of Er:Yb co-doped fiber lasers (EYDFL) is 297 W with output power dependent slope efficiency, i.e. 40% for output power below 150W and 19% for output power above 200W[31]. The drawbacks of EYDFL for further power scaling are the parasitic lasing at 1-1.1μm from Yb and high thermal load. Based on large mode area EDF, a 656 W EDFL

with a slope efficiency of 35.6% is reported[32]. Still, the power level of EDFLs at 1.55μm waveband is lagging behind of YDFL.

Tm is another successful laser dopant that provides high optical gain. Its long wavelength emission adds unique features not available in YDFL. In optical fibers, it is noted that the fundamental mode (LP_{01}) area scales with λ^2. Compared with YDFL at 1 μm, the LP_{01} mode area of Tm^{3+}-doped fiber (TDF) at 2 μm is four times of that at 1 μm of YDF, thus providing a prominent advantage of power scaling. Meanwhile the damage threshold of TDFL is increased accordingly in Brillouin and Raman scattering. And most of the strategies used in YDFLs for power scaling could be translated to TDFLs. For the in-band pumping scheme that Tm^{3+} transferred from level $^3H_6$ to $^3F_4$, power scaling of TDFL is limited by the power level of EYDFL or laser diode. However, with the emerging of high power/brightness laser diodes at ~790 nm, output power of TDFL exceeds the EYDFL in high power fiber laser technology. Besides, TDFL could be utilized as a pump for Ho^{3+}-doped fiber laser, which extends the wavelength of silica based fiber lasers beyond 2.1 μm[33].

2.3 Thulium spectroscopy

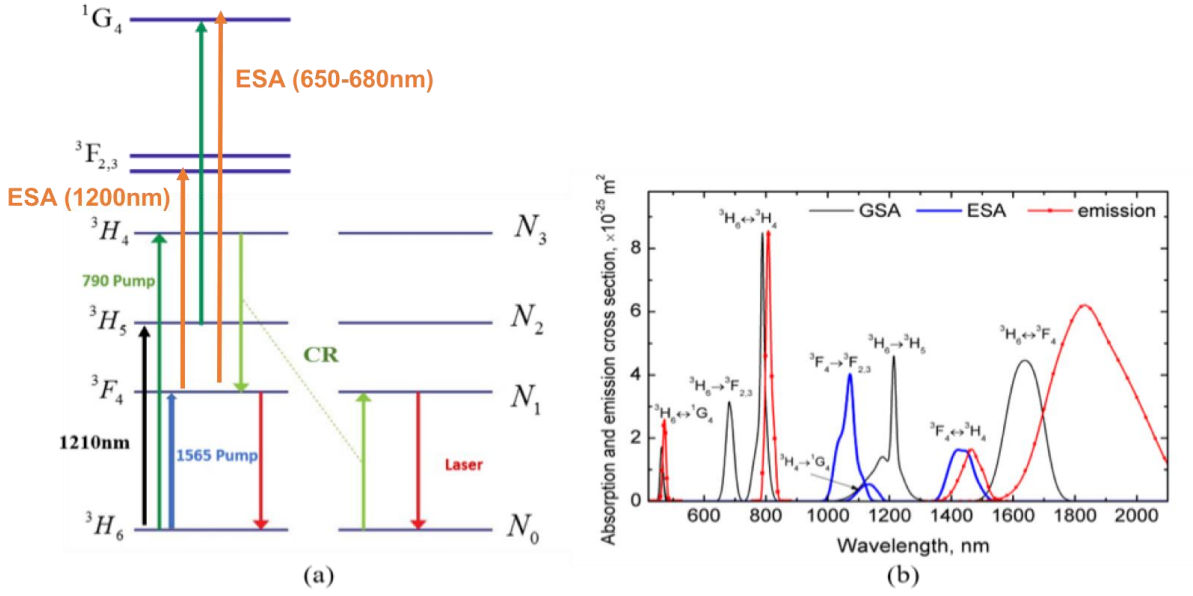

Figure 2. 1 (a) Energy-transfer processes between neighboring Tm^{3+} in Tm^{3+}-doped fiber; (b) the absorption and emission cross-section of Tm^{3+}-doped aluminosilicate fiber in [34].

Tm^{3+} ions have a complicated energy-level structure as shown in Fig. 2. 1a. In the transition of Tm^{3+} ions from the level $^3F_4$ to $^3H_6$ for Tm^{3+} ions, the fluorescence exhibits a seamless and broadband emission spanning from 1600 nm to 2200 nm as illustrated in Fig. 2. 1b, offering a prominently wide gain bandwidth for amplifiers and lasers. From the absorption spectrum of Tm^{3+} ions in aluminosilicate fiber shown in Fig. 2. 1b, there are four possible pumping

wavebands for Tm^{3+}-doped fiber based lasers and amplifiers, i.e., 1500-1750 nm for the transition $^3H_6$-$^3F_4$, ~1200 nm waveband for the transition $^3H_6$-$^3H_5$, 790 nm waveband for the transition $^3H_6$-$^3H_4$ and 650-680nm wavebands for the transition $^3H_6$-$^3F_{2,3}$. However, for the pump wavebands of ~1200 nm and 650-680 nm, they are subject to an excited state absorption (ESA), limiting efficiency in the $^3F_4$ to $^3H_6$ transition. In detail, the 650-680 nm pumping will pump the excited Tm^{3+} in level $^3F_4$ to $^1G_4$, thus triggering the corresponding ESA. Moreover, the Tm^{3+} in level $^3F_4$ could be pumped to the level $^3F_{2,3}$ by the 1200 nm pump photons. The 1500-1750 nm pumping, namely as in-band pumping, is promising for high efficiency operation due to its high Stokes efficiency. While for the 790 nm waveband pump, there is no possible transition from level $^3H_4$ or $^3F_4$ to higher Tm^{3+} level. Although blue fluorescence attributing to the ESA from level $^3H_5$ to level $^1G_4$ is usually observed, ESA is weak since the lifetime of level $^3H_5$ is very short due to the fast non-radiative decay to $^3F_4$, and the decay is suppressed by the cross-relaxation decay from level $^3H_4$ to $^3F_4$. Therefore, the 790 nm waveband and 1500-1750 nm bands are the widely used pump wavebands.

2.4 Cross-relaxation (CR) process and pumping schemes

In this section, I will firstly brief the CR process in TDFL and its connection with Tm^{3+}-doping concentration. Then the choice of pumping schemes is detailed with respect to pump source, and fiber waveguide structure.

The 790nm pumping is attractive due to the resonant CR process. The CR process could be described as follow: one electron is excited from ground state $^3H_6$ to level $^3H_4$ after absorbing a pump photon, and the radiative decay from level $^3H_4$ to $^3F_4$ will pump another ground state electron in level $^3H_6$ to the $^3F_4$. Hence, the CR process will provide two excited electrons in upper state level $^3F_4$ for one pump photon. Meanwhile, the $^3H_4 \rightarrow {}^3F_4$ emission spectrum overlaps with that of $^3H_6 \rightarrow {}^3F_4$ absorption, thus exhibiting a resonant CR process and a quantum efficiency of two ($^3H_4 + {}^3H_6 \rightarrow {}^3F_4 + {}^3F_4$). In theory, one could obtain a slope efficiency of 82%. However, the CR process is dependent on the Tm^{3+}-doping concentration. Higher Tm^{3+}-doping concentration gives a close ion-ion separation, thus obtaining higher CR efficiency. As the slope efficiencies shown in Fig. 2. 2, which is collected from published data[35]. Without CR process, the lasing efficiency is below 40% due to the quantum defect between pump light at ~790 nm and lasing signal at 2 μm waveband. With Tm^{3+}-doping concentration increasing, the slope efficiency will increase accordingly. With Tm^{3+}-doping concentration above 2 wt%, most of the slope efficiencies reported could surpass 40%, proving

the necessity of high Tm^{3+}-doping (Tm^{3+}>2wt %) to utilize the CR process. However, there is no further improvement when Tm^{3+}-doping>3.5 wt%. If the Tm^{3+}-doping is above 4.5 wt%, the lasing efficiency will decrease because of unwanted Tm^{3+} clustering.

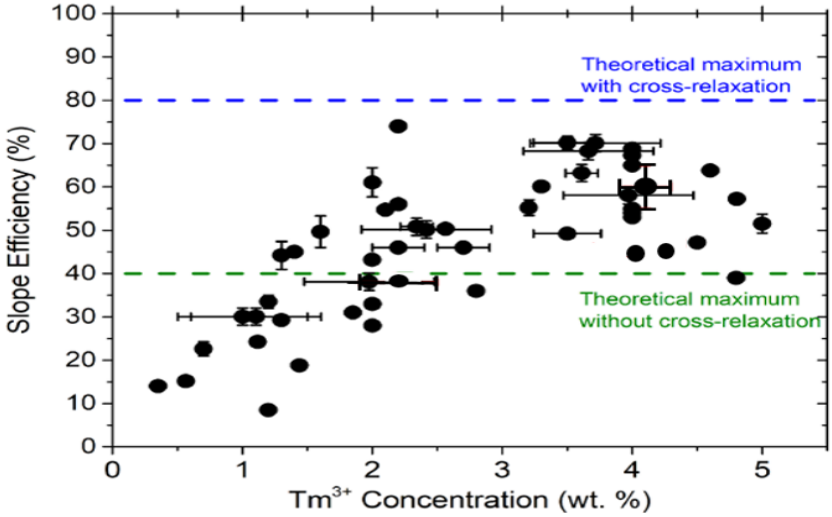

Figure 2. 2 The slope efficiency pumped at 790nm waveband with increasing Tm^{3+}-dopant concentration[35]

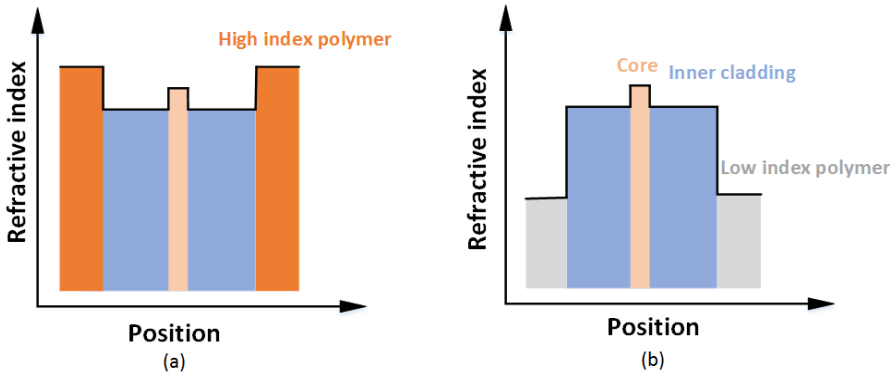

Figure 2. 3 Illustrative refractive index profile of (a) single clad fiber (b) double clad fiber.

Besides the high slope efficiency for the 790 nm pumping with CR process involved, the cladding pumping configuration is normally combined with multimode 790nm LD to achieve high power. Therefore, it is worthwhile to detail the cladding pumping. Firstly, cladding pump is accompanied by the double clad fiber, which is defined by a lower RI of the polymer layer or a fluorine-doped glass layer as illustrated in Fig. 2.3. With the concept of double cladding fiber structure, very high-power rare-earth doped fiber lasers have emerged with the corresponding advantages. Instead of launching into the active core with small numerical aperture (NA) and small core size, pump light is coupled into the inner cladding with larger NA and cladding size, which advantages high pump power. In order to achieve uniform pump absorption along the fiber, as depicted in Fig. 2. 4, non-circular symmetric inner cladding, such

as offset core, D-shape or hexagonal structure, are implemented to avoid the creating of skew rays. Moreover, the emerging of high power rare-earth doped fiber lasers has started with the concept of double cladding fiber structure

Due to available high-power/brightness laser diodes at 780-810 nm waveband, high power and high-efficient TDFLs are demonstrated under the 790nm clad pumping scheme. Moulton et al. demonstrated a 300 W TDFL at 2040 nm with a slope efficiency of 64.5% [36]. In a dual-stage amplifier configuration, output power of 1.05 kW at 2045 nm with a slope efficiency of 53% has been reported in[37].

However, if Tm^{3+}-doping is low, in-band pumping is preferred for higher lasing efficiency due to its low quantum defect. Based on a double-clad TDF with a Tm^{3+}-doing of 1.4 wt%, a 19.2W TDFL at 1991nm with a slope efficiency of 72% pumped by 1565 nm fiber laser has been reported[38]. Owing to the stronger core absorption in TDF, in-band core pumping benefits shorter devices and short wavelength operation. Compared with the 790 nm pumping, the in-band pumping provides a better access to a wide-band lasing tunability due to low quantum defect[38].

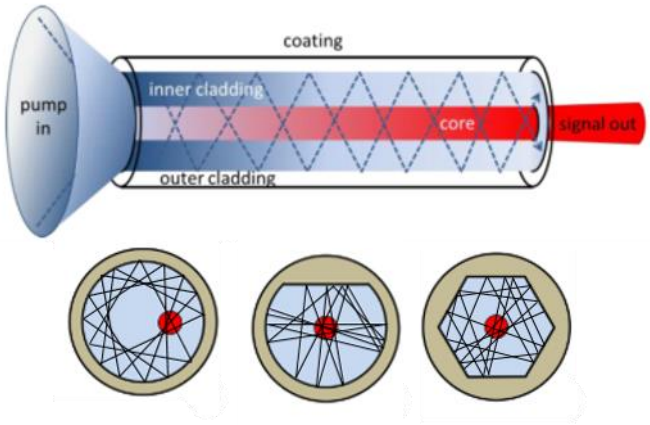

Figure 2. 4 (top) Schematic of cladding pump operation in double-clad fiber. (Bottom) three common double-clad fiber cross sections with propagated pump light in cladding. (From left to right: core offset center, D-shape, hexagonal cladding structure)

2.5 Glass composition of Tm^{3+}-doped fiber (TDF)

In this section, the influences of glass composition of TDF on the capability of Tm^{3+}-doing concentration, emission spectrum and fluorescence lifetime of level $^3F_4$ will be literature reviewed. To reduce the Tm^{3+} clustering, the co-dopants of Al_2O_3 or P_2O_5 are usually added to the main silica glass, thus increasing the Tm^{3+} solubility in silica. However, when P_2O_5 added in silica, the phonon energy is increased and the quantum efficiency in the transition $^3F_4$-$^3H_6$ is

decreased. Sufficient Al_2O_3 is very important to minimize the Tm^{3+} clustering. With the ratio of Al^{3+}: Tm^{3+} above 9:1, the laser efficiency is improved significantly with reduced quenching at $^3F_4$ [39][40]. Therefore, with higher Tm doping concentration and high ratio of Al^{3+}: Tm^{3+} (~10:1), the lasing efficiency surpasses the Stokes limit easily with CR process involved. However, in practice, the Tm^{3+}-doping profile from MCVD process varies across the core, which gives low Tm^{3+}-doping in the core edge. Therefore, CR efficiency is deteriorated by the non-uniform Tm doping profile. In this context, a very high slope efficiency of 70% is achieved based on a double clad TDF with highly Tm-doped (3.6wt %) and flat-top RI profile of Tm-doping[41].

A TDF has a broadest emission bandwidth in the transition from level $^3F_4$ to $^3H_6$ spanning from 1600 nm to 2200 nm. And the emission windows changes for different TDFs with variations of Tm-doping concentration and co-dopants. As shown in Fig. 2. 5, it shows absorption and emission cross-sections for various aluminosilicate-based (Al_2O_3-SiO_2) TDFs. Even though these TDFs exhibits different absorption cross-sections windows, the peaks of absorption cross-section is still beyond 1650nm. Amongst aluminosilicate-based TDFs, the Al/La co-doped TDF has the shortest absorption peak at 1650nm, in addition, Al/La co-doped TDF also exhibits a broadened emission range due to the co-dopants of La[20]. Compared with aluminosilicate-based, Tm^{3+}-doped GeO_2-SiO_2 glass fiber shows a slightly blue-shifted emission spectrum as depicted in [8][21], additionally, GeO_2-SiO_2 glass is more photosensitive. Furthermore, as reported in [42], the shortest wavelength range of TDFL based on Tm^{+}- doped GeO_2-SiO_2 fiber could be tuned down to 1650nm. When the Tm^{+}-doping concentration is low, quenching in TDF is suppressed, which is beneficial for the emission from the transition $^3H_4 \rightarrow {}^3F_4$ in the S-band Meanwhile, the emission from the transition $^3F_4 \rightarrow {}^3H_6$ at the short wavelength edge is accessible due to the realizable high population inversion [43]. In this context, the composition of glass host will influence the emission spectrum in the transition from level $^3F_4$ to $^3H_6$.

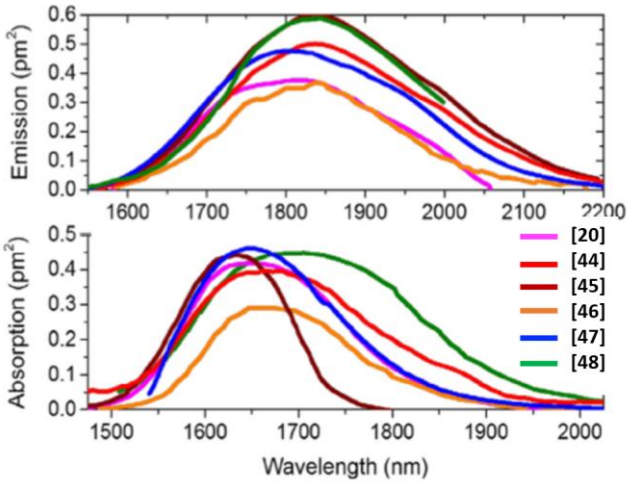

Figure 2. 5 Emission (top) and absorption (bottom) cross-section between level $^3F_4$ and $^3H_6$ for Tm-doped silica fibers reported in **[20] [44][45][46][47][48]**.

As aforementioned analysis, in order to achieve high efficiency TDFL, high Tm^{3+}-doping without Tm^{3+}-clustering is required. However, for silica glass fiber, the Tm^{3+}-doping concentration is limited by the glass structure. Hence, the germanate glass based fiber waveguides are proposed to enhance the capability of Tm^{3+}-doping concentration due to their higher refractive index compared to silica glass. So far, the reported Tm^{3+}-doping concentration in germanate glass fibers are one order of magnitude higher than that in silica glass fiber, showing the prospect of ultra-short fiber devices[49].

Due to the small energy gap between level $^3F_4$ and $^3H_6$, the non-radiative process dominates in decay from level $^3F_4$ to $^3H_6$, which gives a very short upper state lifetime of Tm^{3+}. In the pure silica glass, the measured lifetime from level $^3F_4$ is ~327μs in [50] and 334.7 μs in [45]. However, high Al^{3+} concentration will enhance the lifetime to 430 μs in [34] and 650 μs in [8].

As shown in Fig. 2.6, for SiO_2-Al_2O_3 glass TDFs, the reported lifetime from level $^3F_4$ is in the range of 200 μs to 650 μs, which is close to that in GeO_2-SiO_2 or GeO_2 -Al_2O_3-SiO_2 glass TDFs. It is worthwhile to mention the influence of Tm^{3+} concentration on lifetime. When Tm^{3+} concentration is higher than 3 wt%, self-quenching start to be apparent, and the lifetime from level $^3F_4$ is reduced.

However, for Tm germanate glass fiber, the fluorescence lifetime from level $^3F_4$ is in the range of 0.7 ms to 3ms[45], which is a significant improvement compared with that in silica glass TDF shown in Fig. 2.6 With longer fluorescence lifetime, favoring a population inversion in level $^3F_4$, therefore, the lasing threshold will be lower accordingly and the lasing efficiency will probably be higher[51].

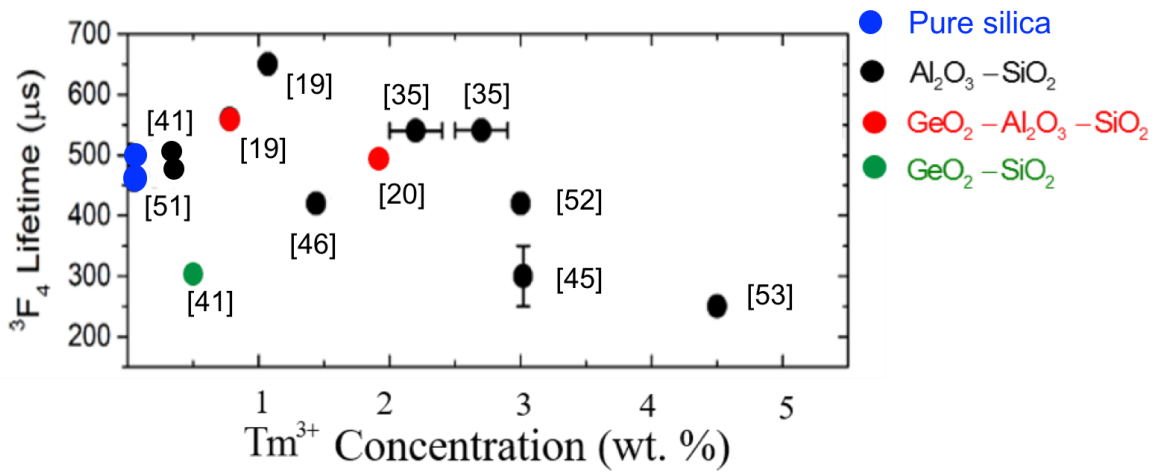

Figure 2. 6 Variation of upper state lifetime from level $^3F_4$ with increasing Tm^{3+}-dopant concentration in silica glass fibers. The fluorescence lifetimes from the level $^3F_4$ to $^3H_6$ for different glass composition based Tm-doped fibers : GeO_2-Al_2O_3-SiO_2: [20] [21], Al_2O_3-SiO_2: [35] [46] [47][52][53][54], GeO_2-SiO_2: [41], Pure silica: [44] [49].

2.6 Review of tunable TDFL

Apart from the eye-safe feature of the 2 μm waveband, TDF emission band also hosts many absorption lines of molecules such as H_2O, CO_2 and NO_2. Particularly, the first overtone vibration of OH locates at 1900 nm, just falling in the emission window of TDF. Therefore, a TDFL with the matched wavelength would be useful in medical applications and atmospheric LIDAR sensing[55][56]. In addition, the emission of TDF locates in the atmospheric window of high transparency, making directed-energy and information delivery feasible in free space optical communication[57][58]. Moreover, the high-power 2 μm fiber laser could performs as a very efficient pump source for Ho^{3+}-doped fiber lasers at wavelength up to 2.2 μm[59]. Furthermore, the 2 μm fiber laser could be used as pump source for mid-infrared optical parametric oscillators with high conversion[60]. To fully implement the potential of the emerging applications, widely tunable fiber lasers in 2 μm waveband are required. Due to the feature of amorphousness in silicate glass, the bandwidth of pump absorption and gain could be very broad. Particularly for TDF, the gain bandwidth could be up to 34 THz , providing the capability of wide-band tuning. In this section, I will review the widely demonstrated tunable TDFLs by different tunable cavity configurations.

2.6.1 Diffraction grating based tunable TDFLs

In the core-pumping scheme with a 788 nm single-mode LD as pump source [42], Barnes et al demonstrated a tunable TDFL in the wavelength range from 1715 to 2000 nm using aluminosilicate TDF, which operated in low power regime (a few mW). Based on the cladding-

pump scheme at 787nm diode-bar pump sources, Clarkson et al demonstrated a tunable TDFL spanning from 1860 to 2090 nm with output power ranging from 3 W to 9 W [61]. In [38], with an Er/Yb co-doped fiber laser as pump, Shen et al reported a high-power TDFL in a core-pump scheme with operating wavelength from 1723 nm to 1973 nm and in a cladding-pump scheme spanning from 1859 to 2061 nm with the maximum output power is 17.4 W at 1941 nm, which is restricted by pump power.

2.6.2 Fiberized grating based tunable TDFLs

With a 3 dB bandwidth of 3 nm tunable filter, Li et al demonstrated a monolithic all-fiber ring cavity TDFL offering tuning range of 250 nm pumped by single-mode 79 0nm LD with maximum output power of 30 mW at 1930 nm[55]. Instead of core pumping, Yin et al first built a tunable TDFL spanning from 1940 to 207 0nm cladding pumped by multimode 793 nm LD. With this tunable TDFL as a master oscillator, a high-power tunable TDFL in a configuration of MOPA system was demonstrated [62].

2.6.3 Fiber Bragg grating (FBG) based tunable TDFLs

With an FBG array including high reflective FBGs at discrete wavelengths, Li et al reported a wavelength switchable cladding-pumped TDFL in the wavelength region from 1997nm to 2125nm[63]. Although lasing threshold is low in the low loss cavity, lasing wavelength is not continuously tuned. Due to the high Tm^{3+}-doping concentration in TDF, the lasing wavelength could be extended to 2200 nm (long emission edge of TDF) by employing a low reflective FBG and a sufficient fiber length.

Additionally, based on a force-induced long period fiber gratings (LPFGs), Sakata et al demonstrated an all-fiber tunable TDFL with operating wavelength in the range from 1845 to 1930 nm under core-pumping by 1.6 μm laser diode [64]. Compared with FBG array, force-induced LPFG could offer a wide tunability when it is manually controlled by changing force and grating period. However, the lasing wavelength is still not seamlessly tuned.

It is obviously observed that all the abovementioned tunable TDFLs are operated in the wavelength range from 1720 nm to 2200 nm. Hence, long wavelength Tm emission (see Fig. 2.5) is fully utilized but short wavelength is less exploited. Lasing at short wavelength is practically difficult due to the prominent reabsorption in the transition from $^3F_4$ to $^3H_6$ and the gain saturation effect caused by ASE in the peak emission region will overrun lasing at short wavelength. However, Daniel et al demonstrated a tunable TDFL in the 1660-1720 nm region

based on a high reflective FBG mounted in a mechanical stage, whereby the tuning of lasing wavelength is realized by compressing FBG[22].

2.7 Short-wavelength fiber lasers below 1750 nm

Recently, intense laser radiation in the spectral range of 1650–1750 nm attracts increasing interest due to its various applications. Firstly, C-H bond stretch resonance are present in many hydrocarbon materials in the wavelength range around 1700 nm, whereby water exhibits a local minimum absorption. Particularly, in the fat rich tissue (high C-H content) of human body, the absorption of fat with local maximum value at around 1720 nm is higher than that of water, allowing many promising medical applications where heating of fat rich tissue is preferentially required [65]. Moreover, the 1700 nm wavelength region attracts growing interest for optical coherence tomography (OCT), so far the applications of OCT is limited by its shallow imaging depth. Compared with the wavelengths of 808 nm and 1300 nm used in the previous OCT techniques, the spectral region near 1700nm show a lower scattering coefficient, which will improve the imaging depth in OCT due to its dependence on scattering coefficient and water absorption[66]. In coherent tomography and multiphoton microscopy, the 1675nm laser improves the signal-to-noise ratio in biomedical tissue, which is beneficial for obtaining information from a larger depth[67][9]. With the wavelength decreased further, the 1650 nm laser radiation in surgery could allow much larger penetration depth in tissue with reduced collateral damages [68]. Based on soliton self-frequency shift, a femtosecond laser at 1650 nm was reported in [8], which show the potential for three-photon imaging of biological tissue.

Due to the broadband emission spanning from 1600-2200 nm, TDF provides access to the lasing below 1750 nm. In the cw regime, a few fiber lasers related to short wavelength below 1750 nm have been reported. Based on the TDF with terbium-doping in cladding for ASE suppressing in 1750-2000 nm region, a tunable TDFL was reported with a lasing wavelength tuned from 1635.6nm to 1766 nm, but the output power was not satisfactory with maximum power of 0.16 mW at 1716 nm[19]. Transmission characteristics of a proposed PCF design could be evaluated based on confinement loss[10]. By controlling the geometrical structure of a particular PCF design, the long cut-off wavelength (such as 1800nm, 1750nm) could be implemented. With a PCF as low-pass filter, Emami et al reported a 1740nm TDFL with only output power of 34 mW [10]. In order to achieve high power at wavelength below 1750 nm, as described in previous section with high pump power, an effectively tunable cw TDFL in the 1660-1750 nm region was demonstrated with the help of compressive FBG, and the output

power at 1726 nm is 12.6W [22]. In [69], using a pair of FBGs as feedback in the laser cavity with low reflective FGB as output coupler, a 1706.75nm TDFL with output power of 3.15 W was achieved. On the other hand, however, TDF based pulsed fiber lasers at wavelength below 1750 nm are only few reported. In[11], Emami reported a tunable mode-locked TDFL in the region 1702-1764 nm with pulse duration around 2.55 ps at 1730 nm.

2.8 Overview of state-of-the-art EDFA and TDFA

In the past decades, EDFA-based transmission systems have shaped the infrastructure of today's telecommunication network. The success of optical communication has seen exponentially increasing internet traffic.

To satisfy the ever-increasing demand of internet traffic, dense wavelength division multiplexing (DWDM) transmission systems are successfully developed, offering a double bandwidth when combine C-band EDFA and L-band EDFA in parallel. To date, with silica-based EDFs, the L-band EDFAs can only covers wavelength up to 1620nm[70]. Other researchers also extended L-band EDFA to the wavelength of 1620nm by exploiting bismuth-based EDF or MCS (antimony silicate) EDF[71][14]. Compared with silica-based or fluoride based EDF, tellurite-based EDF is capable of providing larger emission ($^4I_{13/2}$-$^4I_{15/2}$) cross-section and lower ESA ($^4I_{13/2}$-$^4I_{9/2}$) cross-section in the wavelength region beyond 1600 nm[72]. In addition, the longer operational wavelength limit of EDFA is determined by the intersection between the stimulated emission and ESA. Therefore, tellurite-based EDFs are capable of extending the operating wavelength at long edge, and the measured wavelength of tellurite-based EDFA is extended to 1634 nm with small-signal gain of 8 dB at 1630nm[72]. In order to improve the performance of tellurite-based EDF, the erbium-doped tellurite microstructure fibers (EDTMFs) with enlarged air-to-glass ratio in cladding have been proposed and successfully demonstrated[73]. Based on a novel EDTMF, Jia et al reported a broadband EDFA with positive net gain from 1524 to 1637nm[15], further increasing the capacity of WDM transmission system.

With the combination of C-band and L-band EDFAs, high-capacity DWDM system has been implemented[74][75]. To enhance the capacity of DWDM system, silica-based TDFAs have been exploited as a complement for C-band and L-band in the wavelength region from 1450 to 1530nm from the transition $^3H_4$-$^3F_4$[3][76]. On the other hand, as described in previous section, the broadband emission of TDFs from transition $^3F_4$-$^3H_6$ could cover the wavelength from 1600 to 2200 nm. Compared with EDFs, TDFs could provide significantly broadened amplification bandwidth, indicating potential for high-capacity DWDM system. To date,

different pumping schemes such as 790 nm diode bidirectional pump, 1565nm diode bidirectional pump, and hybrid pump of 790nm and 1565nm diodes, have been employed in various configurations of TDFAs, offering high gain and low noise figure (NF) across the wavelength range of 1700 – 2050 nm as shown in Fig. 2. 7[77][78][79][80], and the wavelength coverage of TDFAs could be controlled by the length of employed gain fibers due to the reabsorption of short wavelength components. With the successful development of HC-PBGFs, exhibiting comparable scattering loss at 2μm window as the insertion loss of silica fibers in 1.55μm window, the TDFA-based data transmission is feasible at 2μm[81]. With effective management of ASE, the short-wavelength amplification edge of the TDFA has further extended down to 1650 nm with a small signal gain of 8dB demonstrated when pumped by 1565nm fiber laser. As above described, there is still a small gap between long wavelength edge of the EDFAs and short wavelength edge of the TDFAs, as shown in Fig. 2.7.

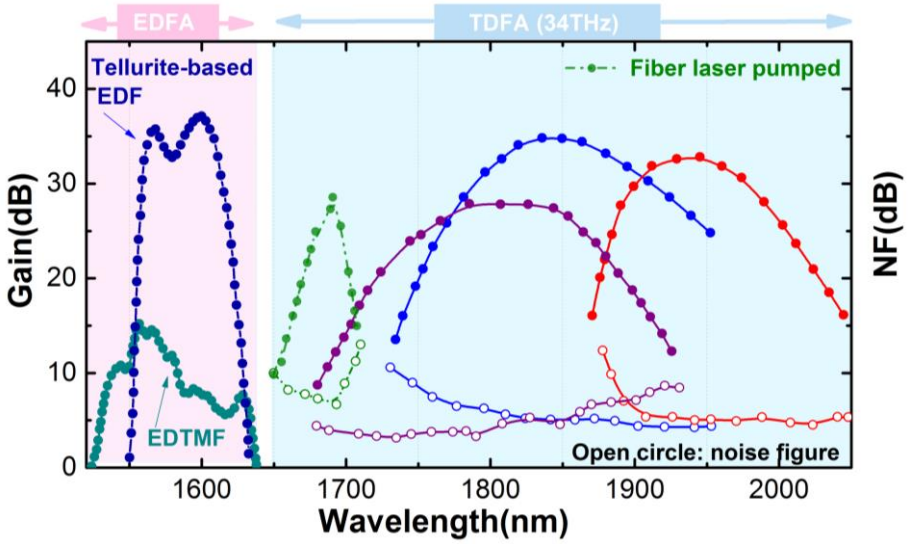

Figure 2. 7 Overall gain and NF of silica-based TDFA, as well as the gain of tellurite-based EDFA in the C+L band. For EDTMF, the gains are measured for input signal with power of -13dBm. In addition, all other gains are measured for input signal with power of -20dBm.

2.9 Atomic-rate equations and TDFA modeling

In the course of the development of broadband TDFAs with high gain and low noise figure for next generation optical fiber communications at 2 μm [82][83], it is essential to optimize the performance of TDFA using theoretical modeling. So far, there are many theoretical modeling works for EDFA[84][85]. Particularly, in [86], accurate modeling of EDFA is realized with Er^{3+}-doping profile, modal profiles of signal and pump incorporated. On the other hand, theoretical modeling of TDFA and TDFL are sporadically reported[87][88]. Generally, there

are two pumping schemes for TDFA, i.e., 790nm (indirect) core-pumping scheme and 1560nm (in-band) pumping scheme. To improve the accuracy of TDFA modeling, CR process and ASE noise are included for both pump schemes, and the simulation result of TDFA is close with the experimental result in [89]. Considering the accurate modeling achieved in EDFAs, the accuracy of TDFA modeling could be further improved by incorporating the Tm^{3+}-doping profile, modal profiles of signal and pump waves.

Hence, the population density $N(r,\theta)$ in level $^3F_4$, $^3H_4$ and $^3H_6$ is transversely dependent due to the effect of modal overlap between pump and signal, which will be depicted in rate equations. In turn, power of pump and signal will be determined by the population density in level $^3F_4$ and $^3H_6$, which will be described in light propagation equations along fiber.

2.9.1 Indirect (790nm) core-pumping scheme

As illustrated in Fig. 2.2a, pump, signal and CR process are indicated clearly between two Thulium-energy levels. For indirect core-pumping scheme from the numerical model in [89], rate equations used to estimate the population density of energy level $^3F_4$, $^3H_4$ and $^3H_6$ are given by[89]:

$$\frac{dN_3}{dt} = R_{03}N_0 - N_3(A_{31} + A_{30}) - C \quad \ldots 2.3$$

$$\frac{dN_1}{dt} = -W_{10}N_1 + W_{01}N_0 - A_{10}N_1 + N_3A_{31} + 2C \quad \ldots 2.4$$

$$\frac{dN_0}{dt} = W_{10}N_1 - W_{01}N_0 + A_{10}N_1 + N_3A_{30} - C - R_{03}N_0 \quad \ldots 2.5$$

$$C = k_{3101}N_0N_3 - k_{1310}N_1^2 \quad \ldots 2.6$$

where A_{ij} is the non-decay rate of level *i* into level *j*. N_0, N_1, N_3 are population density of level $^3H_6$, $^3F_4$, $^3H_4$. R_{03} is the pumping rate from level $^3H_6$ to $^3H_4$, W_{01} and W_{10} are the absorption rate and emission rate respectively. *C* represents the CR process, k_{1310} and k_{3101} are the inverse CR constant and CR constant, which are related to Tm^{3+}-doping concentration, as detailed in [88].

Actually, for core-pumping scheme, pump and signal propagating along the fiber will have a transverse-plane dependent intensity distribution due to the fiber waveguide structure, which could be described by[86]:

$$I(r,\theta) = P \cdot i(r,\theta) \quad \ldots 2.7$$

where *P* is the power of signal or pump in the corresponding modal profile, and $i(r,\theta)$ is the normalized intensity profile of pump or signal mode in TDF.

Hereby, the normalized intensity of signal and pump mode will be achieved with the following depiction. For a given optical fiber waveguide, the finite-element method based COMSOL Multiphysics is called to calculate the electric and magnetic field components of the optical modes in a fiber. In this way, the obtained eigen-solutions are vector modes in terms of electric field and magnetic field. Generally, for weakly guiding fibers, the vector modes obtained from COMSOL could be converted to scalar modes (LP modes) after data processing in MATLAB[90]. Therefore, the normalized intensity profiles of pump modes and signal mode are acquired by:

$$i(r,\theta) = \frac{E_{x,LP}^2 + E_{y,LP}^2}{\iint (E_{x,LP}^2 + E_{y,LP}^2) r dr d\theta} \quad \ldots 2.8$$

where Ex and E_y is the electric field. Based on the transverse-plane dependent intensity profile for pump and signal, the pump rate, absorption rate and emission rate could be written as follows[89][90]:

$$R_{03} = \lambda_p \frac{\sigma_a(\lambda_p)}{hc} I_p(r,\theta,z) \quad \ldots 2.9$$

$$W_{01} = \lambda_s \frac{\sigma_a(\lambda_s)}{hc} I_s(r,\theta,z) \quad \ldots 2.10$$

$$W_{10} = \lambda_s \frac{\sigma_e(\lambda_s)}{hc} I_s(r,\theta,z) \quad \ldots 2.11$$

where $\sigma_a(\lambda_p)$ is absorption cross-section at pump wavelength, $\sigma_a(\lambda_s)$ and $\sigma_e(\lambda_s)$ are the absorption and emission cross-section at signal wavelength respectively. c is speed of light in vacuum. h is Planck's constant.

At a steady state, we have $\frac{dN_i}{dt} = 0$, i=0, 1, 3, and $N_0 + N_1 + N_3 = N_t$ with N_2 ignored. Besides that the mode profiles of signal and pump are transverse-plane dependent, the doping concentration N_t in TDF is also transverse-plane dependent. According to the equations 2.2-2.5, and 2.8-2.10, N_1, and N_3 could be given in terms of N_0 and N_3 as follows:

$$N_1(r,q) = \frac{\overline{\sigma_a}(\lambda_p)\frac{I_p(r,\theta)}{I_{sat,p}} + \overline{\sigma_a}(\lambda_s)\frac{I_s(r,\theta)}{I_{sat,s}} + 2A_{30}\tau + A_{31}\tau}{\overline{\sigma_e}(\lambda_s)\frac{I_s(r,\theta)}{I_{sat,s}} + \overline{\sigma_e}(\lambda_p)\frac{I_p(r,\theta)}{I_{sat,p}} - 2A_{30}\tau - A_{31}\tau + 1} N_0(r,q) - \frac{2A_{30}\tau + A_{31}\tau}{\overline{\sigma_e}(\lambda_s)\frac{I_s(r,\theta)}{I_{sat,s}} + \overline{\sigma_e}(\lambda_p)\frac{I_p(r,\theta)}{I_{sat,p}} - 2A_{30}\tau - A_{31}\tau + 1} N_t(r,q) \quad \ldots 2.12$$

$$N_3(r,q) = \frac{-\frac{I_s(r,\theta)}{I_{sat,s}} - \frac{I_p(r,\theta)}{I_{sat,p}} - 1}{\overline{\sigma_e}(\lambda_s)\frac{I_s(r,\theta)}{I_{sat,s}} + \overline{\sigma_e}(\lambda_p)\frac{I_p(r,\theta)}{I_{sat,p}} - 2A_{30}\tau - A_{31}\tau + 1} N_0(r,q) + \frac{\overline{\sigma_e}(\lambda_s)\frac{I_s(r,\theta)}{I_{sat,s}} + \overline{\sigma_e}(\lambda_p)\frac{I_p(r,\theta)}{I_{sat,p}} + 1}{\overline{\sigma_e}(\lambda_s)\frac{I_s(r,\theta)}{I_{sat,s}} + \overline{\sigma_e}(\lambda_p)\frac{I_p(r,\theta)}{I_{sat,p}} - 2A_{30}\tau - A_{31}\tau + 1} N_t(r,q) \quad \ldots 2.13$$

$$where, I_{sat,p} = \frac{h\nu_p}{(\sigma_a(\lambda_p)+\sigma_e(\lambda_p))\tau}, I_{sat,s} = \frac{h\nu_s}{(\sigma_a(\lambda_s)+\sigma_e(\lambda_s))\tau}, \tau = \frac{1}{A_{10}}$$

$$\overline{\sigma_a}(\lambda_p) = \frac{\sigma_a(\lambda_p)}{(\sigma_a(\lambda_p)+\sigma_e(\lambda_p))}, \overline{\sigma_a}(\lambda_s) = \frac{\sigma_a(\lambda_s)}{\sigma_a(\lambda_s)+\sigma_e(\lambda_s)}, \overline{\sigma_e}(\lambda_s) = \frac{\sigma_e(\lambda_s)}{(\sigma_a(\lambda_s)+\sigma_e(\lambda_s))}, \overline{\sigma_e}(\lambda_p) = \frac{2\sigma_e(\lambda_p)}{(\sigma_a(\lambda_p)+\sigma_e(\lambda_p))}$$

where, $\overline{\sigma}_\alpha(\lambda_p)$, $\overline{\sigma}_e(\lambda_p)$, $\overline{\sigma}_\alpha(\lambda_s)$ and $\overline{\sigma}_e(\lambda_s)$ are the corresponding normalized absorption- and emission cross section for pump and signal respectively.

With $N_1(r,\theta)$ and $N_3(r,\theta)$ substituted into equation 2.5, we have

$$k_{1310}N_1^2 - k_{0131}N_0N_3 + (\sigma_a(\lambda_p)N_1 - \sigma_e(\lambda)N_3)\frac{I_p(r,\theta)}{h\nu_p} - (A_{30}+A_{31})N_3 = 0 \quad \ldots 2.14$$

Therefore, based on the equations 2.11-2.13, the concentration $N_1(r,\theta)$ and $N_0(r,\theta)$ could be solved. Due to the transvers-plane dependent of pump and signal, i.e, $I_p(r,\theta)$, $I_s(r,\theta)$ and the Tm^{3+}-doping profile of $N_t(r,\theta)$ in fiber core, $N_1(r,\theta)$ in level $^3F_4$ and $N_0(r,\theta)$ in $^3H_6$ are transverse-plane dependent.

Moreover, instead of using a confinement factor for pump and signal modes as in [89] , in this model, the transvers-plane dependent profiles are incorporated in the propagation equations, which describes the distribution of pump power, signal power and ASEs along fiber length as in [89].

$$\frac{dP^{\pm}{}_{p}(z)}{dz} = \pm P^{\pm}{}_{p}(z)(\iint_{S} \sigma_a(\lambda_p)(\eta(\lambda_p)N_1(r,\theta) - N_0(r,\theta))i_p(r,\theta)rdrd\theta - \alpha_p) \quad \text{... 2. 15}$$

$$\frac{dP_s(z)}{dz} = P_s(z)(\iint_{S} \sigma_a(\lambda_s)(\eta(\lambda_s)N_1(r,\theta) - N_0(r,\theta))i_s(r,\theta)rdrd\theta - \alpha_s) \quad \text{...2. 16}$$

$$\frac{dP_{ASE,\,forward}(z)}{dz} = P_{ASE,\,forward}(z)\cdot\sigma_a(\lambda_{ASE})(\iint_{S}(\eta(\lambda_{ASE})N_1(r,\theta) - N_0(r,\theta))i_s(r,\theta)rdrd\theta - \alpha_s) +$$

$$2h\frac{c^2}{\lambda^3}\Delta\lambda(\iint_{S}(\sigma_e(\lambda_{ASE})N_1(r,\theta))i_s(r,\theta)rdrd\theta \quad \text{... 2. 17}$$

$$\frac{dP_{ASE,backward}(z)}{dz} = -P_{ASE,backward}(z)\cdot\sigma_a(\lambda_{ASE})(\iint_{S}(\eta(\lambda_{ASE})N_1(r,\theta) - N_0(r,\theta))i_s(r,\theta)rdrd\theta - \alpha_s) -$$

$$2h\frac{c^2}{\lambda^3}\Delta\lambda(\iint_{S}(\sigma_e(\lambda_{ASE})N_1(r,\theta))i_s(r,\theta)rdrd\theta \quad \text{... 2. 18}$$

where $\eta = \frac{\sigma_e}{\sigma_a}$, $P^{\pm}{}_{p}(z)$ corresponds to the forward and backward pump power at position z, $P_{ASE,\,forward}(z)$ and $P_{ASE,backward}(z)$ are the corresponding power of forward ASE and backward ASE, and $\Delta\lambda$ is the bandwidth of the ASE around signal wavelength.

2.9.2. In-band (1565nm) core-pumping scheme

Although the CR process will be very weak due to low population density in level $^3H_4$ for in-band pumping, the CR process will also be included in the rate equations to keep consistent with that of indirect core pumping scheme, and the rate equations are given by:

$$\frac{dN_3}{dt} = -N_3(A_{31} + A_{30}) - C \quad \text{...2. 19}$$

$$\frac{dN_1}{dt} = R_{01}N_0 - R_{10}N_1 - W_{10}N_1 + W_{01}N_0 - A_{10}N_1 + N_3A_{31} + 2C \quad \text{... 2. 20}$$

$$\frac{dN_0}{dt} = -R_{01}N_0 + R_{10}N_1 + W_{10}N_1 - W_{01}N_0 + A_{10}N_1 + N_3A_{30} - C \quad \text{... 2. 21}$$

$$C = k_{3101}N_0N_3 - k_{1310}N_1^2 \quad \text{... 2. 22}$$

At the steady-state, the rate equations could be solved similarly as indirect core-pumping scheme.

For indirect core-pumping and in-band core-pumping schemes, given the boundary condition of pump and signal for the first order differential equation 2.15 and equation 2.16, the power of pump and signal could be numerically solved by MATLAB based on the Runge-

Kutta fourth-order method. Due to the low-power input signal, the forward ASE and backward ASE along the fiber will saturate the gain of TDFA. On the other hand, ASE is very important to evaluate the NF of TDFA. Hence, an accurate evaluation of forward ASE and backward ASE is necessary. For single-mode TDFA, the shooting method is generally used as a trial-and-error approach. Firstly, the boundary condition of backward ASE at z=0 is guessed with an initial value. After integration from z=0 to z=L, the backward ASE at z=L is obtained, which is compared with the ideally value of 0 at z=L. Afterwards, the initial backward ASE of the subsequent trials is corrected by the difference. After lots of integration iterations, the backward ASE at z=L will be finally converged and close to 0. Based on the calculated power of signal and ASE at output end, gain (G) and NF as two most important figure-of-merits of optical amplifier could be calculated[91] :

$$G = 10\log_{10}\frac{P_s(z)}{P_S(0)} \quad \text{... 2. 23}$$

$$NF = \frac{P_{ASE}}{h\nu\Delta\nu G} + \frac{1}{G} \quad \text{... 2. 24}$$

Chapter 3 Tm/Ge co-doped Fiber Characterization

3.1 In-house built Er/Yb co-doped fiber laser

For the applications of Tm^{3+}-doped fiber in lases and amplifier, an in-band pump source is a necessity for core-pumping scheme throughout this thesis. Therefore, at the first stage, I have built an Er/Yb co-doped fiber laser at the wavelength of 1565nm for the PhD project. As shown in Fig. 3.1, the linear fiber laser cavity is formed by a pair of apodized FBGs centered at 1565nm, i.e., high reflection (HR 99% with BW of 1nm) FBG and low reflection (LR 5% with BW of 0.6nm) FBG. Here I used six multimode 915nm laser diodes (LDs) as pump source for the 1565nm fiber laser, and the pump power were launched through (6+1) ×1combiner. In addition, the gain fiber is a 5m double-clad Er/Yb co-doped fiber (Nufern 12/130μm) with a core NA of 0.2 and first cladding NA of 0.46. Moreover, the residual pump was stripped out by high refractive index glue, which is close to the splicing point between Er/Yb co-doped fiber and SMF28 fiber. Furthermore, the laser output was coupled out through LR FBG, which was connected to a 1550nm isolator in case of parasitic lasing.

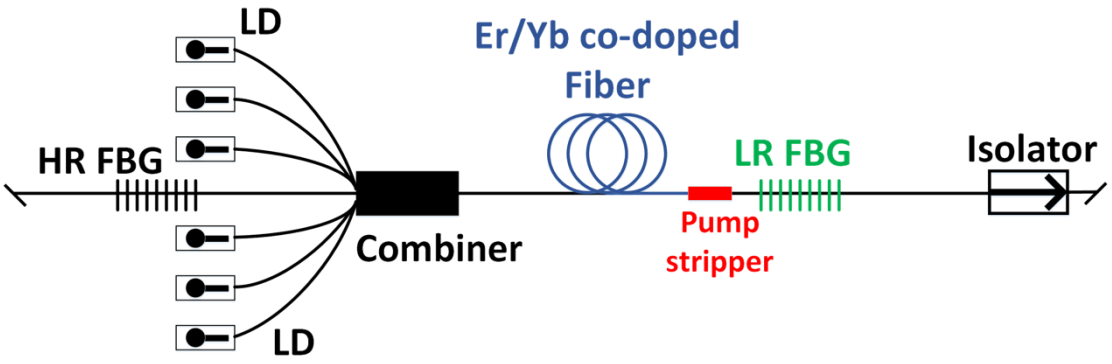

Figure 3. 1 schematic of in-house built Er/Yb co-doped fiber laser

The LDs (JDSU-6397, 8W) used in Er/Yb co-doped fiber laser shown in Fig. 3. 1 are driven simultaneously by power supply (Lumina LD driver) with input current varying from 0 to 9.5 A. Fig. 3. 2a shows the laser output at different pump power. The lasing threshold of the six LDs are around 0.5 A. With the increment of pump power up to 16 W, the lasing output of each individual LD could reach to the power level ranging from 6.5 W to 7 W. The corresponding lasing efficiency of LDs vary from 40% to 43%. Moreover, the operation wavelength of LD will have a red shift of 13 nm with a BW broadened when drive current is increased to 9 A from 1 A. As shown in Fig. 3. 1, the output power of six LDs are combined as a pump source for pumping the 1565nm fiber. Fig. 3. 3 summarizes the output power and spectra of the in-

house built 1565nm fiber laser. The lasing threshold is 2.6 W from the launched pump power from LDs. With increasing the pump power, the output power could reach 5 W with the lasing efficiency of 23.95% at 1565 nm. With pump power increased further; the laser output power becomes unstable, resulting from the unstable power of LDs when operated at high driven current. Regardless of the input current varying from 1.5A to 4A, the lasing spectra were nearly identical fixed at 1564.5nm.

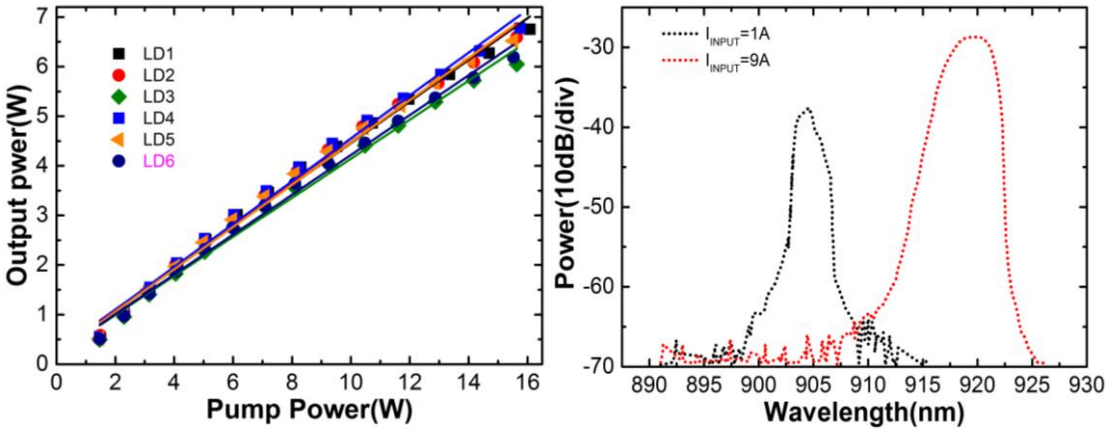

Figure 3. 2(a) the laser output vs. electrical pump power of six 915nm laser diodes in Fig. 3.1 (b) The laser spectra of a 915 nm laser diode at two pump levels with input current set at 1A and 9A respectively. The spectra were measured using OSA with a resolution of 1nm.

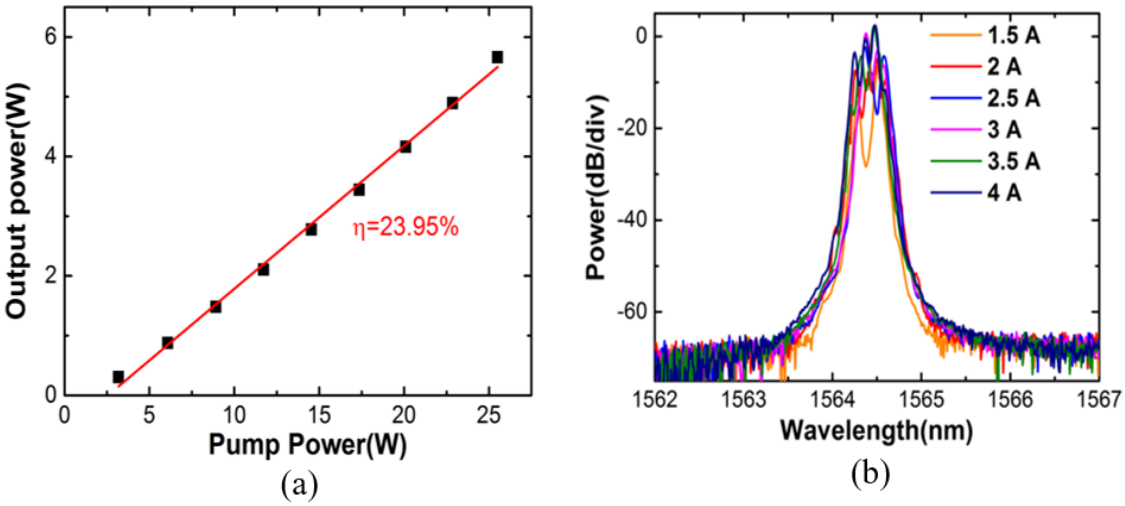

Figure 3. 3 . (a) The output power of Er/Yb co-doped fiber laser with respect to the launched pump power from six laser diodes. (b) The laser spectra of Er/Yb co-doped fiber laser pumped with different input currents. The spectra were measured using OSA with a resolution of 0.1nm.

3.2 Preparation of Tm/Ge co-doped preform

The preform was prepared with a typical MCVD process, during the core layer deposition, MCVD reagents such as $SiCl_4$ and $GeCl_4$ were introduced inside a high purity silica tube. Tm

was introduced through a solution doping process. The prepared preformed was doped with high Ge but with low Tm. And the measurement of Ge and Tm doping were carried out using the electron probe micro analysis (EPMA) along the direction shown in Fig. 3. 4b, which is the scanning electron microscopy image. As shown in Fig. 3. 4b, the measured average Ge doping concentration is 20wt% with Tm doping of <0.1wt%. In addition, the central dip in the index profile is due to the evaporation of germanium from the central region of preform in the process of collapsing and sealing passes. In order to reduce the central dip profile, temperature optimization of germanium deposition and pre-deposition collapse techniques were necessary. The fabricated preforms with core diameter of 0.7 6mm and outer cladding diameter of 18 mm were drawn to fibers with core size of 4.4 µm and cladding of 104 µm in the conventional drawing tower.

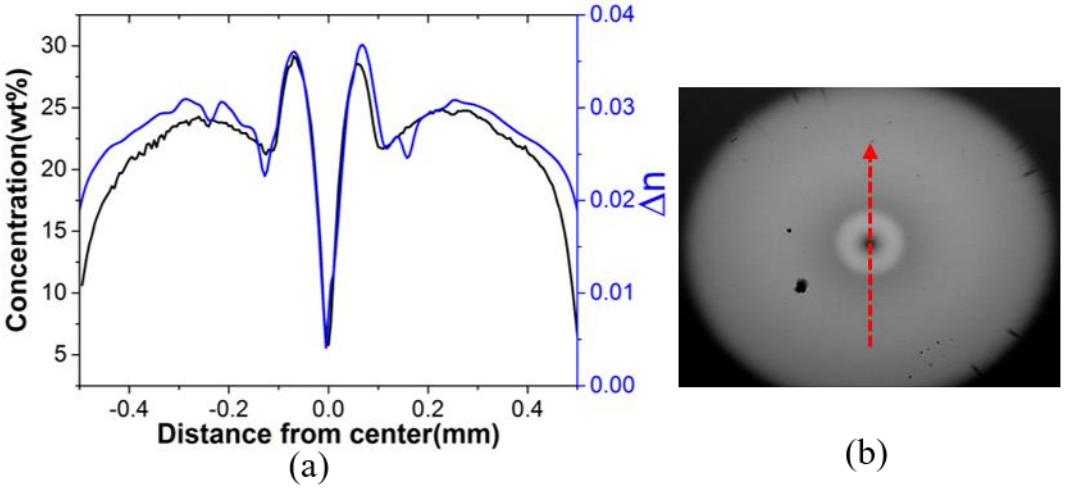

Figure 3. 4 The measured Ge doping concentration (wt %) in prepared preform at step size of 5µm and 1µm respectively along the arrow shown in (b).

3.3 Absorption of Tm/ Ge co-doped fiber

The in-house fabricated Tm/Ge co-doped fiber was characterized for the background loss, absorption and splicing loss. In detail, the Tm/Ge co-doped fiber has an NA of 0.28 with core size of 4.4µm, with the cut-off wavelength of 1.4 µm. Without the dopant of Al_2O_3, the thulium doping concentration is limited to a low level otherwise clustering will dominate. As shown in Fig. 3. 5, the experimental setup was built with a supercontinuum (SC) source (Fianium WhiteLase 400-2400nm). An objective lens was employed to couple the collimated SC source into the Tm/Ge co-doped fiber under test. To protect the objective lens from damage by high power, a beam splitter and an attenuator were employed to obtain power value less than <20 mW. Based on the cutback technique, the fiber background loss was measured with a loss of

~0.6 dB / m at 980 nm cutting from 50m to 1m. Similarly, with the cutback method, the absorption of the Tm/Ge co-doped fiber was measured. Fig. 3. 6a illustrates the measured absorption curve. Similar as other Al co-doped Tm-doped fibers, the fabricated Tm/Ge co-doped fiber has three absorption peaks, corresponding to the transitions from level $^3H_6$ to $^3F_4$ with 38dB/m at 793nm, level $^3H_6$ to $^3H_5$ with 24dB/m at 1210nm and level $^3H_6$ to $^3H_4$ with 18dB/m at 1585nm respectively. Interestingly, compared with Tm/Al co-doped fiber (OFS TmDF200, NA=0.26, MFD=5μm at 1700nm) in the transition from level $^3H_6$ to $^3H_4$, the absorption curve of Tm/Ge co-doped fiber is 65 nm blue-shifted. According to the work of Agger et al[20], it is envisaged that the emission profile of Tm/Ge co-doped fiber will also be blue-shifted enabling shorter wavelength operation as compared to Tm-doped aluminosilicate fiber. Clearly, the Tm/Ge co-doped fiber has a lower thulium concentration than TmDF200 fiber, which helps further in assisting lasing and amplification at short wavelengths (<1700nm).

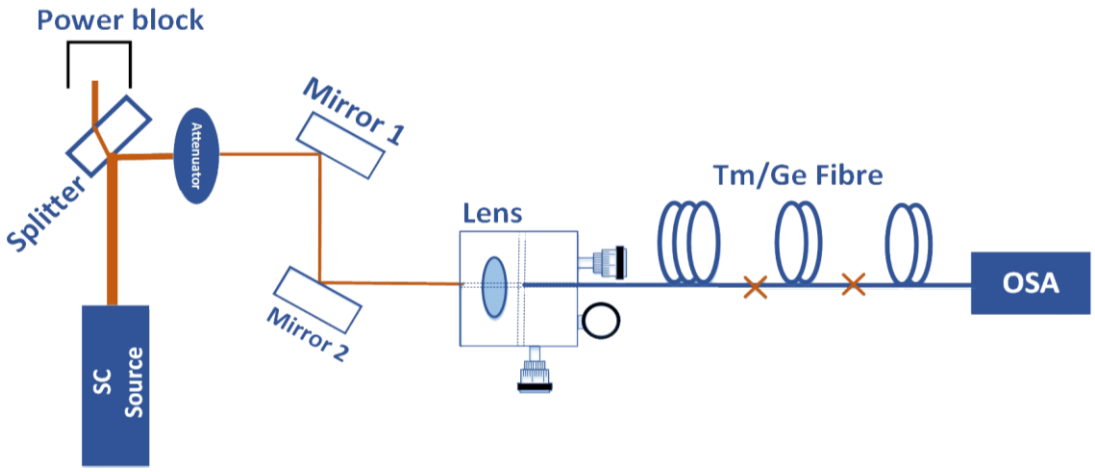

Figure 3. 5 The experimental setup for absorption measurement. SC source: supercontinuum source.

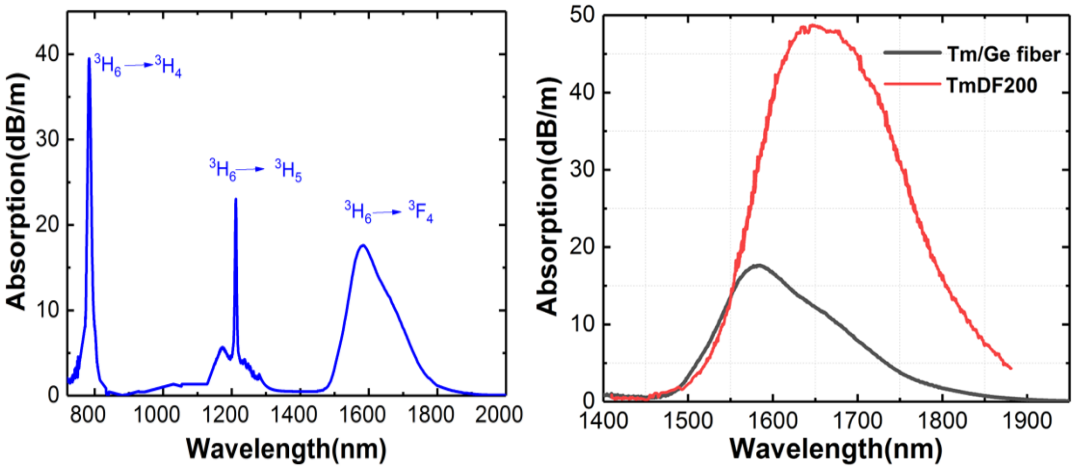

Figure 3. 6 (a) the measured absorption curve in the wavelength region from 800nm to 2000nm. (b) Absorption versus wavelength of TmDF200 and Tm/Ge co-doped fiber from $^3H_6 \rightarrow {}^3F_4$ transition.

3.4 Fluorescence characterization

In order to obtain the emission cross-section, I firstly measured the fluorescence spectra from level $^3F_4$ to $^3H_6$. From literatures[50][92], there are two methods to obtain the emission fluorescence from two energy levels for rare-earth doped fibers, which depending on the test sample; either preform or fabricated fiber. For a preform slice, as illustrated in Fig. 3. 7, a single mode laser beam from a 790nm LD (Lumics) with maximum power of 250 mW after collimating lens could be incident on the core of preform to excite the Tm ions. Backward emission could be captured using a large core multimode fiber. However, for the prepared Tm/Ge preform (0.76mm/18mm) with low thulium doping, the fluorescence emission was difficult to capture and carry sufficient power to be detected in the OSA region of 1200-2400nm. Therefore, this was abandoned. Considering the low thulium doping concentration in the Tm/Ge co-doped fiber, the fluorescence could be measured using a short length of Tm/Ge fiber to avoid ASE building. As shown in Fig. 3. 8a, we employed a 2×2 multimode (MM) fiber beam splitter (50:50 Thorlabs 105/125μm) to connect the 790nm LD and the fiber under test (FUT). The port 4 of the coupler serves as a monitoring port to check 790nm LD pump power. At port 3, the coupled backward emission (low power) from the FUT is collected at the OSA. The unconnected end of the FUT was angle-cleaved to avoid undesired feedback, and a few short lengths down to a few cm were tested to ensure collecting fluorescence undistorted by ASE. Thus the measured backward ASE could be regarded as fluorescence without emission reabsorption and optical gain. Here, I have investigated Tm/Al fiber and Tm/Ge co-doped fiber, for the fluorescence measurement. The backward ASE was measured using OSA (Yokogawa AQ6375). Compared with Tm/Al fiber, the fluorescence emission of Tm/Ge fiber is ~35nm blue-shifted with the maximum intensity peaking at 1690nm.

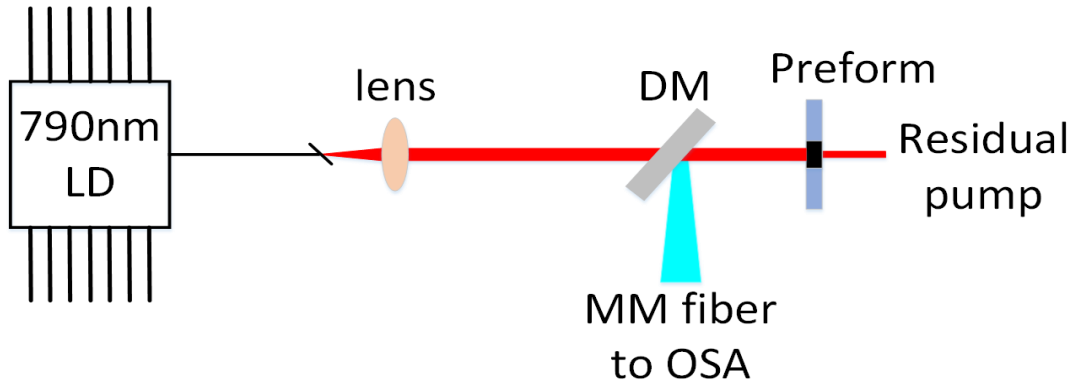

Figure 3. 7 Schematic setup for fluorescence measurement using Tm/Ge preform. DM: dichroic mirror. MM fiber: multimode fiber. OSA: optical spectral analyzer.

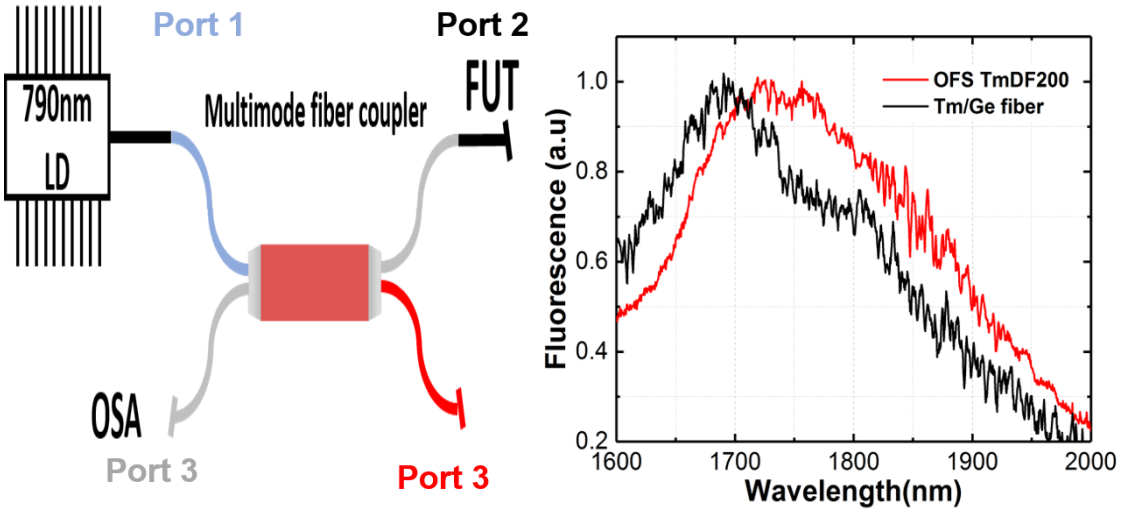

Figure 3. 8 (a) The schematic setup for fluorescence measurement and (b) the measured fluorescence of Tm/Ge co-doped Tm/Al co-doped fiber (OFS TmDF200).

3.5 Cross-section and gain coefficient

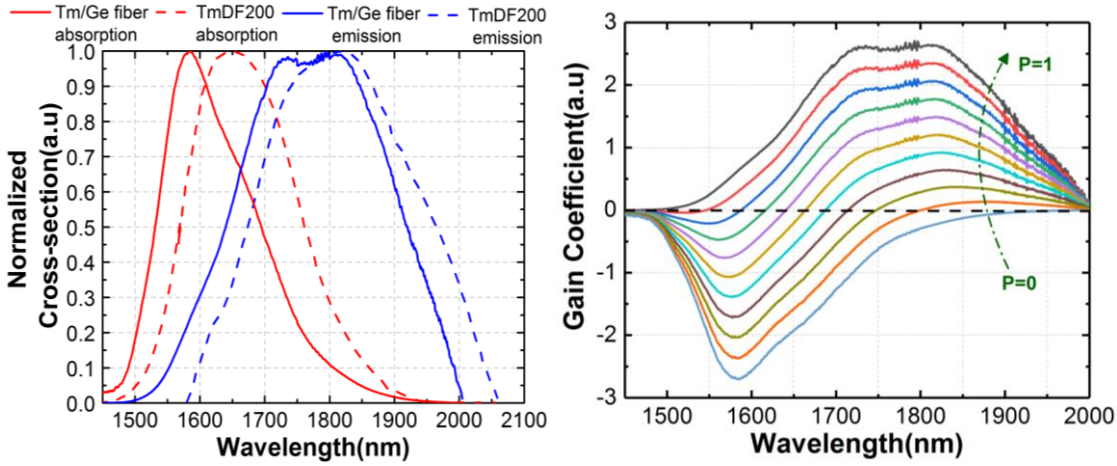

Figure 3. 9 (a) Normalized absorption and emission cross-sections for Tm-doped fiber (OFS TmDF200) and in-house fabricated Tm/Ge co-doped fiber, respectively, and (b) the calculated normalized gain coefficient of Tm/Ge co-doped fiber. *p* represents a fraction of excited population

As compared to commercial Tm-doped aluminosilicate fiber (OFS TmDF200), the absorption spectrum of the Tm/Ge co-doped fiber is significantly blue shifted (65nm shorter) as shown by the red solid line in Fig. 3. 9(a) with a peak absorption of ~20 dB/m at 1580nm. According to the McCumber analysis[93][94], the derived emission cross-section of Tm/Ge co-doped fiber is also blue-shifted by about 50 nm compared to TmDF200 fiber. Therefore, it is anticipated that the proposed Tm/Ge co-doped fiber can be used for efficient signal amplification at wavelengths much shorter than1650 nm. Given the Tm/Ge proposed fiber NA, core and cladding size, the mode profile guided in the fiber could be calculated using a mode

solver (COMSOL). Based on the assumed step-index doped Thulium doping profile, the absorption cross-section could be calculated by[20]:

$$\sigma_a(\lambda) = \frac{GSA(\lambda)}{2\pi \int \rho(r)\phi^2{}_S(\lambda) r dr} \tag{1}$$

where $GSA(\lambda)$ is the ground-state-absorption, $\rho(r)$ is the doping concentration profile, and $\phi_s(\lambda)$ is the normalized mode profile of fiber. Moreover, based on the measured fluorescence and reasonable estimation of radiative lifetime by Judd-Ofelt analysis, the emission cross-section could be calculated by the Fuchtauer-Ladenburg equation[54]:

$$\sigma_e(\lambda) = \frac{\lambda^5 I(\lambda)}{8\pi\tau_r n^2 c \int \lambda I(\lambda) d\lambda} \tag{2}$$

where $I(\lambda)$ is the fluorescence intensity, τ_r is radiative lifetime from ${}^3F_4 \rightarrow {}^3H_6$, and c is light speed.

Moreover, it is useful to examine the wavelength dependence of net gain as a function of population of the upper laser level (population inversion). The net gain coefficient, G(λ), can be expressed by the following equation[49]

$$\mathrm{G}(\lambda) = \mathrm{N}[\mathrm{p}\sigma_\mathrm{e}(\lambda) - (1-\mathrm{p})\sigma_\mathrm{e}(\lambda)] \tag{3}$$

where *p* represents the population fraction in the upper laser level, and N stands for the total number of Tm^{3+} ions. As shown in Fig. 3. 9b, the gain spectrum strongly depends on the population inversion and the gain peak shifts to shorter wavelengths as the inversion level is increased. Therefore, to achieve efficient signal amplification below 1700 nm, more than 30 % population inversion is required, necessitating optimization of the fiber length for a given pump wavelength.

3.6 Lasing efficiency test

In this section, I investigate the laser efficiency of Tm/Ge co-doped fiber in a free-running laser setup. Fig. 3. 10 illustrates the experimental setup with a 793nm multimode laser diode with maximum power of 7 W as a pump source. Lenses (Thorlabs AR C-coated) are employed to couple light from fiber to free space and vice versa. Both ends of Tm/Ge co-doped fiber are perpendicularly cleaved for a broadband 4% reflection, thus performing as the laser cavity. The length of the Tm/Ge co-doped fiber was optimized by testing various lengths of 12 m down to 10m, 8m, 2m and 1m. A pair of dichroic mirrors (800nm HT/2000nm HR) are used to split

pump and laser signal. Residual pump is directed to power dump. And the output measured using an OSA and two thermal power meters (Ophir 3A-FS).

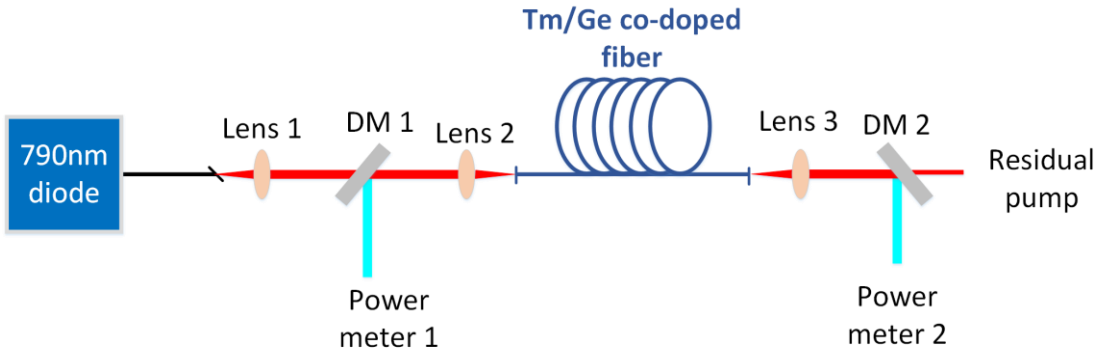

Figure 3. 10 A schematic of experimental setup for the laser efficiency test. DM: dichroic mirror; lens 1, 2, 3: AR C-coated with focal length of 11mm.

Fig. 3. 11a showcases the laser spectra at different lengths of Tm/Ge co-doped fiber. For the energy transition from level $^3H_6$ to $^3H_4$ when pumped by 793nm laser diode, Tm ions decay fast to level $^3F_4$ and behave with a characteristic of quasi three level between level $^3H_6$ and $^3F_4$. Therefore, when the fiber length shortened, the ASE peak will continuously blue-shift. When fiber length is cut from 12m down to 8m, the corresponding laser wavelengths is blue-shifted from 1910nm to 1890nm. At the fiber length of 2 m, the lasing wavelength is centered at 1825nm. Compared with the lasing at 8m, 10m or 12 m, the laser BW at 2 m is broadened with higher lasing threshold. With fiber length shortened further to 1 m, it is difficult to get lasing even with maximum pump power of 5 W because the gain in the fiber with length of 1 m is not sufficient to overcome the cavity loss. Fig. 3. 10b shows the laser output power at fiber lengths of 8m,10m and 12m respectively, and the corresponding lasing efficiencies are 37.2%, 33.6% and 35.1%. From the experimental record, the maximum lasing efficiency is gradually decreased from 37% when fiber length decreased with a step size of 2m. For the in-house fabricated Tm/Ge co-doped fiber with doping concentration <0.1wt%, the maximum lasing efficiency without cross-relaxation should be less than 40% [35], which is in accord with the measured maximum lasing efficiency of 37.2%.

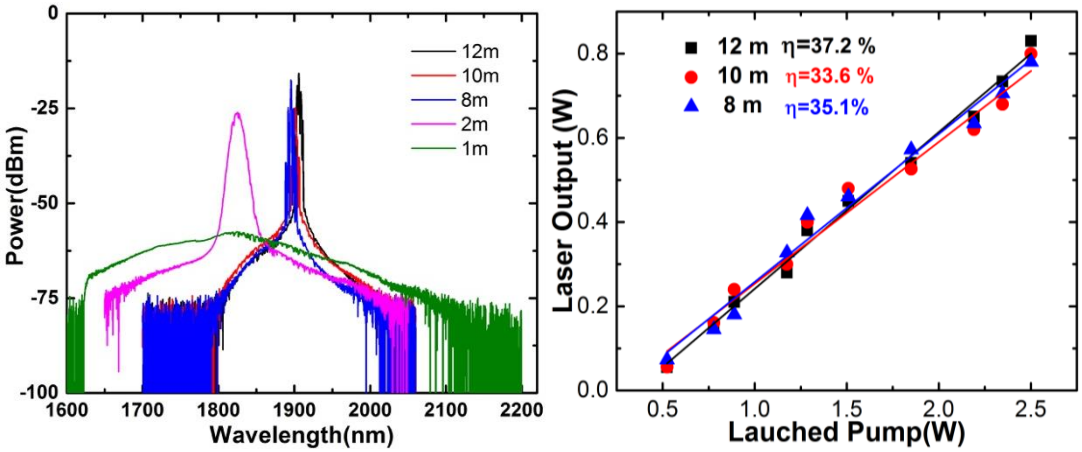

Figure 3. 11 (a) the free running lasing spectra at different fiber length (b) laser efficiency at different fiber lengths of 8m, 10m, and 12m.

3.7 Splicing optimization

Since I would like to build all-fiber devices using the Tm/Ge co-doped fiber, therefore, in this section, I investigated the splicing loss between SMF and Tm/Ge co-doped fiber using the 1310nm superluminescent diode (SLD). I chose 1310 nm SLD as an investigation light source since the absorption of Tm/Ge fiber is negligible, thus the splice loss could be measured accurately. Regarding to the Tm/Ge co-doped fiber with NA of 0.28 and core diameter of 4.4 μm, the mode field diameter (MFD) is 4.2 μm at 1310 nm. However, the MFD of SMF28 is 9.6 μm at 1310 nm. Therefore, the direct splicing loss resulting from MFD mismatch could be calculated by the equation:

$$\text{Loss} = 20\log\frac{\text{MFD}_1^{\,2} + \text{MFD}_2^{\,2}}{2\times\text{MFD}_1\times\text{MFD}_2} \tag{4}$$

The calculated splicing loss is $2.68\,\text{dB}$, which is comparable to the measured splice loss of 3.1 dB. The typical method of reducing the splicing loss between MFD fibers is to optimize the splicing recipe, thus achieving an optical intermediate area where MFD matches. For the abovementioned Tm/Al co-doped fiber(OFS TmDF200) with NA of 0.26 and a core size of 4 um, the significant splicing loss with SMF could be reduced to $<0.3\,\text{dB}$ when implementing offset splicing and repeatedly applying multiple arcs with 60 μm offset on the side of Tm/Al co-doped fiber. However, high Ge concentration in the Tm/Ge co-doped fiber lowered softening temperature and induced higher diffusion coefficient of Ge, provoking difficulty in MFD matching between the two fibers despite the abovementioned offset-arc splicing method. And the resultant loss is always around $3\,\text{dB}$. However, it is obvious to find that the MFD between Tm/Ge co-doped fiber and Tm/Al is closely matched. Therefore, I introduced the

Tm/Al co-doped fiber with a length of 5mm as an intermediate fiber between SMF and Tm/Ge co-doped fiber. The resultant splicing is significantly reduced. As shown in Fig. 3. 12, the 1310 nm SLD was employed to measure the splice losses for the scheme of SMF-Tm/Al-Tm/Ge-Tm/Al-SMF. The measured total splicing loss is 1.5 dB, i.e. the splicing loss between SMF and Tm/Ge co-doped fiber is 0.75 dB by average.

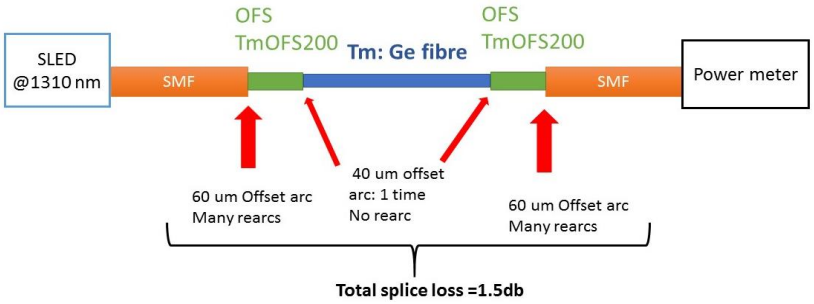

Figure 3. 12 Optimized splicing scheme for Tm/Ge co-doped fiber.

3.8 Chapter Summary

In this chapter, I have built an Er/Yb co-doped fiber laser with a maximum pump power of 5W as the pump source for all the experiments pumped by the 1565nm in this thesis, and I tested this 1565nm pump source regarding to lasing efficiency and spectrum at different pump powers. Using the preform with new glass composition (GeO_2-SiO_2) prepared by MCVD method, the Tm/Ge co-doped fiber is fabricated with cut-off wavelength at 1.4μm. Based on the in-house fabricated Tm/Ge co-doped fiber, fiber characterization including absorption, fluorescence, cross-sections and lasing efficiency are conducted. Moreover, splicing optimization is implemented between SMF and Tm/Ge co-doped fiber using the commercial Tm/Al co-doped fiber as an intermediate fiber.

Chapter 4. Applications of Tm/Ge co-doped Fiber in Lasers and Amplifier

Thulium-doped silica glass can be used to generate emission spanning from 1600- 2200 nm and thulium doped fiber has subsequently emerged as an attractive gain medium for power scalable laser sources operating in this "eye-safe" wavelength band[37]. Based on Tm^{3+}-doped silica fibers, many applications such as fiber lasers, amplifiers and mode-locked fiber laser have been widely studied.

Broadly tunable fiber lasers, particularly in the 2 μm wavelength region, have already made significant impact in many diverse fields of science and technology. Tm-doped, Ho-doped and Tm/Ho co-doped fiber have all been used to make high performance tunable laser devices. For example, using an external diffraction grating, Clarkson et al demonstrated a TDFL tunable from ~1860 - 2090 nm[60]. Moreover, Guo et al reported a tunable TDFL with wavelength a tuning range from 1895 - 2109 nm[95]. However, developing a TDFL operating below 1750 nm in the Tm emission band is challenging due to the increasingly three-level nature of the transition at short wavelengths. With a highly wavelength selective fiber Bragg grating (FBG), Daniel et al demonstrated a TDFL tunable over the 1660 - 1750 nm wavelength band[22]. In order to access the sub 1750 nm wavelength band, ASE filtering was incorporated in an all fiber thulium amplifier to introduce substantial loss at wavelengths >1750 nm to avoid parasitic lasing. Similarly, thulium fiber co-doped with terbium in the core or cladding provided preferential loss at wavelengths >1750 nm, thus allowing operation at shorter wavelength[19]. Whilst these methods enable an access to the sub-1750 nm waveband, the associated conversion efficiencies are typically extremely low (<0.2 %) and the tunability is limited, typically to less than 100 nm. Using different lengths of a Tm-doped GeO_2-SiO_2 fiber in a low loss cavity configuration, Barnes et al demonstrated a TDFL tunable from 1650 nm to 1870 nm[42]. In this implementation a highly reflective output coupler (R>90%) was used to lower the lasing threshold to a few mW. Therefore, to date, based on the available Tm^{3+}-doped fiber, the shortest wavelength of TDFL is 1650nm with low output power, and the tunability of TDFL is less than 250nm.

With the growing demand for capacity in optical fiber transmission, considerable research has been devoted to the 1.6-2μm wavelength region as an emerging transmission window for next generation optical communications based on hollow-core photonic-bandgap fibers (HC-PBGFs) [96]. As the low loss window of silica fiber extends up to 1.7μm, and with the continual improvement of background loss in HC-PBGFs, the possibility of future optical

communications networks operating seamlessly from 1.55 to 2 μm is emerging, requiring efficient optical fiber amplifiers covering the entire 1.55-2 μm wavelength band. Various configuration of thulium-doped fiber amplifiers (TDFAs) have been demonstrated offering high gain and low noise performance across the wavelength 1700 – 2050 nm range. With effective management of amplified spontaneous emission (ASE), the short-wavelength amplification edge of the TDFA has further extended down to 1650 nm with a small signal gain of 8dB demonstrated[77]. This is a great improvement but a ~30 nm spectral gap still exists between operating windows of the L-band EDFAs and TDFAs.

Moreover, the third near-infrared (NIR) optical window (1600 to 1870 nm) has recently attracted interest from a bio-imaging community owing to the rapid developments of relevant fiber laser technologies. Compared to shorter wavelengths, the third optical window has the merits of reduced optical attenuation and diminished photo-toxicity[9], and is therefore advantageous for imaging of deep and turbid scattering tissues. Up to now, a series of imaging modalities such as three-photon microscopy, optical coherence tomography[97], and optical coherence microscopy[98] have all been demonstrated at the 1700 nm optical waveband. However, N.G Horton et al[9] has shown that one promising strategy for deep-tissue multiphoton imaging is to implement three-photon excitation with wavelengths in the 1600–1700 nm range. This provides three advantages: (1) three-photon excitation ensures a better confinement of the excitation than two-photon excitation when focusing deep inside scattering media, (2) this wavelength window provides optimal penetration in biological tissues owing to the somehow reduced absorption of water in this specific range [9], and (3) it matches the three-photon excitation spectra of red fluorochromes commonly used in biology[9][99].

To date, few short wavelength TDF operations are implemented either via high fractional ion excitation of the gain fiber or introducing loss to long wavelengths[100] [24][25]. Despite a few demonstrations of cw fiber laser in 1600-1800 nm range, there are only a couple of ultra-short pulsed fiber laser reported in this wavelength band all operating beyond 1700 nm. Li et al. demonstrate a soliton mode-locked thulium-doped fiber laser based on nonlinear polarization rotation (NPR) with wavelength of 1787 nm[101]. Noronen et al demonstrate a tunable thulium-holmium mode-locked fiber laser for the 1700-1800 nm wavelength through combination of an intra-cavity acousto-optic tunable filter and NPR technique [102]. Emami et al. present a tunable thulium-doped mode-locked laser from 1702 to 1764 nm and 1788 to 1831 nm by utilizing a PCF to suppress long wavelength ASE and NPR as the mode-locker[11]. However, the lasing wavelength in mode-locked regime is still above 1700nm.

In this Chapter, based on the Tm/Ge co-doped silica fiber, an ultra-wide broadband cw TDFL laser spanning from 1679nm to 1992nm is presented in section 4. 2. With dispersion compensating fiber (DCF) introduced as an ASE filter, a much broader tunable TDFL from 1650nm to 2000nm is demonstrated in section 4. 3. Furthermore, with diffraction grating replaced by compressively tunable FBGs, an ultra-short wavelength tunable TDFL from 1620 nm to 1660 nm could be built and studied in section 4. 4. Considering the blue-shifted cross section of Tm/Ge co-doped fiber, a short wavelength TDFA from 1628nm to 1655nm is briefed in section 4. 5. In addition to the applications of the in-house fabricated Tm/Ge co-doped fiber as tunable lasers and amplifier, I also studied the soliton and noise-like pulse mode-locked fiber laser in the 1650 nm waveband incorporating a chirped FBG as band pass filter, showing as a promising candidate as an ultra-fast laser source in 1700 nm waveband for the bio-imaging community.

4.1 Reflective diffraction grating

Reflective diffraction gratings could be used as wavelength selector in fiber laser. With a periodic structure on the surface of reflective diffraction grating, the incident light after diffraction is diffracted in a dedicated angle, depending on the incident light wavelength and spatial frequency of its periodic surface. The incident light and diffracted light follow the characteristic diffraction equation:

$$d(\sin\theta_{in} + \sin\theta_{d}) = m\lambda \tag{5}$$

where d is the period of surface grating, θ_{in} and θ_{d} are the incident angle and diffracted angle with respect to the grating normal, m is the diffraction order, and λ is the incident light wavelength. Usually, reflective diffraction gratings have a wide wavelength coverage, thus they could be used in tunable fiber lasers in a Littrow configuration as shown in Fig. 4. 1.

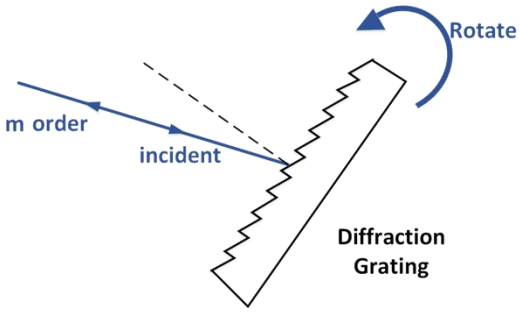

Figure 4. 1 Reflective diffraction grating in a Littrow configuration

Reflective diffraction gratings could work as retroreflector in fiber laser with external cavity because diffracted angle equal to incident angel, described by the equation:

$$2d\sin\theta_{in} = m\lambda \tag{6}$$

Typically, commercial diffraction gratings have the designed wavelength and the most intense order (m). In this context, the variation of incident angle could be implemented simply by rotate the diffraction grating, thus achieving wavelength tuning.

4.2 Ultra-wideband Operation of a Tunable Thulium Fiber Laser offering Tunability from1679-1992 nm

In this section, I present a tunable TDFL incorporating an in-house fabricated Tm/Ge co-doped silica fiber to access the sub 1700nm wavelength regime. Meanwhile, a short length of commercially available Tm-doped aluminosilicate fiber (OFS TmDF200) was added to the cavity to realize more than 300nm tuning range spanning from 1679 nm to 1992 nm.

4.2.1 Experimental setup

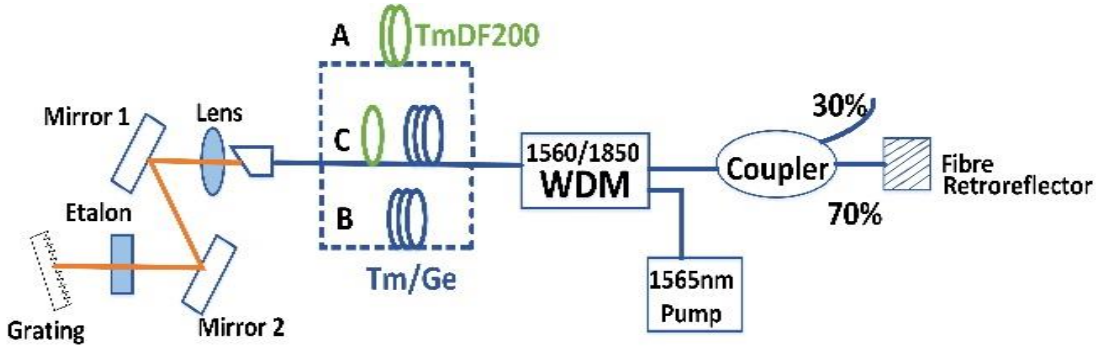

Figure 4. 2 Schematic diagram of the tunable TDFL. WDM, wavelength division multiplexer. Lens: AR C-coating (1050-1620), f=11.0 mm.

Fig. 4.2 depicts the experimental setup of the tunable TDFL with an external cavity comprising a bulk grating operated in a Littrow configuration whereby the first order-diffracted beam is retro-reflected back to the gain fiber under test. A silver-coated fiber retroreflector formed the other end mirror of the laser cavity. The tunable TDFL was core-pumped by an in-house built 1565 nm fiber laser through a 1565/1850nm wavelength division multiplexer (WDM). The 30% port of a 70/30 tap coupler was used to extract the output power from the TDFL and the output measured using the OSA and a thermal power head (Ophir 3A-FS). Wavelength tuning was achieved by tuning the angle of the grating (for coarse tuning) and the etalon (for fine tuning).

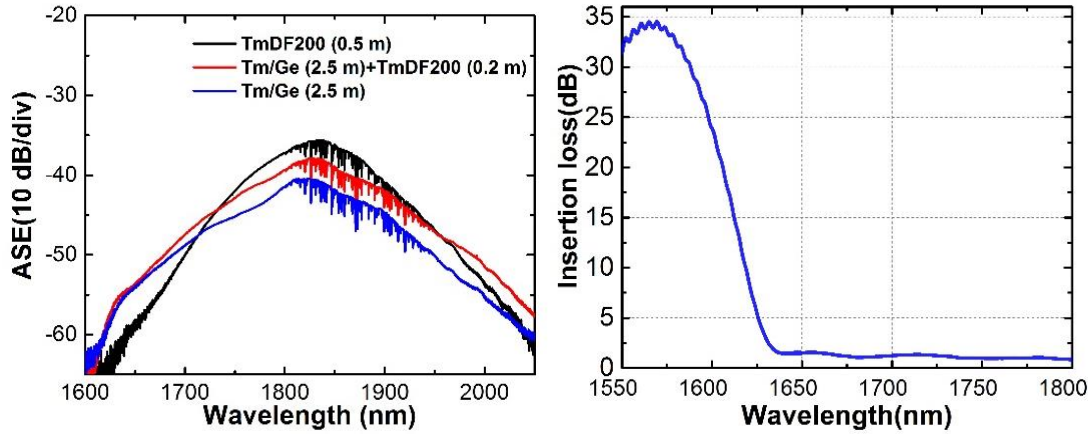

Figure 4. 3 (a) ASE spectra of the TmDF200 fiber (TDFL-A), Tm/Ge co-doped fiber and the combination of 0.2 m TmDF200 (TDFL-C) and 2.5 m Tm/Ge co-doped fiber (TDFL-B)(Measured with 0.5 nm OSA resolution). (b) Measured insertion loss of the 1560/1850nm filter based WDM.

4.2.2 Results and discussion

As shown in Fig. 4. 2, we investigated three different cavity configurations designated as TDFL-A/B/C, respectively. TDFL-A incorporated only a 0.5m length of TmDF200 fiber, while TDFL-B comprised only Tm/Ge co-doped fiber of ~2.5 m length. The lengths of TmDF200 and Tm/Ge co-doped fiber were selected via a series of cut-back measurements so as to yield the maximum tuning range without parasitic lasing when operating at extreme wavelengths. TDFL-C incorporated ~0.2 m of TmDF200 and ~2.5 m of Tm/Ge co-doped fiber spliced together so as to extend the operating bandwidth both at the shorter and longer wavelength edges. The (sub-threshold) ASE spectra at the output of the three fiber cavities, i.e. TDFL-A/B/C were measured with 0.5 W pump power at 1565 nm. The ASE spectra plotted in Fig. 4. 3a clearly indicate that the Tm/Ge fiber generates relatively higher ASE intensity at wavelengths shorter than 1740 nm as compared to TmDF200 fiber. However, the TmDF200 fiber was able to provide higher gain at wavelengths beyond 1750 nm, with a ~6 dB higher ASE peak at 1820 nm. The combination of the 2.5 m length of Tm/Ge co-doped fiber a 0.2 m length of TmDF200 fiber could maintain the ASE intensity at shorter wavelength region (sub 1750 nm) while increasing the ASE intensity at longer wavelength, thus broadening the overall ASE bandwidth. The rapid drop in ASE of TDFL-B/C below 1625 nm results from the rapidly increasing loss of the WDM at short wavelengths, which rises to 5 dB at 1625 nm as illustrated in Fig. 4. 3b. Due to an excess loss of the free space external cavity shown in Fig. 4. 2, higher pump power is required to overcome the loss of the cavity, especially at the shorter wavelength edge where a high excitation fraction is required in the $^3F_4$ level.

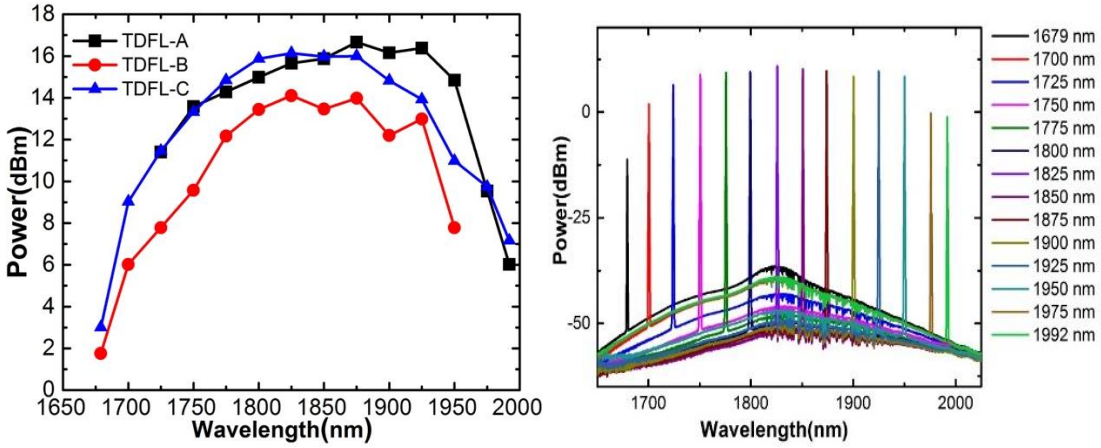

Figure 4. 4 (a) Output power versus laser wavelength. The three tuning curves correspond to TDFL-A/B/C respectively. (b) Output optical spectra of the TDFL-C laser operating at different wavelengths from 1679 nm to 1992 nm

At the maximum available pump power of 3 W, the highest output powers achieved from TDFL-A/B/C were 46.4, 25.8 and 41.1 mW respectively. When pumped at 3W, TDFL-A could be tuned from 1726 nm to 1980 nm yielding a total tuning range of 254 nm as shown in Fig. 4.4a. By contrast, the overall tuning range of TDFL-B was 282 nm, spanning from 1679 nm to 1961nm. The most important feature of this cavity is that the operating wavelength is blue-shifted by about 47 nm thanks to the introduction of the Tm/Ge co-doped fiber. Overall, the average output power over the entire tuning range for TDFL-B is almost 3 dB lower than that of TDFL-A and this is believed to be due to pump saturation in the Tm/Ge co-doped fiber resulting in inefficient pump absorption. At the shortest operating wavelength of 1679 nm, the output power was measured to be about 1.5 mW. In TDFL-C, where a 0.2 m length of TmDF200 fiber was spliced to the 2.5m long Tm/Ge co-doped fiber, the tuning range was further broadened, extending from 1679 nm to 1992 nm with a total tuning range of 313 nm which is the highest demonstrated to date from a single Tm-doped fiber laser cavity. The average output power at 1679 nm was increased to 2 mW. However, at wavelengths beyond 1700 nm the average output power is ~3 dB higher than TDFL-B, which exhibits similar behavior to that to TDFL-A. The corresponding output spectra are plotted in Fig. 4. 4b. A maximum optical signal to noise ratio (OSNR) of 60 dB was measured at the gain peak of 1820 nm whilst a minimum OSNR of 30 dB was measured at the shortest operating wavelength of 1679 nm. It is anticipated that further extension of the tuning range should be possible with a further increase in pump power since no parasitic lasing was observed even at the extreme operating wavelengths. Moreover, replacing the 70/30 coupler with a 90/10 coupler as well as using a wavelength selective FBG instead of a diffraction grating in a ring cavity configuration

will reduce losses and enable lasing at much shorter wavelength with increased optical conversion efficiency. TDFL-C gave the best performance amongst the three laser configurations in terms of tenability and output power. Exploiting Tm/Ge co-doped fiber, which provides enhanced gain in the sub 1750 nm wavelength region, a record 313nm tuning range is achieved for a thulium doped fiber laser which covers from 1679 nm to 1992 nm.

4.3 Ultra-wide tunability TDFL down to 1650nm from 2000nm

4.3.1 DCF as discrete ASE filter

As demonstrated in previous section, TDFL-C with Tm/Ge co-doped fiber possess the tunability from 1679 nm to 1992 nm. However, even with the Tm/Ge co-doped fiber, the peak emission is still located in the 1800 nm region (Please, see Fig. 4.3(a)). In order to push the lasing wavelength below 1679nm, one option is to implement ASE filtering at wavelength >1800nm without inducing extra loss at the wavelength <1700 nm. Due to the bend-induced loss in optical fiber as a function of wavelength and bend radius [103], the strategy of fiber bending is frequently used to achieve single mode operation by significantly introducing high losses for high order mode[104]. Similarly, in this section, a dispersion compensating fiber (DCF) under bended condition is introduced as a long wavelength ASE filter to suppressing emission at wavelength beyond 1800nm, thus facilitating lasing at wavelength<1679nm. A 20 m DCF (Thorlabs DCF38) with MFD of 6μm was selected as the ASE filter. To select filtering edge wavelength, a bending scheme is adopted. The bending loss of DCF is wavelength and bending diameter dependent. And the bend losses at different bend diameters were measured using the same setup with SC source for absorption test as presented in section 3.3. Fig.4. 5 shows the transmission curve of DCF fiber bended at the diameters of 25cm, 12.5cm, 10cm and 5.5cm. At the bend diameter of 25cm, the transmission curve is flat with bend loss <1.5dB. With tighter bending diameter to 12.5cm or 10cm, the transmission loss at wavelength <1750nm remains unchanged. However, the transmission loss at wavelength>1750nm increase, marking a 3 dB loss at 1800 nm when coiled at 10cm diameter. Moreover, when DCF is bended further to 5.5cm, the transmission loss is significant increased, bringing up the loss of 7.5 dB and 20 dB at 1800nm and 1900nm, respectively. The tighter bending also induces high loss at the target short wavelength (<1700nm).

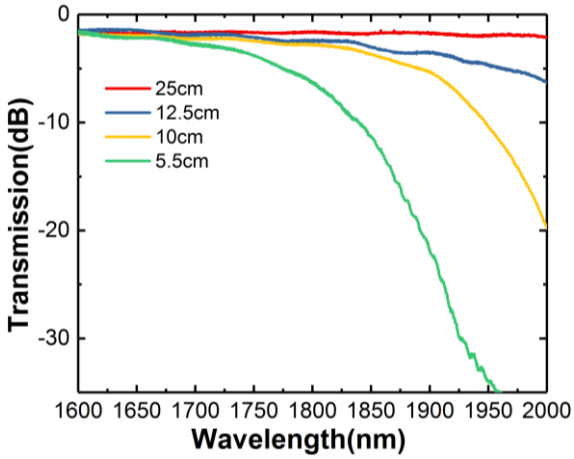

Figure 4. 5 Transmission curves of DCF at different bend diameters, i.e. 25cm, 12.5cm, 10cm and 5.5cm.

4.3.2 Experimental setup

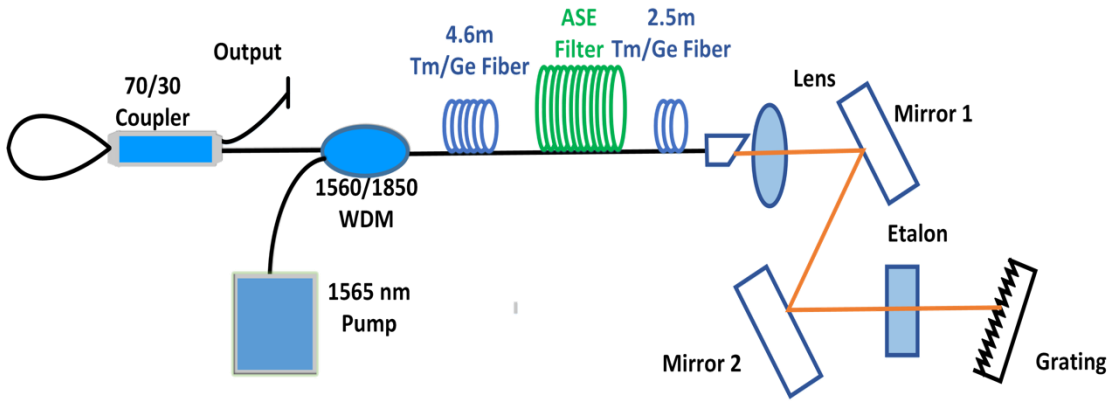

Figure 4. 6 Schematic diagram of the tunable TDFL. WDM, wavelength division multiplexer. Lens: AR C-coating (1050-1620), f=11.0 mm.

Compared with the tunable TDFL in the previous section, the tunable TDFL laser setup illustrated in Fig. 4. 6. The setup is composed of two segments of Tm/Ge co-doped fiber with optimal fiber lengths of 2.5m and 4.6m, and a long DCF of 10 m as a ASE filter to suppression emission at longer wavelength. Instead of using a fiber retroreflector as cavity feedback, a Sagnac loop mirror with low loss was employed to provide feedback of 30% as well as output coupling of 70%. All other components are same as those illustrated in Fig. 4. 2, and the output of spectra and power are measured with the same procedure as described in section 4.2.

4.3.3 Results and discussion

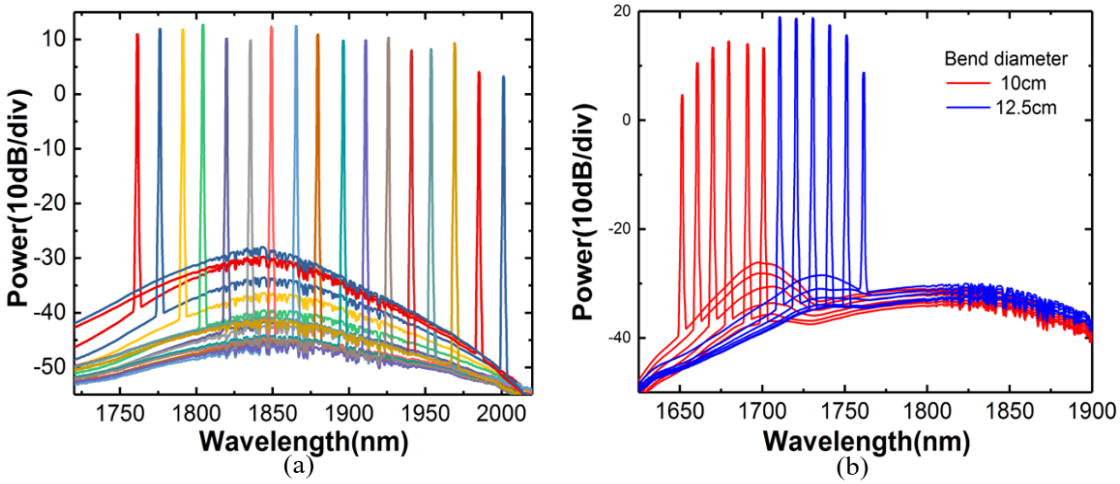

Figure 4. 7 Output optical spectra of the TDFL with a DCF ASE filter bended at different diameters ϕ : (a) ϕ =25cm when pumped by 1565nm fiber laser with power of 1.5W; (b) ϕ =12.5cm and ϕ =10cm with pump power of 4W.

Lasing wavelength tuning was achieve using bulk grating and etalon in the external cavity. At a bending diameter of 25cm with pump power of 1.5W, the TDFL showed tuning performance from 1760nm to 2000nm as shown in Fig. 4.7. Lasing at the emission edges ($\lambda <$ 1760nm or >2000nm) were difficult to achieve. Due to the strong ASE peak at 1850nm, the lasing threshold will be higher at shorter wavelength. Particularly, at high pump power, ASE peak will overrun the laser wavelength at short wavelength edge of the emission. For lasing at wavelength beyond 2000nm, it will be achievable using longer active fiber length if the small emission cross-section at the long wavelength is overcome. My target is to explore the shorter wavelength regime, and the ASE around 1850 nm is anticipated as the main challenge to overcome. The DCF fiber with strong bending would help suppress the ASE. Then, the remaining questions include low emission fluorescence below 1760 nm (10 dB lower than at 1850 nm as shown in Fig. 4. 7a), and possible extra loss induced by the ASE filter at the shorter wavelength under tight bending. It seems to suggest that higher pump power is necessary to address the questions. At the bending diameter of 12.5cm, the ASE peak is shifted from 1850nm to 1730nm. With tighter bending at a diameter of 10 cm, the ASE peak is shifted down to 1690 nm. At a pump power of 4 W, Fig. 4. 7b shows the seamlessly tunable TDFL spectra from 1750nm to 1650nm with DCF bending diameter adjusted from 12.5cm to 10cm. As shown in Fig. 4. 7, the OSNR of lasing spectra from 1760nm to 2000nm is above 50 dB . Even though the OSNR at wavelength from 1750nm to 1650nm is lower, it is still larger than 40 dB , sufficient for many applications.

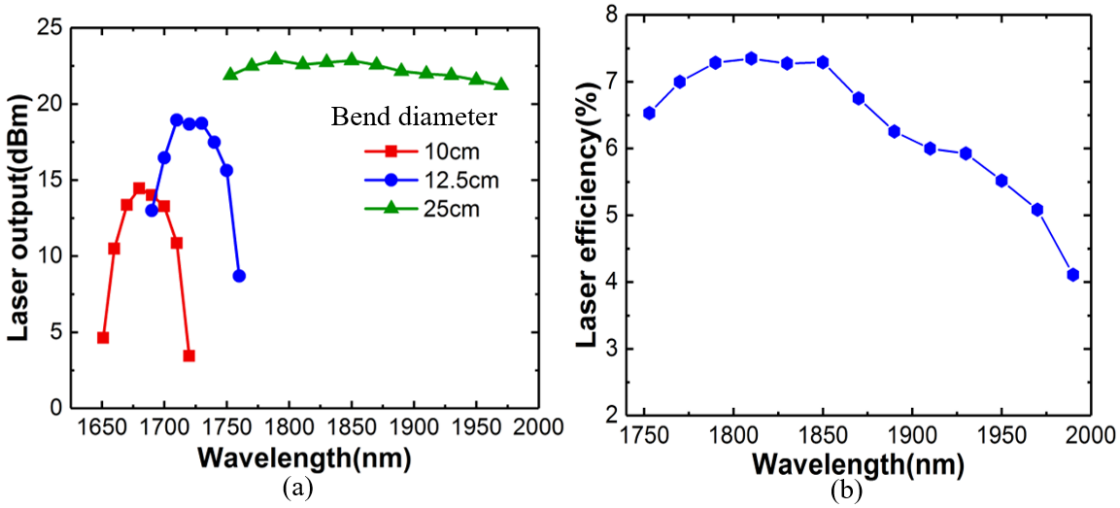

Figure 4. 8(a) Laser output power of the tunable TDFL with a DCF ASF filter bended at different diameters of 25cm, 12.5cm and 10cm with pump power of 4W. (b) Lasing efficiency of the tunable TDFL from 1750nm to 1975nm with DCF bending diameter of 25cm for the pump power of 4W.

Fig. 4. 8a shows the laser output with respect to different bending diameters for the pump power of 4 W at 1565 nm. At a bending diameter of 25 cm for DCF, the powers of more than 20dBm were achieved in the wavelength range from 1750nm to 1975nm, and the variation of power was less than 3dB . In addition, the slope efficiency of the tunable 1750nm-1975nm TDFL is shown in Fig. 4. 8b with respect to the lasing wavelength at the pump power of 4W. When the coiled DCF was bended at a diameter of 12.5cm, the built TDFL could be tuned continuously from 1690nm to 1760m, and the peak of laser output was located at 1710nm with power of 18.5dBm . The low power at 1690nm is attributed to the low gain coefficient at the emission edge. Similarly, with DCF bended further to 10cm, the tunability range of TDFL becomes in 1650nm - 1725nm with peak power of 14.8dBm at 1680 nm. Further reducing the bending diameter will increase the lasing threshold. Subsequently, lasing performance is compromised by the significant bending loss from coiled DCF. Considering the maximum pump power from the 1565nm fiber laser and the maximum handling power in WDM, it is difficult to push the lasing wavelength less than 1650nm. When the tunable TDFL operated with DCF at different bending diameters, the corresponding spectral range could overlap with each other, thus achieving a seamlessly tunable TDFL from 1650nm to 2000nm (corresponding to a frequency bandwidth of 31.8THz).

4.4 Ultra-short wavelength operation of a thulium doped fiber laser in a 1620-1660 nm wavelength band

Broadband operation of tunable thulium doped fiber lasers (TDFL) have been extensively investigated over the past few years and efficient laser emission can readily be achieved in the 1700nm to 2050nm wavelength range [2-3]. However, it is challenging to achieve shorter wavelength operation in a Tm-doped silica fiber, due to the fact that Tm exhibits a strong three-level behavior and as such requires a high population inversion (thus high pump intensity) and a low cavity loss to achieve reasonable lasing at this waveband. Recently, a tunable TDFL operable over the 1660 - 1750 nm has been demonstrated using a highly wavelength selective fiber Bragg grating (FBG) and a low loss all fiber laser cavity [4]. In addition, by suppressing the amplified spontaneous emission (ASE) at the longer wavelength region (1800-2000nm), Li et al have demonstrated a thulium-doped fiber amplifier (TDFA) working in the 1650-1700 nm range with a small signal gain of up to 29 dB [5]. Operation of Tm-doped fiber devices at or below 1650 nm remains a topic of great interest as it could potentially provide for seamless silica based rare-earth doped amplifier solutions extending from the S-band (exploiting erbium doping) right up to the IR absorption edge of silica fiber.

In section 4.3, I have reported a ultra-wide tunable Tm^{3+}-doped fiber laser in the wavelength spanning from 1650 nm to 2000 nm using a diffraction grating for wavelength tuning and DCF as ASE filter. Still, there is a 30 nm unfilled gap to the L-band edge of 162 0nm. In this follow-on work, I focus on ultra-short wavelength operation of the TDFL and present the first demonstration of a tunable TDFL (based on an in-house fabricated Tm/Ge co-doped silica fiber) operating over the 1620-1660nm wavelength band, i.e. extending operation down to the long wavelength edge of the L-band. This results represent by far the shortest laser wavelengths ever achieved for a TDFL.

4.4.1 Fiber Bragg grating (FBG)

In Section 4.3, the reflective diffraction grating is employed as retroreflector in laser cavity. Although the diffraction grating could provide broadband tunability, the reflection will degrade with lasing wavelength away from the designed wavelength, thus bringing in extra loss for laser cavity. To provide broader operating window, FBG is introduced to replace the diffraction grating as fiber retroreflector to construct all-fiber laser without any free space elements. FBG is a periodic refractive index modulation written directly in fiber core by exposing to periodic pattern of ultraviolet light.

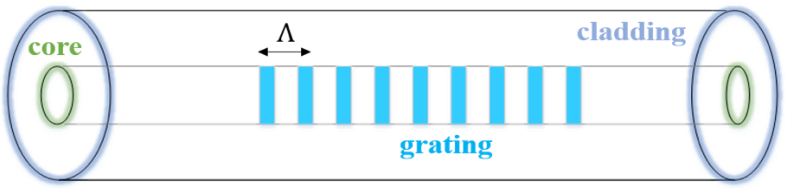

Figure 4. 9 The illustration of Fiber Bragg grating

The reflected Bragg wavelength for a FBG is described by:

$$\lambda_{FBG} = 2n_{eff}\Lambda \tag{7}$$

where Λ is the grating period and n_{eff} is the effective refractive index of propagating mode in fiber core. A high reflective FBG (>99%) with narrow bandwidth (<1nm) could be achieved when a propagating mode strongly overlaps with grating index modulation which is adjusted by controlling grating length and strength. In order to achieve a high quality FBG with suppressed side-lobes, apodization of refractive index is required over the grating length. Interestingly, Bragg wavelength of FBG could be tuned up to a certain range through optoelastic and thermo-optic effects which influence Λ and n_{eff}. For instance, the grating pitch is somewhat tunable by applying mechanical strain on the Bragg grating. On the other hand, temperature induced tunability of FBG wavelength is also possible albeit limited to a few nm range. Hence, the mechanical strain based tuning was investigated. The grating separation Λ could be increased when stretching FBG, which gives a red-shifted Bragg wavelength. However, increased tension would result in creating micro-cracks, which limits this approach and corresponding tunability of less than 10nm.

Instead, compressed strain would enable a broader tuning range. I introduce an in-house built tunable HR FBG. As depicted in Fig. 4. 10a (top), a FBG was mounted on an elastic beam sandwiched by flexible slabs. The FBG became under compression by moving the movable block inward, thus leading to blue-shifted FBG wavelength. According to [105], the wavelength shift could be calculated by:

$$\Delta\lambda = 0.78 \cdot \left(\frac{\theta \cdot d}{L_b}\right)\lambda_{FBG} \tag{8}$$

where θ is the angle formed between deformed elastic beam and idle position, d is the thickness of flexible slab, L_b is the elastic beam length and λ_{FBG} is the central wavelength of FBG.

As shown in Fig. 4. 10a (bottom), a tunable FBG was built using a FBG (Of-link) with a central wavelength of 1675nm in the lab. By compressing the FBG, the central wavelength could be tuned down to 1600nm from 1675nm, which covering the whole U-band of optical communication. Even though the wavelength could be blue shifted further with larger compression stress, the main concern is that at high pump power regime, high intensity due to strong compression stress will burn the fiber written with FBG. With a SC source (Fianium WhiteLase) and 1675nm circulator, the reflection of tunable FBG was characterized and the result is shown in Fig. 4. 10b. The reflection of the tunable FBG is more than 80% throughout the tunable range from 1675nm to 1638nm with narrow BW (<0.5nm). With the Bragg wavelength blue-shifted further down to 1615nm, the reflection of FBG decreased gradually, i.e. 65% at 1617.5nm. Moreover, with the compression of FBG on the mounted stage, the grating period along the gratings are nearly linear changed, thus the compressed FBG performed like a chirped FBG with broadened bandwidth at shorter wavelength, exactly as shown in Fig. 4.10 (b). Even though the decreased reflection at shorter wavelength, the compressively tunable FBG provides better reflectivity as compared to the external cavity bulk grating. Therefore, this high reflective FBG became a key element to improve the performance of CW lasing in the U-band.

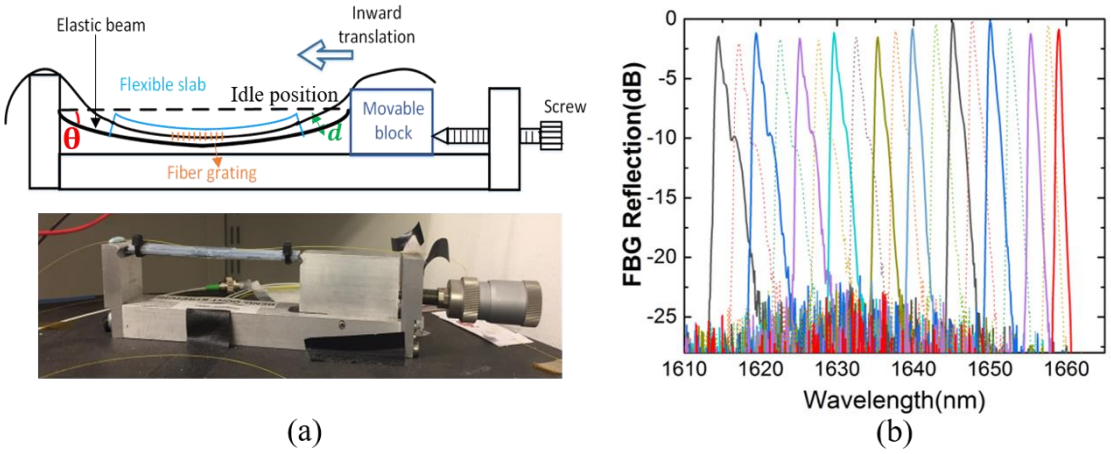

Figure 4. 10 (a) (Top) the scheme structure of tunable FBG, and (bottom) the corresponding in-house made tunable FBG; (b) the measured reflection of FBG with central wavelength tuned from 1660nm to 1600nm.

4.4.2. Experimental setup

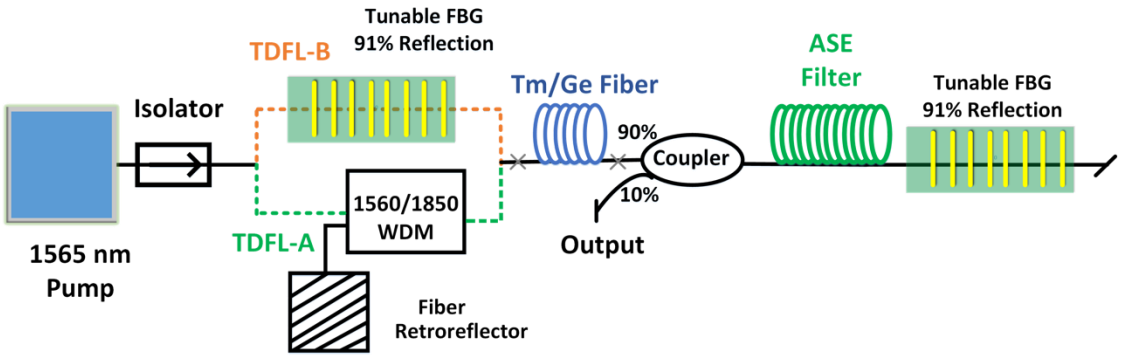

Figure 4. 11 Schematic of the TDF, showing the two laser configurations studied, hereafter referred to as TDFL-A (Green) and TDFL-B (Brown).

Fig. 4. 11 shows the experimental setup of the all-fiber tunable TDFL illustrating the two laser configurations studied. The setup comprises an in-house built Er/Yb fiber laser at 1565nm with maximum output power of 5 W as the pump source and a ~4.5 m length of in-house fabricated Tm/Ge co-doped fiber with high Ge concentration (19 mol%). The core diameter and NA of the fiber were measured to be 4.4µm and ~0.28, respectively. In TDFL-A, the pump light is coupled into the Tm/Ge co-doped fiber through a broadband, filter-based, 1560/1850 nm WDM. In order to build the cavity, the signal port of the WDM was spliced to a silver coated fiber retro-reflector, whereas a highly wavelength selective compressible fiber Bragg grating (FBG) with a central wavelength of ~1675nm was spliced to the other end of the gain medium. The FBG could be tuned from 1620 nm throughout to 1660nm by compression tuning. The measured reflectivity and bandwidth of the FBG varied from 80% to 94% and from 0.67 nm to 1 nm respectively, depending on the operating wavelength. The 10% port of the 90/10 tap coupler was used to extract the output from the TDFL. A coiled 20 m long DCF was used as an ASE filter. The bend diameter was optimized to provide low transmission loss at wavelengths below 1700 nm, whilst exhibiting high transmission loss at longer wavelengths. Fig. 4. 5 shows the bend dependent loss of the coiled DCF for an optimized bend diameter of 5 cm. The insertion loss of the WDM was also measured (see Fig. 4. 3b), and it was found that the loss increases significantly at wavelengths shorter than 1640nm. Therefore, for improved performance at wavelengths below 1660nm the TDFL-B configuration was used. Here the WDM and retro-reflector were replaced with a second compressible FBG, thereby avoiding the high insertion loss of the WDM. Given that the FBG is wavelength selective, it was possible to couple 1565nm pump power through the FBG without introducing additional cavity loss. Tuning of the laser cavity was realized by simultaneously compressing the two FBGs (mounted on mechanical stages) whilst ensuring wavelength synchronization between the two. Splicing

the Tm/Ge co-doped fiber and the SMF-28 fiber pigtails of the passive components together resulted in a high splice loss of ~3dB due to the large mode field diameter mismatch and this compromised the short wavelength operation of the cavity. To reduce this splice loss, a short section (~1cm) of OFS TmDF200 was used as an intermediate fiber between SMF-28 and Tm/Ge co-doped fiber and the optimized splice loss was reduced down to 0.8 dB. The 90/10 output coupler has an insertion loss of around 0.4dB in the 1550-1750nm waveband. The output characteristics of the tunable laser was measured by using a Yokogawa OSA (AQ6375) and a thermal power meter (Ophir 3A-FS).

4.4.3 Results and discussion

As shown in Fig. 3. 6, the in-house fabricated Tm/Ge co-doped fiber exhibits a blue-shifted absorption curve with a peak absorption of ~20dB/m at 1580nm, significantly shorther than the commerical Tm-doped aluminosilicate fiber. Moreover, according to McCumber theory, the emission profile of Tm/Ge co-doped fiber will also be blue-shifted, enabling shorter wavelength operation. In the TDFL-A configuration, the high insertion loss of the WDM coupler and ASE filter as well as the splice losses between SMF-28 and Tm/Ge co-doped fibers give an aggregate single pass cavity loss of 6 dB at 1650 nm, which increased further at shorter wavelengths. To achieve short wavelength operation, a short Tm/Ge co-doped fiber length is preferred in order to avoid signal reabsorption, with the minimum usable fiber length determined by the requirement to achieve sufficient total gain to overcome the large cavity loss. In our experiment, we found that the optimal fiber length was 4.5 m (for a pump power of 3.5W). The blue colored plot in Fig. 4. 12a shows the output power as a function of operating wavelength for the maximum available pump power. A highest output power of ~15 mW was obtained at a wavelength of 1660 nm. The shortest lasing wavelength was measured to be 1637nm with an output power of ~5mW. The red colored plot in Fig. 4. 12a shows the output power as a function of operating wavelength for the TDFL-B laser configuration. The same pump power and fiber length were used to ensure a fair comparison between the two laser configurations. We found that the lasing threshold for 1660 nm operation decreased from 1.6 W to 0.9 W, resulting in a much higher laser output power. Also, an almost constant output power was achieved over the entire tuning range from 1620 nm to 1660 nm which highlights the importance of avoiding passive components whose insertion loss varies with wavelength (i.e. the WDM coupler). The highest output power of about 22 dBm from the 10% port of the coupler was recorded at 1660 nm. At 1620 nm, a measured laser output power is 17 dBm, the shortest wavelength we could reach with the current tunable gratings. Moreover, when the

10/90 coupler was replaced by 30/70 coupler, at the pump power of 3.5W, the laser outputs were improved by 3dB overall in the 1620-1660nm. Particularly, when lasing at 1660nm, the slope efficiencies are 5.0% and 6.24% for the couplers with ratio of 10/90 and 30/70 respectively.

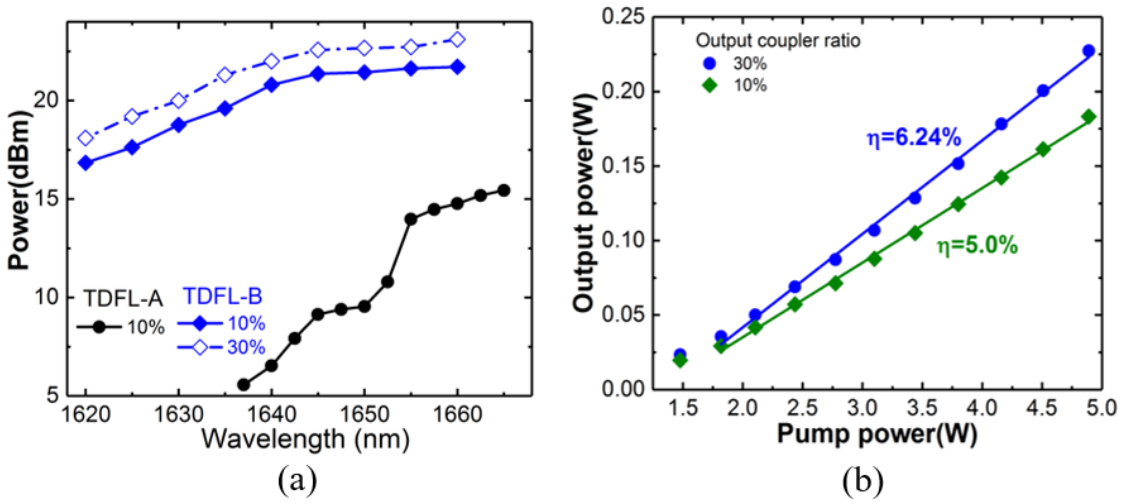

Figure 4. 12(a) Output powers of TDFL-A and TDFL-B at different lasing wavelengths, and (b) The laser outputs at 1660nm for different output couplers, (10% and 30% respectively).

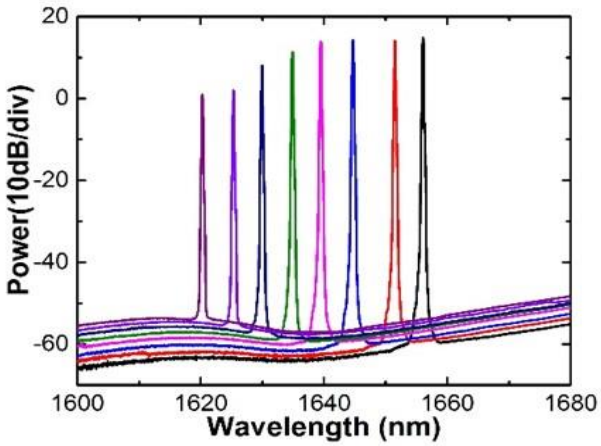

Figure 4. 13 Output optical spectra of the TDFL-B laser configuration (measured with 0.1nm OSA resolution).

Since the output from the laser cavities was extracted after reflection from the FBG on the right side depicted in Fig. 4.11, the out-of-band ASE was well suppressed, resulting in a high optical signal-to-noise ratio (OSNR) albeit at a slightly lower output power. Fig. 4. 13 plots the spectral characteristics of TDFL-B. An OSNR of more than 45 dB was successfully achieved across the full tuning range from 1620 nm to 1660nm (up to 60 dB OSNR from 1640nm to 1660nm). The 3dB bandwidth of the laser lines were measured to be <0.3nm. We believe that the output power and lasing efficiency could be further improved by optimizing the ASE filter to provide a much sharper wavelength cutoff and the Tm/Ge fiber glass composition.

4.5 Ultra-short Wavelength Operation of Thulium-doped Fiber Amplifier in the 1628-1655nm Waveband

Based on the fabricated Tm/Ge co-doped fiber using new glass composition (particularly, a thulium (Tm) and germanium (Ge) co-doped silica fiber), in section 4.4, I have successfully demonstrated a tunable Tm-doped fiber laser in the wavelength range of 1620-1660 nm [97]. With the distinctive feature of blue-shifted absorption and emission spectra, the Tm/Ge co-doped fiber provides the intriguing possibility of bridging the gap between the long wavelength edge of the L-band EDFA and short wavelength edge of the TFDA. In this section, I report amplification of the short TDF wavelengths encouraged by the successful TDFL operation in the ultra-short wavelength region. This presents the first realization of a silica-based TDFA operating down to as short as 1628 nm.

4.5.1 Experimental setup

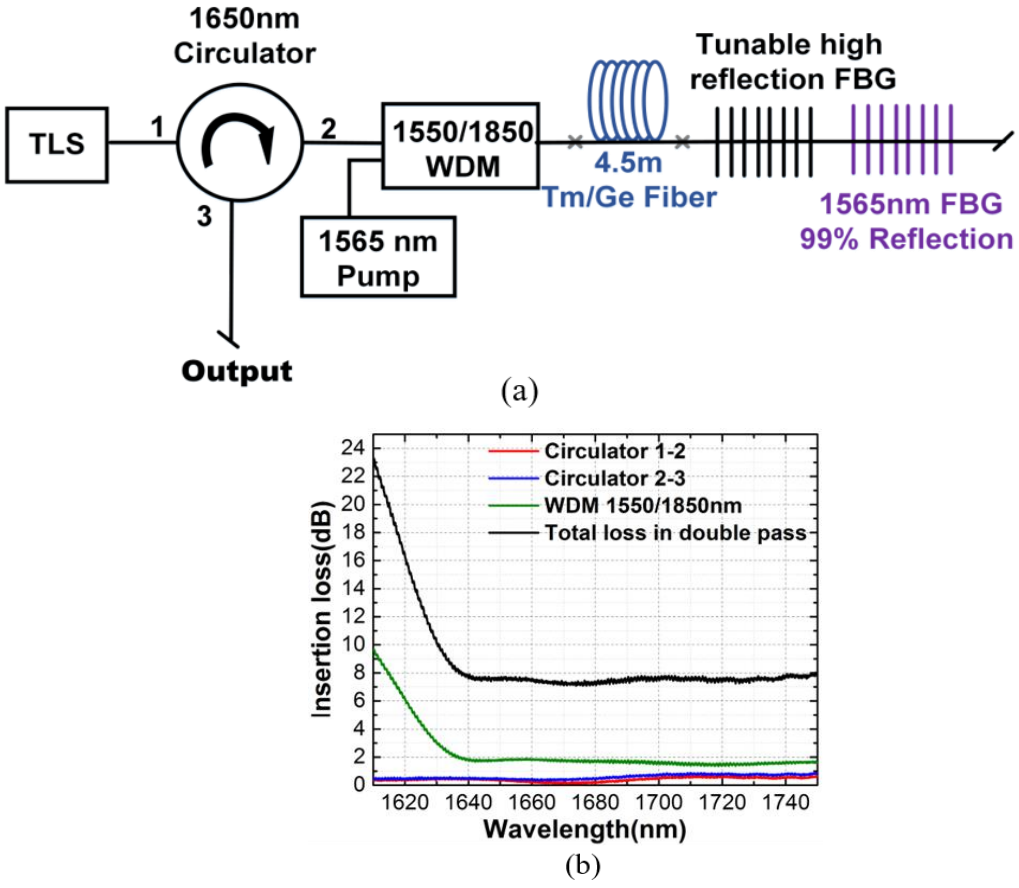

Figure 4. 14(a) Schematic of the TDFA, TLS: tunable laser source; (b) insertion losses of the WDM coupler (green) and circulator (blue and pink) used in the setup, and the total optical loss of the double pass cavity.

Fig. 4. 14a shows a schematic of the TDFA. In our experiment, a commercially available tunable laser source (Tunics T100S-HP) covering the wavelength range of 1500-1680 nm was

used as a seed source with an input power of -20 dBm and 0 dBm for small and saturated signals, respectively. An optical circulator optimized at 1650 nm and with high optical isolation (>40 dB at center wavelength) and low insertion loss (0.45 dB) was employed as depicted in Fig. 4. 14(a). In order to extract enough gain at short wavelengths, a high population inversion is required and an in-house built high-power Er/Yb fiber laser operating at 1565 nm was used as a pump source with a maximum output power of 4.35 W (36.3 dBm). A dielectric filter-based 1550/1850 nm WDM was used for combining the pump and signal. As shown in Fig. 4. 14b, the insertion loss of the WDM coupler was less than 2dB but this sharply increased at wavelengths shorter than 1640 nm. In addition, Fig. 4. 14b also shows the total optical loss in a double pass configuration including the loss of an optical circulator, a 1550/1850nm WDM coupler as well as the optimized splicing loss of 0.8 dB between standard SMF and Tm/Ge co-doped fibers. To realize short wavelength operation, a tunable FBG was used in our experiment as an ASE filter as well as a narrowband signal retroreflector to realize a double pass implementation.

The FBG can be tuned from 1620 nm throughout to 1660 nm by using an axial compression mechanism. The measured reflectivity and bandwidth of the FBG varied from 80 % to 94 % and from 0.67 nm to 1 nm respectively, depending on the operating wavelengths. Moreover, a 1565 nm FBG with ~99% reflection was incorporated to recycle the residual pump light (~0.4 W). The external gain and NF of the amplifier was measured by an optical spectrum analyzer (Yokogawa AQ6375) and a thermal power meter (Ophir 3A-FS).

4.5.2 Result and discussion

Fig. 4. 15a shows the gain and NF performance of the proposed TDFA. An external small-signal gain of 19 dB was achieved at 1655nm, 8dB at 1632nm and 4dB at 1628nm. Compared to the previous demonstration of a short wavelength TDFA in Section 2.9, I have successfully extended the short wavelength edge of the silica-based TDFA from 1650 nm to 1628 nm. The saturated gain shows similar behavior and varies from 7 dB to 17.2 dB with only 2.5 dB difference as compared to the small signal gain. The external NFs for saturated signal and small signal were as low as 4.6dB and 4.4dB at a wavelength of 1655 nm but increased towards shorter wavelengths. This is mainly due to the high insertion loss of the WDM coupler and strong re-absorption of signal light by Tm ions in their ground state.

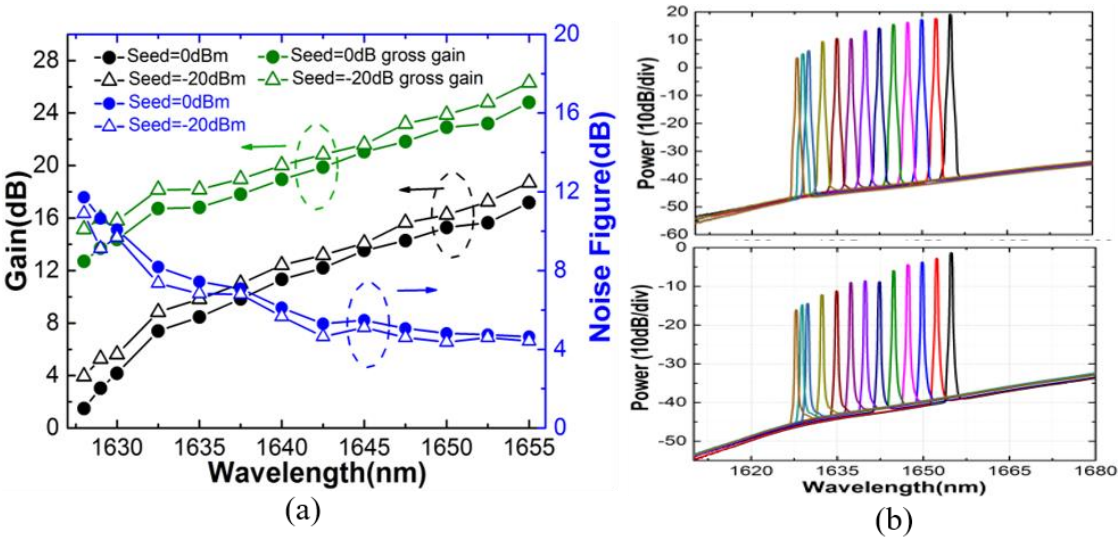

Figure 4. 15(a) Gain and NF performances of the TDFA. Amplified spectra for (b) saturated and small signals, measured with 0.5nm OSA resolution.

By considering the total insertion loss of the amplifier with the double-pass architecture, the gross (or internal) small-signal gain is around 15-26dB in the 1628-1665 nm. Therefore, further improvement in the performance of the TDFA is expected with higher pump powers (or indeed a different choice of pump wavelength such as 793nm, which has been theoretically investigated with the conclusion that the gains at shorter wavelengths will be enhanced compared to 1550nm pumping[106]). In addition, further optimization of both the passive fiber components and splicing loss between the active and passive fibers are expected to improve the performance. Fig. 4. 15b shows the amplified optical spectra for the saturated and small signal regime in the upper and the lower plots, respectively. The amplified small signal has 30–38dB in-band OSNR across the entire amplification band while the amplified saturated signal exhibits over 50 dB in-band OSNR.

4.6 Ultra-short wavelength mode-locked fiber laser at 1650nm waveband

Fiber laser system based on TDF have been demonstrated as efficient way which covers a wide wavelength band from 1800 nm to over 2200 nm in both CW and mode-locked regimes[107][108] [9], because of its high optical gain and optical conversion efficiency. The fluorescence of Tm in silica glass is originated from the $^3F_4 - {}^3H_6$ transition, which allows the operation ranging from 1600 nm to 2200 nm. The peak of the emission is usually located between 1800 and 1850nm[106]. However, the quasi-three-level nature of TDF emission leads to strong re-absorption of the light at the short wavelength region and TDF lasers generally operate at wavelengths longer than 1900 nm.

In order to achieve ultra-fast fiber laser below 1700 nm by mode-locking, there are two key elements need to be concerned, i.e., higher gain below 1700nm and suitable saturable absorber (SA). Fortunately, as described in previous section, I have the fabricated Tm/Ge co-doped fiber, which providing a higher gain at short wavelength edge below 1700nm than other Tm^{3+}-doped fiber available so far[44][109]. Moreover, I introduced a 1650 nm chirped FBG with BW of 20 nm as a band pass filter for lasing at 1650nm waveband. Firstly, compared with HR FBG with BW of 0.5nm, the 20nm BW of chirped FBG ensures an ultra-short pulse duration when operated in a soliton regime as well as noise-like pulse. Secondly, the chirped FBG performs like a band pass filter with high reflectivity (>90%) at 1650nm, which introduce less loss than the aforementioned long wavelength ASE filters such as PCF and DCF.

Recently, higher energy pulse TDFL below 1750nm is requested from the perspective of applications. Despite the conventional soliton and dissipative soliton, noise-like pulses have attracted attentions due to their high pulse energy and broadband spectrum. Compared with SAs such as semiconductor saturable absorber mirror (SESAM), carbon nanotubes and other physical SAs, NPR or NOLM could be used as artificial SA to achieve high energy pulsed fiber laser due to its easy implementation and low cost. In addition, mode-locking based on the technique of NPR or NOLM allows ultra-fast pulsed laser to operate in both soliton and noise-like regimes, which is determined by pump power. At high pump power, soliton pulse could be switched to the noise-like pulse by simply adjusting the polarization controllers (PCs). Particularly, the energy of noise-like pulse will increase accordingly with increment of pump power. Unlike conventional soliton pulse, the energy of noise-like pulse will not be restricted by the cavity dispersion and nonlinear effect[110]. Horowitz et al described a theoretical explanation to the formation of noise-like pulse, indicating that the noise-like pulse could be achieved in a birefringent laser cavity comprising a gain fiber and a nonlinear transmission element [111] .

For a soliton pulse fiber laser based on Tm^{3+}-doped fiber, the shortest wavelength reported so far is 1702nm [11]. For noise-like pulse TDFL, Sobon et al achieved an ultra-broadband noise-like pulse from a normal dispersion mode-locked TDFL with a 10 dB bandwidth of over 300nm spanning from 1830nm to 2140nm[112]. Li et al studied both soliton and noise-like pulse at 2017.33nm based on Tm^{3+}-doped fiber [113]. To date, the central wavelengths of all noise-like pulses are around the 2 μm band.

In this section, I discuss on a self-starting all-fiber passively ultra-short wavelength mode-locked TDFL based on nonlinear optical loop mirror (NOLM) in both soliton and noise-like

pulse regimes. Stable soliton pulses centered at 1656.1nm with 0.55 nm FWHM were produced at a repetition rate of 1.28MHz with pulse duration of 5.32 ps and pulse energy of 109 pJ. As pump power increases, the oscillator can also operate at the noise-like (NL) regime. Stable NL pulses with coherence spike width of 890 fs and pulse energy of up to 20 nJ was achieved with a central wavelength of 1656.2nm with 4.51nm FWHM. To the best of my knowledge, this is the shortest wavelength operation of a mode-locked thulium-doped fiber laser.

4.6.1 Nonlinear optical loop mirror

In this section, I will introduce the NOLM as an artificial SA for the mode-locked fiber lasers in section 4.6.4 and 4.6.5. As illustrated in Fig. 4. 16, a NOLM could be built based on a 2×2 fiber coupler with power-coupling ratio of α : 1-α , where α ≠ ½. The input beam will be split into two counter propagating beams with unequal intensity in the right hand side loop. Phase shift ϕ occurs between the two mismatched counter propagating beams due to the intensity dependent phase velocity. If dispersion is ignored, the transmission of a NOLM is given by [114]

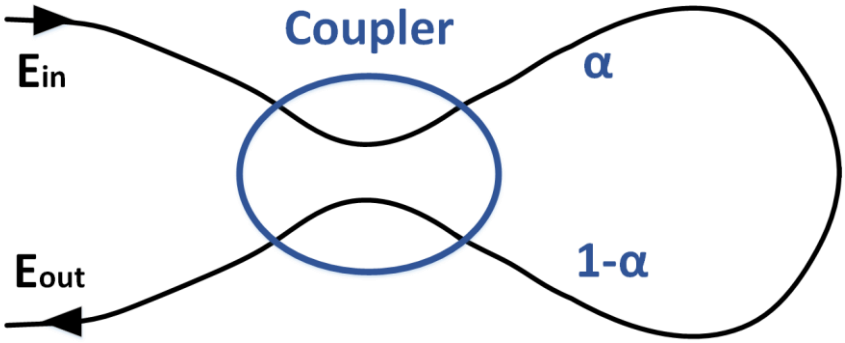

Figure 4. 16 the loop mirror configuration

$$\phi = |E_{in}|^2 \times \frac{2\pi n_2 L}{\lambda}]$$
$$T_S = \frac{E_{out}}{E_{in}} = 1 - 2\alpha(1-\alpha)\{1+\cos[(1-2\alpha)\phi]\} \quad (9)$$

where ϕ is the phase shift accumulated when a beam propagate a fiber length of L. n_2 refers to the nonlinear (Kerr) coefficient of the fiber, $|E_{in}|$ is the output field from the TDFA. T_s denotes transmissivity of the nonlinear loop, $\alpha:(1-\alpha)$ is the coupling ratio of the coupler. It is obvious that the transmission of a NOLM is intensity dependent, and before the first transmission peak, the increase of transmission with respect to intensity is similar with the performance of a fast SA. When a NOLM is placed in a laser cavity as a nonlinear phase shifter, pulse self-shaping occurs just as real SA. In a laser cavity incorporating NOLM, passive mode-locking is expected.

4.6.2 Experimental setup

The experimental arrangement for the mode-locked TDFL based on a NOLM is depicted in Fig. 4. 17 The left loop is a ring oscillator and the right one is the nonlinear loop mirror. The above mentioned 3.8 m Tm/Ge co-doped fiber was used in the ring oscillator Moreover, the small-signal gain of ~5.8 dB/m at 1655 nm was observed when pumped at 36.3 dBm power at 1565 nm. A commercial CW 1560 nm fiber laser (SPI) was used to pump the active fiber through a 1560/2000 nm wavelength-division multiplexer (WDM, AFR). This WDM provides maximum 5 W for the pump and 2 dB insertion loss at 1650 nm. A chirped fiber Bragg grating (20 nm bandwidth at a central wavelength of 1650 nm with 90% reflection, OF-LINK) in conjunction with a circulator (1.5dB loss, OF-LINK) was used as a wavelength selective filter and anomalously/normal dispersive element. The 10% port of a 90:10 coupler was used to extract output from the all-fiber mode-locked laser. A 2 ×2 fused fiber coupler with a coupling ratio of 60:40 at 1650 nm was used to join the loop on the left hand side (LHS) to the NOLM on the right hand side (RHS). A 140 m long SMF-28 fiber was used to ensure enough nonlinear phase shift for mode-locked operation. Two PCs were placed close to the 60:40 coupler in the NOLM section to control the polarization state of the counter clockwise (CCW) and clockwise (CW) beams to initiate mode-locked operation. An isolator working at 1650 nm with an insertion loss of 0.5 dB and an extinction ratio of 48 dB was inserted in the ring oscillator to ensure unidirectional laser operation.

Length of the total cavity was about 161 m including 3.8 m Tm/Ge co-doped fiber, 140 m SMF-28 fiber, 3 m SMF-28 fiber in PCs and 14.2 m SMF-28 pigtail fibers from the pump combiner, isolator, circulator, CFBG and the tap couplers. The anomalous dispersion values of the SMF-28 fiber at 1.65μm was about $-0.034 ps^2/m$. The anomalous dispersion values of the FBG at 1.65 μm was about -8 ps^2, which is provided by the producer (OF-LINK). Unfortunately, I have not measure the dispersion of the home-made Tm/Ge co-doped fiber. I assumed slightly anomalous dispersion from the active fiber, which is ignored. Hence, the net dispersion in the cavity was estimated to be about $-13.44 ps^2$. For the measurements of the laser output, an InGaAs photodetector (EOT ET-5000F) with a response time of approximately 60 ps was connected to a 20 GHz oscilloscope (Tektronix CSA 803A). The detection system was used to measure the pulse train and pulse waveforms whilst the actual pulse duration was

measured by a commercial autocorrelator (APE). The pulse spectra were measure by an optical spectrum analyzer (Yokogawa AQ6375)

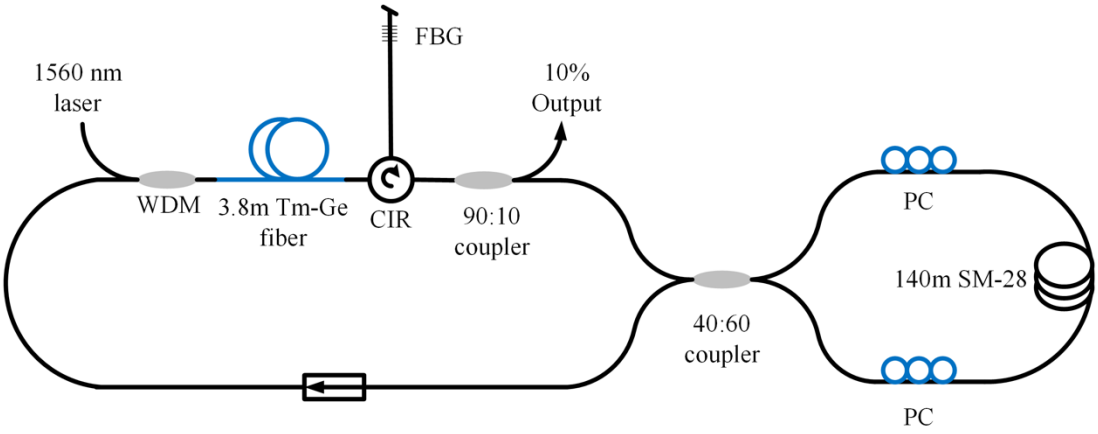

Figure 4. 17 Schematic of the mode-locked TDF laser. WDM-Wavelength-division multiplexer, PC- Polarization controller, CIR- Circulator, FBG- Fiber Bragg grating.

4.6.3 CW fiber laser at 1656nm

The oscillator started to operate at a cw regime after reaching the launched pump power of 1.9 W. With the increment of pump power, the cw lasing output at 1656 nm increased linearly. At pump power of 5 W, the lasing output reaches 33.8 mW . The measured lasing spectrum is shown in Fig. 4. 18.

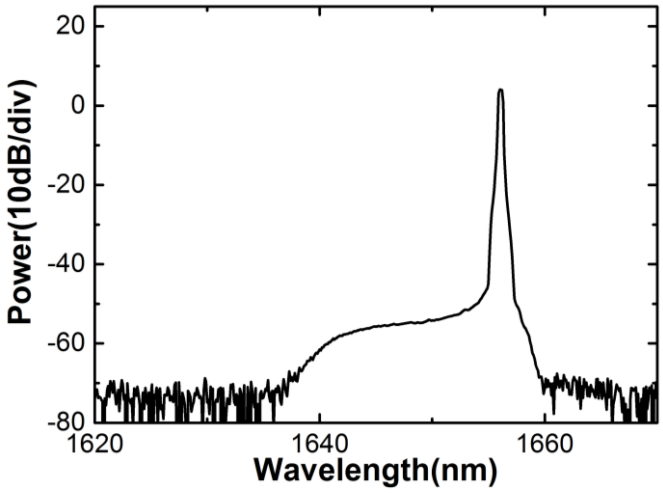

Figure 4. 18 The optical spectrum of all-fiber ring cavity laser incorporated with 1650nm band-pass FBG.

4.6.4 Soliton mode-locked fiber laser at 1656nm

In this section, I report the demonstration of an ultra-short wavelength mode-locked fiber laser at 1656 nm by using an in-house fabricated Tm/Ge co-doped silica fiber as the gain medium.

It employs the NOLM structure, and large net anomalous dispersion operates at both soliton and NL pulse regimes. The 5.32 ps soliton pulses with pulse energy of 109 pJ and SNR of ~60 dB, and 890 fs noisy double-scale pulses with pulse energy of 20 nJ and SNR of ~63 dB were achieved, respectively. It represents by far the shortest lasing wavelength ever achieved from a TDFL producing soliton optical pulses.

The oscillator started to operate at a cw regime with a threshold launched pump power of 1.9W. With appropriate adjustment of the PCs, stable soliton mode-locking operation was achieved as shown in Fig.4. 19a at a launched pump power of 2.1W. The measured repetition rate of 1.288MHz matches well with the cavity length dependent theoretically value suggesting that the oscillators operates with a single pulse per round trip. The inset of Fig.4. 19a shows the waveform at the 2 ns range suggesting no multi-pulse operation. The mode-locking state could be maintained up to a launched pump power of 2.15W, generating a maximum average output power of 140 μW and pulse energy of 109 pJ. Once the mode locking achieved by the initial adjustment of the polarization controllers, the soliton pulses were self-starting and no further adjustment of the PCs was required, and the operation is stable when pump power is increased gradually or even the pump power is re-switched. Fig. 4. 19b shows the RF spectrum of the output at a scanning range of 180 kHz with a resolution of 1 Hz at the launched pump power of 2.15 W. The signal to noise ratio (SNR) of ~60dB and the absence of modulation in 12 MHz broad RF spectrum [see inset of Fig. 4. 19b] indicated that the oscillator operated at stable CW mode-locking regime.

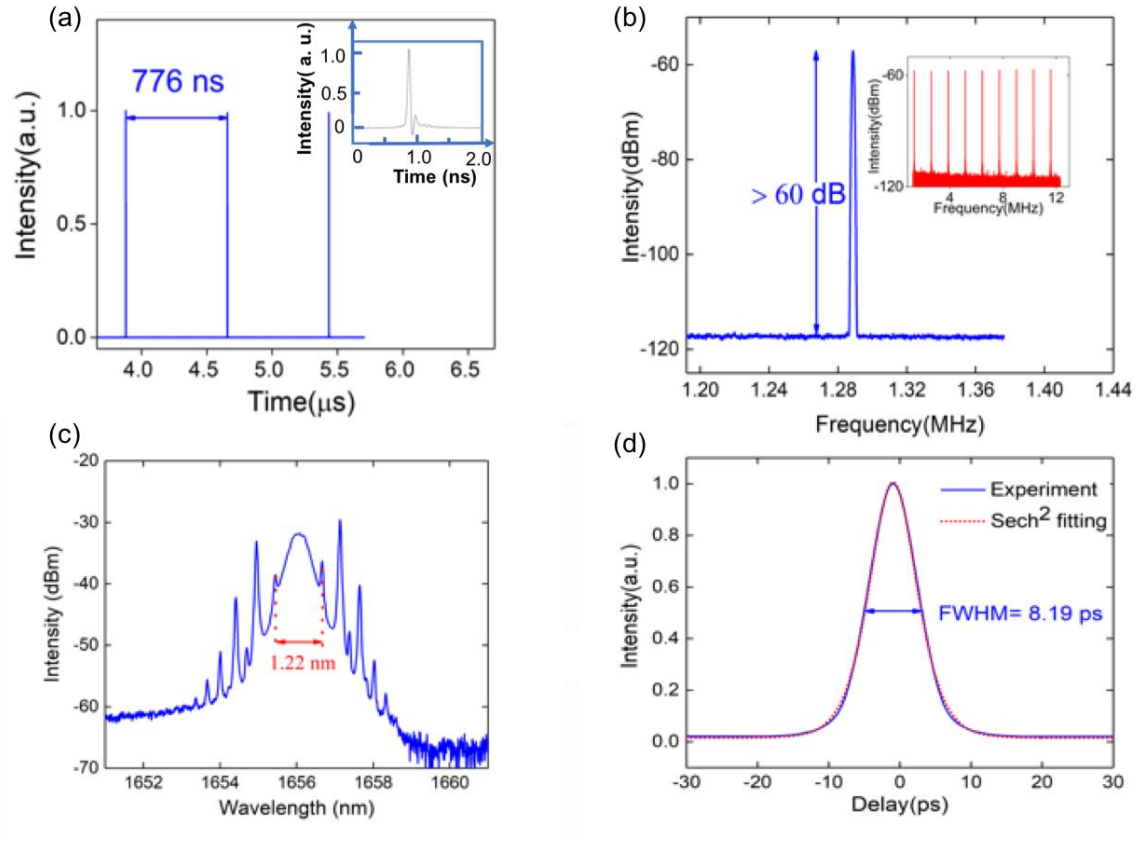

Figure 4. 19 Mode-locked laser under soliton operation: (a)Pulse train and waveform (insert with 2ns range); (b) Ratio frequency (RF) spectrums with scanning range of 180kHz and 12 MHz (inset); (c) optical spectrum; (d) autocorrelation trace with sech^2-pulse fitting, FWHM- Full width at half maximum.

Fig. 4. 19c shows the measured optical spectrum of the soliton pulses at the launched pump power of 2.15W with a resolution of 0.05nm. The central wavelength and FWHM were 1656.1nm and 0.55nm respectively. Typical Kelly sidebands originating from spectral interference of dispersive waves suggested the operation in this case was the conventional solitary mode-locking. The separation of 1.22nm between first-order Kelly sidebands agrees well with the estimated net cavity dispersion of −13.34ps^2 according to the formula:

$$\Delta\lambda = \frac{\lambda^2}{\pi c \tau_0}\sqrt{\frac{4\pi {\tau_0}^2}{|\beta_2|} - 1}\ [115] \qquad (10)$$

where τ_0 denotes pulse duration at half of the maximum intensity, β_2 refers to the net cavity dispersion. Noted that the cw component with narrow spectral line generally started with the Kelly sideband if the PCs shifted from the optimum positions. Fig. 4. 19d shows the measured autocorrelation trace of the mode-locked pulses at a scanning range of 60 ps. A background- and side-lobe free autocorrelation trace measurement shows the laser operates at single soliton pulse as well. The FWHM is 8.19 ps. The experimental data were fitted by a sech^2-pulse profile

very well, and the pulse duration was estimated to be 5.32 ps. Consequently, the time-bandwidth time (TBP) was calculated to be 0.319 indicating the pulse is almost transform-limited. Further increasing the pump power, soliton splitting initially appeared in temporal domain due to energy overflow of single soliton pulse.

4.6.5 Noise-like mode-locked fiber laser at 1656nm

In this section, we report the demonstration of an ultra-short wavelength mode-locked fiber laser at 1656 nm by using an in-house fabricated Tm/Ge co-doped silica fiber as the gain

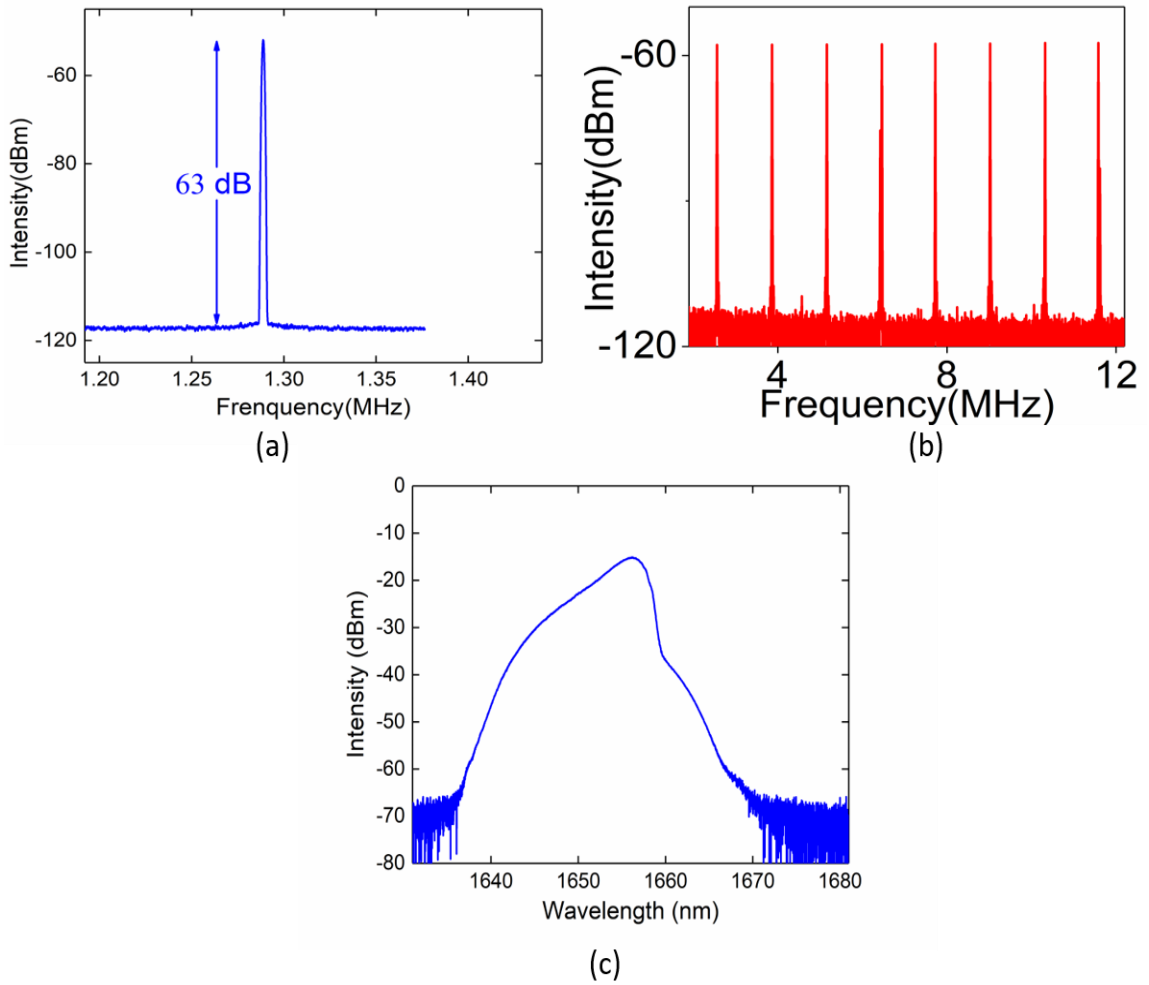

Figure 4. 2 Mode-locked laser under NL pulse operation: RF spectrums with scanning range of (a) 180kHz and (b) 2MHz; (c) optical spectrum

medium. It also employs the NOLM structure and large net anomalous dispersion which can operate at NLP regime. The 890 fs noisy double-scale pulses with pulse energy of 20 nJ and SNR of ~63 dB were achieve. It also represents by far the shortest lasing wavelength ever achieved from a TDFL producing noise-like optical pulses.As the launched pump power was increased to 2.48W, the oscillator switched to a NL pulse regime producing stable pulses with further adjustment of the PCs. At this launched pump power, the measured average output power was 3 mW. Moreover, once the mode locking was started by the initial tuning of the

polarization, the pulses were self-starting without the request of polarization tuning when the pump power was switched on and increased. The NL mode-locking state can be maintained up to the maximum launched pump power of 5W with an average output power of 25.6 mW. Fig. 4. 20a demonstrates the RF spectrum with 63dB SNR at a scanning range 18kHz with a resolution of 1 Hz at the launched pump power of 2.48 W. The measured repetition rate of 1.28 MHz is same as soliton pulses, indicating that the oscillator operated at the fundamental mode-locking regime. Given the achieved highest average power of 25.6mW, the maximum achieved single pulse energy can be calculated as high as 20 nJ. Similarly, the RF spectrum at a range of 12MHz with a resolution of 1kHz was free of modulation indicating no Q-switching instability. Fig.4. 20c shows the measured optical spectrum of the NL pulses with a resolution of 0.05 nm at the launched pump power 2.48W. The smooth spectrum had a typical shape of NL pulses as reported at 1.5 and 1.9 μm regions [116][117]. The center wavelength and FWHM were 1656.2 nm and 4.51 nm, respectively. Gradually increasing the pump power to maximum, the spectral profile was essentially unchanged, and the output power and pulse-width increase linearly, which was the typical feature of mode-locked pulses operating at NL regime. As in Fig. 4. 21, it shows the measured pulse width and laser output with respect to the pump power. Unlike the limited power value of mode-locked laser in soliton regime, the maximum output power could reach 25 mW . The pulse duration shown in Fig. 4. 21 is measured based on the fast photodiodes (60ps response time) and 20GHz oscillator (Tektronix CSA 803A).

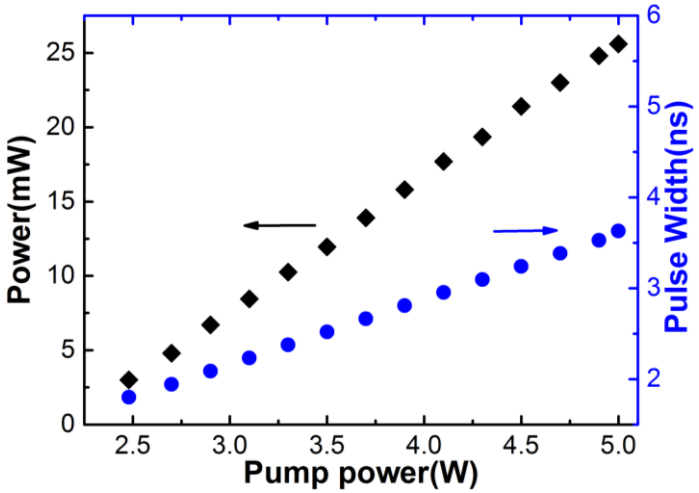

Figure 4. 21 The variation of pulse width and output power with respect to pump power

.

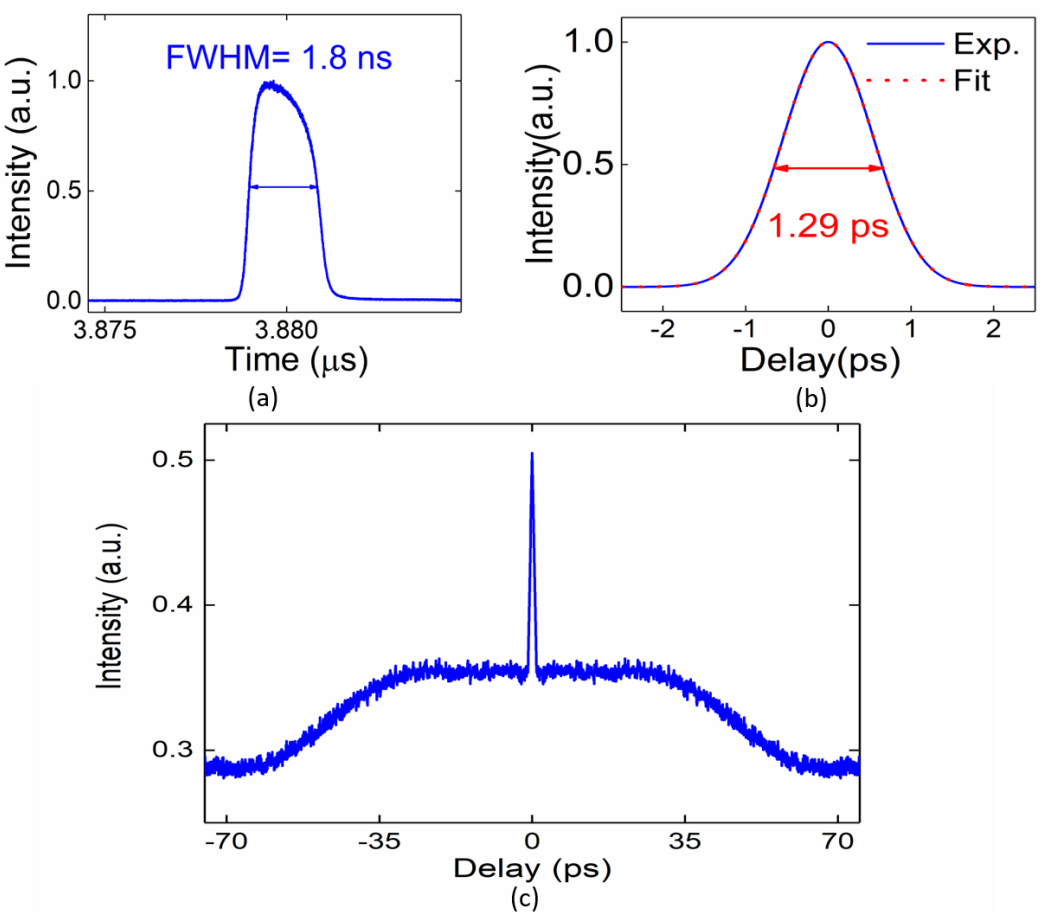

Figure 4. 22(a) The pulse temporal profile with FWHM of 1.8ns; (b) presents the autocorrelation trace at 5ps range; (c) measured 140ps autocorrelation trace of the pulse.

At the pump power of 2.48 W, the measured pulse duration was 1.8 ns of FWHM illustrated in Fig. 4. 22a. Fig. 4. 22b shows a FWHM of 1.29ps at a scanning range of 5 ps. If a Gaussian-pulse profile is assumed, the width of the coherent spike is 895 fs with time bandwidth product of 0.442. Fig. 4. 22c shows the measured autocorrelation trace at a scanning range of 140 ps, a narrow spike riding on a broad pedestal was observed. The wide shoulders that extended over the entire width of measurement window suggested that the pulse duration was longer than 140 ps at launched pump power of 2.48W.

To investigate the influence of the cavity dispersion in our case, we reverse the direction of the CFBG without other variation of the cavity thus inverting the dispersion of the CFBG to be $+8ps^2$. The net dispersion of the cavity is estimated to be $+2.56ps^2$. The oscillator started to operate at a cw regime after reaching the launched pump power of 1.9W which is the same as the net-anomalous regime discussed in the earlier section. The NL pulse was achieved under the lunched pump power of 2.4W with adjusting the PCs. This result agrees with that the NL pulse could be generated in dispersion-mapped cavities with either net-anomalous dispersion

(NAD) or net-normal dispersion (NND)[118][119][120]. The influence of SMF length in the RHS loop mirror for the mode-locking operation was investigated in[114].

Note that the coupling ratio chosen in this experiment was 60:40 instead of 50:50 to increase the nonlinear phase shift difference between the counter clockwise and clockwise directions so as to increase the transmissivity of the NOLM to meets the condition that light with high intensity has a higher transmissivity than that of light with low intensity. We also replaced the previous 140 m SMF-28 fiber by 110 m and 80 m SMF-28 fiber, respectively. The CW operation thresholds for 110 m and 80 m fibers were decreased to 1.85 W and 1.8 W, respectively, as a result of the reduced total cavity loss. From equation 9, the shorter length of fiber requires higher pulse energy entering into the NOLM under the fixed nonlinearity and the fixed coupling ratio to start the function of the NOLM for mode-locking. Hence for the 80 m fiber, the soliton pulses cannot be achieved due to the signal energy required for NOLM was beyond the soliton regime. For the 110 m fiber, the soliton pulses cannot be self-started, but can be achieved by increasing the launched pump power until multiple pulses were observed. The multiple pulses remained when the pump power was slightly decreased. This is because enhanced nonlinear phase shift difference was induced by higher peak power of multiple pulses [113]. For both 110 m and 80 m fibers, the stable NL can be achieved at threshold of 2.55W and 2.8W respectively.

4.7 Chapter Summary

In Section 4.3, I have reported a ultra-wide tunable Tm^{3+}-doped fiber laser in the wavelength spanning from 1650 nm to 2000 nm using a diffraction grating for wavelength tuning and DCF as ASE filter.

In Section 4.4, I have successfully demonstrated an all-fiber tunable TDFL operating over the 1620 nm to 1660 nm range (communication U-band) by using Tm/Ge co-doped fiber. This unique glass composition effectively shifts the emission cross-section of the Tm ions to shorter wavelengths as compared to conventional Tm-doped fiber using an aluminosilicate host. This greatly improved short wavelength operation and allowed us to bridge the gap between the prior EDFLs and TDFLs. Using two FBGs as cavity mirrors and a long wavelength ASE filter, more than 17 dBm output power with >45dB OSNR was achieved over the entire tuning range.

In section 4.5, by constructing a double-pass amplifier, we have demonstrated a silica-based TDFA operating from 1628 nm to 1655 nm, a ~2THz gain bandwidth extension compared to the previous best report. Up to 19 dB small signal gain (external) and a NF as low as 4.4 dB were achieved at 1655 nm with >30dB in-band OSNR.

In Section 4.6, I have experimentally demonstrated an ultra-short wavelength soliton and noise-like mode-locked TDFL based on a NOLM. Both stable soliton and NL mode-locked pulses at all-anomalous-dispersion regime were observed. The oscillator produced 5.32 ps soliton pulses with energy of 109 pJ and SNR of ~60 dB centered at 1656.1 nm with a FWHM of 0.55 nm. The oscillator can also produce NL pulses centered at 1656.2nm with duration of 1.8ns and pulse energy as high as 20nJ. The measured SNR of~63dB suggests its higher stability compared with typical NL pulses. Although the NL pulses in most of cases are not the ideal pulses due to its large pulse duration and broad pedestal, the highly energetic NL pulses with high SNR in this case is of great potential in deep-tissue multiphoton imaging and producing femtosecond-level pulses with high energy that could lead to a wide range of applications [8]. To the best of my knowledge, this is the shortest wavelength of operation of a mode-locked thulium-doped fiber laser. Energetic ultra-short 1.65 μm mode-locked pulses operating at dissipative soliton regime were also expected by developing a normal dispersion cavity based on the above structure.

Chapter 5. Large Mode Area (LMA) Tm^{3+}-doped Germanate Glass Fiber laser and Amplifier at 2 μm

Due to the important applications for telecommunication, LIDAR, remote sensing, medical surgery and mid-infrared frequency generation, fiber lasers in the wavelength regime of 2μm have attracted intense attention for its feature of broadband emission linewidth from 1.6μm to 2.1μm[37][121]. Moreover, Thulium (Tm^{3+})-doped fiber lasers have a significant advantage of high slope efficiency over other rare-earth ions, which could exceed the Stoke limit. Particularly, when pumped by the wavelength near 800nm ($^3H_4 \rightarrow {}^3H_6$), the cross-relaxation energy transfer process happens thus exhibiting a quantum efficiency of 2. However, the efficient one-for-two energy transfer requires high Tm^{3+} doping concentration resulting from the close proximity of Tm^{3+} ions. In order to obtain high Tm^{3+} -doped fibers, the option of the host glass is momentous. For the state-of-art Tm^{3+} doped silica fibers, very high doping concentration has not achieved yet because of the defined waveguide structure in silica glass. Compared with silica glass host, germanate glass with lower phonon energy (~900 cm^{-1}) enhance the luminescence quantum efficiency[122]. Multi-component glasses (e.g. germanate glass, silicate glass, tellurite glass and bismuthate glass) are better Tm^{3+} glass host due to their higher Tm^{3+} solubility. Furthermore, the highly Tm^{3+} -doped (typically up to 10^{21} ions/cm^3) germanate glass fiber increases the ability to reach a large pump absorption and high gain per unit length of the fiber, which leads to mitigate the nonlinear effect, reduce the background loss, and narrow emission linewidth.

On the other hand, some of the abovementioned applications require high power pulse or CW laser with good beam quality, which could be accomplished by the configuration of a MOPA [123]. For silica-based glass fiber MOPA system, the conventional approach is to develop low NA, LMA fibers because LMA fibers reduces both the peak power of pulse intensity propagating through the active core region and the fiber length required to achieve appreciable amplification, thus overcoming nonlinear effects for high power application. However, pulse distortion due to nonlinear effects remains a key issue and further improvements are still required. Therefore, with the capability of highly Tm^{3+}-doping concentration, Tm^{3+}-doped germanate glass LMA fiber would be an efficient approach to further mitigate nonlinearity in high power application.

In this Chapter, I will introduce the in-house fabricated Tm^{3+}-doped germanate glass fiber (TGF) and its application in lasers and amplifiers. Based on the prepared core glass and cladding glass

with novel multi-oxide composition, a single-clad LMA (20µm) TGF have been in-house fabricated. After preliminary fiber characterization of in-house fabricated LMA TGF, I have demonstrated a CW TDFL with maximum power of 1.5 W operating at 1952nm by core-pumping at 1565nm. A high slope efficiency of 55.9% with respect to absorbed pump power and nearly diffraction-limited beam quality are achieved. Moreover, a D-shape double-clad LMA TGF was also fabricated. A TGF based amplifier spanning from 1880nm to 2000nm has been demonstrated with peak gain of 13dB and 10dB at 1930nm for small signal and saturated signal respectively. In addition, a pulse-MOPA fiber system incorporating double-clad LMA TGF as main amplifier has been demonstrated with output power of 3.7W, corresponding to an energy of 0.27µJ with pulse duration 57ps.

5.1Fabrication and characterization of germanate glass

Glass samples used in this work was fabricated by the conventional melting-quenching technique using high purity chemicals (99.9% minimum). Tm^{3+} doped multi-component germinate glass (core glass) with molar composition of $61GeO_2$-15PbO-10ZnO-$3ZnF_2$-$6Na_2O$-$4Nb_2O_5$-$0.6Tm_2O_3$-$0.4GdF_2$ was obtained. The cladding glass (without Tm^{3+}ions) had a slightly different composition from the core glass with molar composition of $61GeO_2$-14PbO-11ZnO-$3ZnF_2$-$6Na_2O$-$4Nb_2O_5$-$1GdF_2$. For each glass, well mixed materials were melted at 1230ºC for about 3 hours in a Platinum crucible under dry O_2/N_2 atmosphere to eliminate OH-content. The melts were stirred with a platinum rod to homogenize the glass, remove bubbles and avoid the cluster of the melt. Thereafter, the glass was cast into a brass mold preheated at a temperature around the transition temperature, Tg, for 4 hours to relieve internal stresses before it was cooled to room temperature. After the annealing process, glass samples were cut and polished for optical and spectroscopic characterization. Two glass compositions, namely Ge_01 (doped with 3.10^{20} ions/cm3) and Ge_02 (undoped Tm^{3+}), were prepared to be thermo-mechanically compatible when used as core/cladding glass pairs for fiber fabrication.

5.1.1 DTA, CTE and Refractive index of germanate glass

Differential Thermal Analysis (DTA) was carried out using a PerkinElmer Diamond TG/DTA instrument with a heat rate of 5°C/min from 40°C to 1350°C under N_2 atmosphere, in order to detect the transition (Tg) and the crystallization (Tx) temperatures.

Thermal analysis using DTA was carried out in order to measure the characteristic temperatures Tg and Tx. With these data, one can calculate the stability parameter of a glass, $\Delta T = Tx - Tg$, which give an indication of the stability of the glass and his tendency to devitrification. The

glass transition temperatures were measured to be 485°C and 489°C for Ge_01 and Ge_02, respectively. In Fig. 5. 1 the typical DTA curve for the core composition glass is reported. The difference between the crystallization temperature and the glass transition temperature is 260°C, a quite high value, higher than the one reported by Wen et al[124]. Such high transition temperatures and high thermal stability, as compared to other reported germanate glass compositions, make the fabricated glasses suitable for manufacturing glass lasing structures able to handle high average powers without the risk of crystallization and devitrification[125].

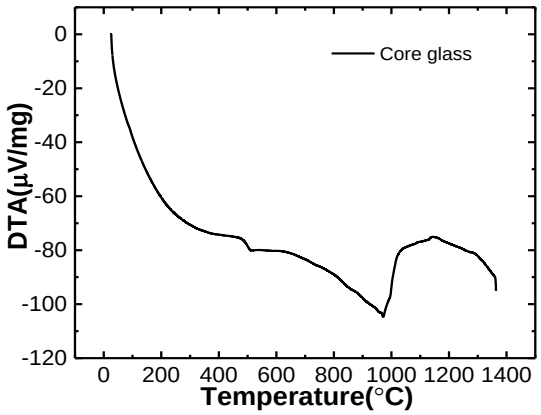

Figure 5. 1 The curve DTA versus temperature of Ge_01 core glass

The coefficient of thermal expansion (CTE) was measured using a PerkinElmer Diamond TMA instrument in the 30°C-400°C temperature range at a rate of 10°C/min under a constant compressive force of 100mN. The CTE was reported in table 2 and the value of core and cladding glasses were 7.18×10^{-6}/°C and 6.46×10^{-6}/°C, respectively. The difference between the core and germanate cladding glasses is 7.2%. Because of the little discrepancy, it can be stated that the drawing of the fiber can be performed without residual stresses at the interface. The density of the two glass samples was also reported in table 1. The density of the cladding is lower than the core glass, according to the less amount of PbO in the composition.

The refractive indexes of the glasses was measured by ellipsometry using a MC05-Woolham-Ellipsometer. The absorption spectra was performed on a UV-visible NIR double beam spectrometer for wavelengths ranging from 200 to 2000 nm. The refractive indexes of core and cladding glasses at 632.8 nm are 1.834 and 1.833, respectively. The NA was as low as 0.07 ± 0.001. This value is suitable for developing a single mode fiber with a large core diameter at 2µm.

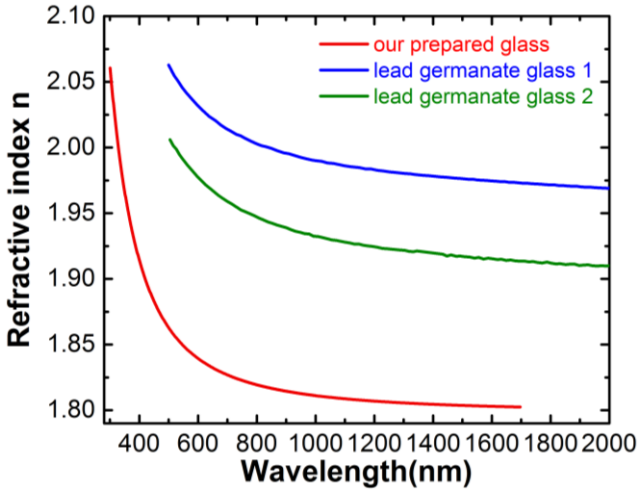

Figure 5. 2 Refractive indexes of in-house developed Tm Germanate glass fiber, lead germanate glasses in[126].

As shown in Fig. 5. 2, the refractive index of Tm germanate glass with respect to wavelength was measured in the visible and near IR region. Based on the measured result, the refractive index could be fitted by Sellmeier equation as in [126]:

$$n^2(\lambda)=1+\sum_{i=1}^{3}\frac{B_i\lambda^2}{\lambda^2-C_i} \qquad (1)$$

And the value of Sellmeier coefficients after fitting are given in table 1. Compared with other germanate glasses doped with lead [126], the refractive index is much lower, therefore, our prepared germanate glass is promising to have lower nonlinear coefficient γ. In summary, the physical properties of germanate glasses (core glass and cladding glass) including glass density, the characteristic temperatures of Tg and Tx in DTA, refractive index at 632.8nm and the CTE, are listed in table 2.

Glass	B_1	B_2	B_3	C_1	C_2	C_3
Tm Germanate	1.03441	0.17048	1.03029	0.0319	0.15771	0.03189

Table 1 Sellmeier coefficients for Tm germanate glass and the calculated RI at 2 μm

	Density(g/cm^3) ± 0.05	Tg(°C) ±3	Tx(°C) ± 3	ΔT(°C) ± 3	*Refractive index at 632.8 nm*± 0.001	*CTE($10^{-6}C^{-1}$)*
Core(Ge_01)	5.38	485	745	260	1.834	7.18

Cladding (Ge_02)	5.11	489	734	245	1.833	6.46

Table 2 Property summary of germanate glasses (Ge_01 and Ge_02) in this work

5.1.2 Absorption and lifetime of germanate glass

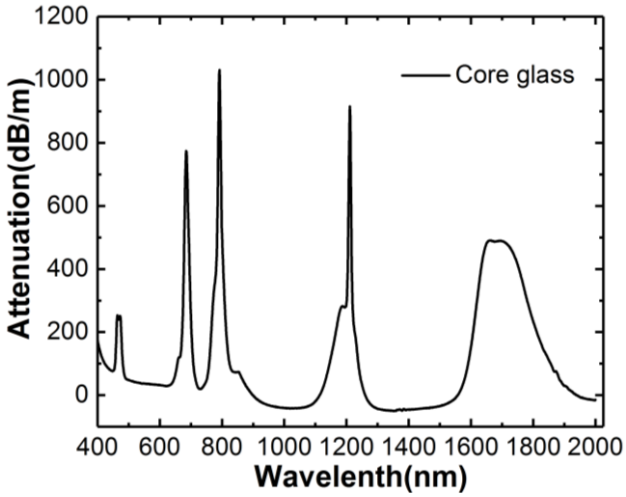

Figure 5. 3 Absorption spectrum of Tm germanate core glass

The absorption UV-Vis-NIR measurement of core glass in the wavelength regions of 400-2000 nm is shown on Fig. 5. 3 The spectrum is characterized by five characteristic absorption bands located at 468 nm, 682 nm, 790 nm, 1210 nm and 1652 nm which can be ascribed to the corresponding transitions from $^3H_6$ ground state to the different excited states $^1G_4$, $^3F_3$, $^3F_2$, $^3H_4$, $^3H_5$ and $^3F_4$ of Tm^{3+}, respectively as shown in Fig.2. 1. In detail, the absorption peaks at 792nm and 1662nm are 1030 dB/m and 490 dB/m respectively, which make the prepared germanate glass a promising candidate for compact fiber devices. Also, the pump sources at 792nm and 1550nm wavelength bands are commercially available.

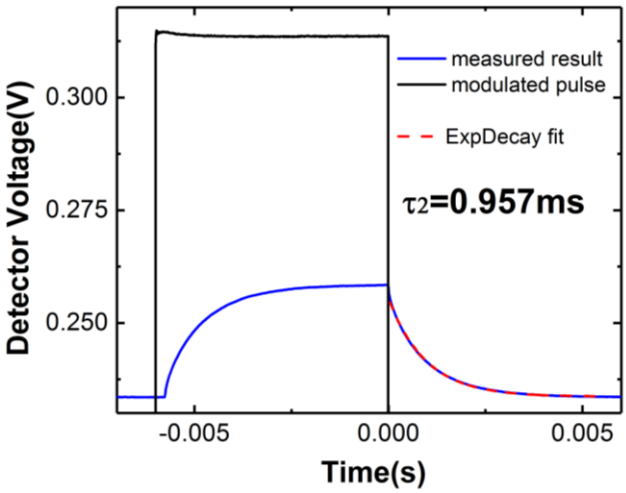

Figure 5. 4 Lifetime measured for the core bulk glass using a 793nm LD

The fluorescence lifetime is defined as $\frac{1}{\tau_{fl}} = \frac{1}{\tau_r} + \frac{1}{\tau_{nr}}$, with τ_r and τ_{nr} corresponding to the radiative and non-radiative lifetime. Because of non-radiative quenching, measured fluorescence lifetime is shorter than that of calculated radiative lifetime by Judd-Ofelt analysis[127]. In addition, the quantum efficiency from level $^3F_4$ to level $^3H_6$ is define by the ratio of $\frac{\tau_{fl}}{\tau_r}$. The fluorescence lifetime from level $^3F_4$ to level $^3H_6$ is usually discrepant, with reported value in the range of 0.67ms-2.25ms for germanate glass fiber, and the corresponding radiative lifetime varies from 2.2ms to 5.3ms as shown in table 3, where the difference in radiative lifetime is expected relating to Tm doping concentration and possibly co-dopants. Moreover, fluorescence lifetime is relates to temperature described by glass multi-phonon energy-gap law. In order to better understand and model the pump and lasing properties of the in-house fabricated Tm germanate glass fiber, it is necessary to characterize the fluorescence lifetime of $^3F_4$ level in advance. In our experiment, the fluorescence lifetime was measured at room temperature, we used a modulated 790nm laser diode by PRO8000 (Thorlabs) temperature controller (TEC) and LD controller with an output of 6-ms-duration pulse as pump, which is coupled to the bulk Tm germanate glass. Moreover, we employed the InGaAs photodetector (PDA10D-EC) to measure the emission fluorescence from the level of $^3F_4$, the modulated pulse pump, fluorescence response and its decay curve are depicted in Fig. 5. 4. And the fluorescence lifetime of fabricated Tm germanate glass fiber was also measured, which was in accord with the reported fluorescence lifetime of Tm germanate glass in table 3. By comparison, the fluorescence lifetime of Tm silica doped glass have a shorter fluorescence

lifetime (0.3ms to 0.7ms) but longer radiative lifetime (4.56ms-7ms). Therefore, Tm germanate glass provide a high quantum efficiency since longer fluorescence lifetime favors population accumulation and generally lower lasing threshold. With the exponential fitting applied to the fluorescence decay curve in Fig 5.4, Tm germanate glass has a lifetime of 0.957ms.

	Glass	**Fluorescence lifetime $^3F_4$ level**	**radiative lifetime (ms)**	**Thulium doping concentration**
Tm: Germanate glass	$61GeO_2$-10ZnO-$3ZnF_2$-15PbO -$4Nb_2O_5$-$6Na_2O$-$0.6Tm_2O_3$-$0.4GdF_2$ (our work)	0.957	--	0.6 mol% ($3\times10^{20}/cm^3$)
	$36Bi_2O_3$-$29GeO_2$-$25Ga_2O_3$ -$10Na_2O$-$1Tm_2O_3$ [122]	1.63	2.25	1mol%
	$36Bi_2O_3$-$29GeO_2$-$25Ga_2O_3$ -$10BaF_2$-$1Tm_2O_3$ [122]	2.25	2.46	1mol%
	$20BaO$-$15Ge_2O_3$-$60GaO_2$ -$3.2(La_2O_3+Y_2O_3)$-$1.8Tm_2O_3$ [49]	0.7	--	1.8mol% ($7.6\times10^{20}/cm^3$)
	--	3 [46]	5.3	$6.24\times10^{20}/cm^3$
Tm_2O_3 Silica	Tm, Al, La [19]	0.3-0.7	4.56-7	$8.4\times10^{19}/cm^3$

Table 3. Comparison of fluorescence lifetime, radiative lifetime, and doping concentration of different Tm^{3+} doped glasses

5.2. Fabrication and characterization of LMA single mode fiber

5.2.1 Optical fiber development

As illustrated in Fig. 5. 5, the rod-in-tube technique is used for fiber fabrication. Firstly, the Ge_02 glass billet was extruded into a tube with an out diameter of 9.5mm and inner diameter of 1.7mm in a funnel through a die channel by force. An initial rod (120mm long and 11.5mm in diameter) of Ge_01 glass was prepared as described in section 4.1. This rod was then drawn into a cane of 1.3 mm in diameter on a drawing tower. The preform was prepared with the Ge_01 glass cane inserted in the Ge_02 glass tube as shown in Fig. 5. 5b, thereafter, the preform was drawn into a fiber of 130 μm at a speed of 5.4 m/min. During the fiber drawing process, the cane did not show any sign of crystallization. For the fabrication of LMA fiber, we have developed a 20 μm core effectively single mode fiber using Ge_01 glass as core and Ge_02

glass as cladding. The physical properties of the obtained fiber is reported on table 4. The fabricated fiber was again pristine with no apparent sign of crystallization. A cross-sectional view of the fiber is shown in Fig. 5. 6a.

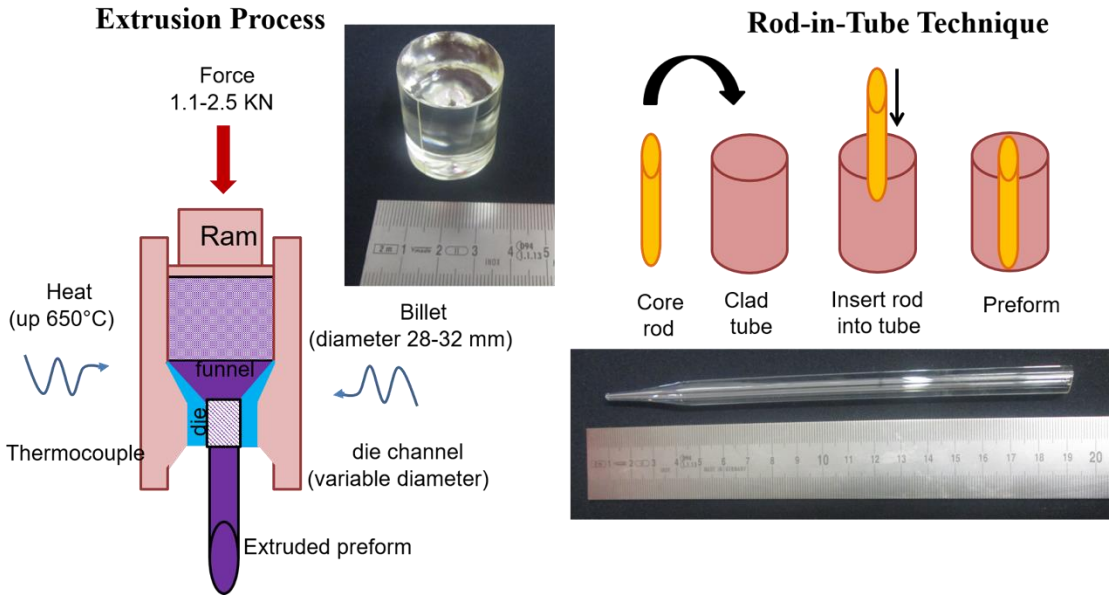

Figure 5. 5 (a) the extrusion process to obtain clad tube (b) illustration of the Rod-in-Tube technique for fiber drawing.

Fiber	$\emptyset_{ext}$[µm] ±1 µm	$\emptyset_{core}$[µm] ±1 µm	*NA* at 632.8 nm
LMA fiber	130	20	0.07

Table 4. Ge_01 core glass with a Ge_02 glass cladding

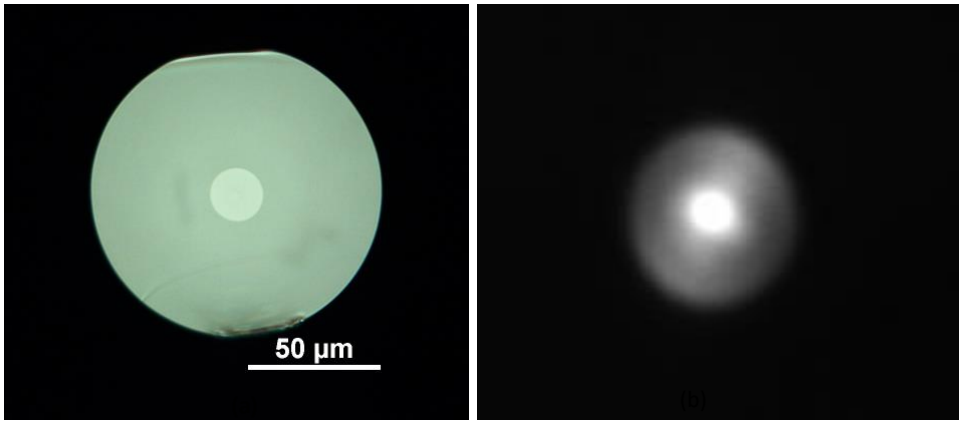

Figure 5. 6(a) Transmission micrograph and (b) near field imaging through a 4.8m length of fiber made from our prepared Tm germanate glass

5.2.2 Fiber background loss of Tm germanate glass fiber

The LMA fiber was successfully developed in-house using the rod-in-tube technique. As one can see on Fig. 5. 6a, there are no signs of residual stresses or bubbles at the interfaces between the core and cladding, which demonstrates the compatibility of these glasses and their CTE and the goodness of the drawing process. The background loss of the fiber was assessed by the cut-back technique using a laser source operating at a wavelength of 980 nm over a length of 5.3 m. The attenuation was calculated through a linear fit of the experimental data. The measured loss of 1.14 dB/m, confirming the absence of crystallization, otherwise it would have induced a significantly higher loss value. It also indicates that the glass can withstand the double thermal cycle necessary for fiber fabrication, without crystallizing. Moreover, a white light source is used to measure the background loss of the fabricated Tm germanate glass fiber also using cut-back technique, and the corresponding background loss is around 0.96 dB/m, which is in accord with the value measured by 980 nm laser diode.

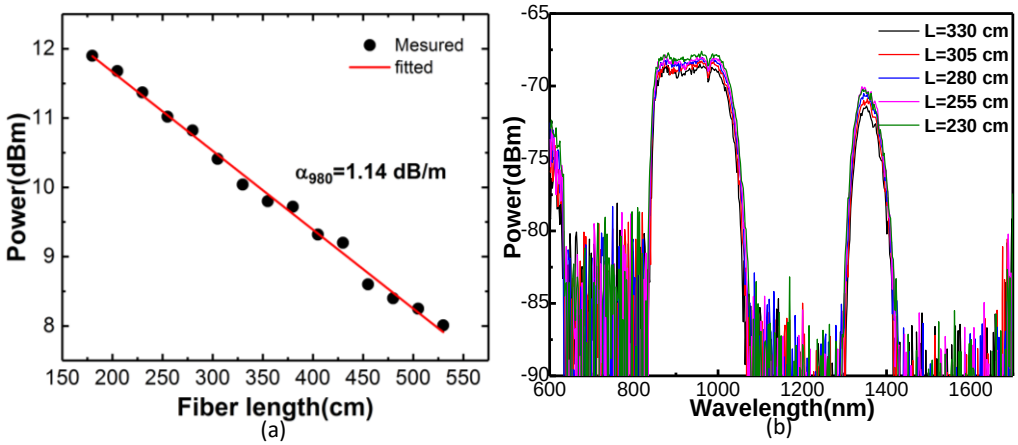

Figure 5. 7 (a) Fiber loss measured by the cut-back technique at 980nm; (b) the measured transmission curves for fabricated Tm germanate glass fiber based on cut-back methods using a white light source.

5.2.3 Absorption and emission cross-section of Tm germanate glass fiber

For the fabricated Tm germanate glass fiber, absorption measurement was first conducted by supercontinuum source (Fianium) by cutting-back technique. It could be found from Fig. 5. 8 that the transmission curves for the tested Tm germanate fiber have the characterization of oscillation below 1800nm, originating from the interference between LP_{01} and LP_{11} mode. Moreover, when fiber length is 8.9 cm, the transmission curve is overlap with the noise level of OSA because of the high absorption spanning from 1600nm to 1800nm. By calculation, the

absorption is around 500dB/m at 1700nm, which is very close to the value calculated in core glass in Fig. 5. 3, i.e. 490 dB/m.

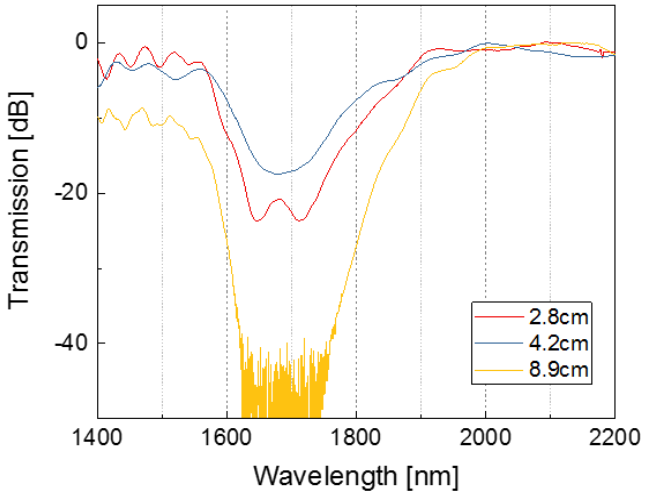

Figure 5. 8 Tm doped Germanate glass fiber absorption tested with a SC source. (Both ends of Tm Germanate fiber spliced with SMF)

Absorption and emission cross-sections are very important spectroscopic properties of in-house developed Tm germanate glass fiber for the evaluation of laser performance from level $^3F_4$ .Given absorption and Tm^{3+} doping concentration; it is straightforward to calculate the absorption cross section. Assuming the in-house developed Tm germanate glass fiber with a step-index refractive index profile, absorption cross-section could be calculated by equation (1). Moreover, based on the measured fluorescence and reasonable estimation of radiative lifetime (2.4ms) by Judd-Ofelt analysis, the emission cross-section could be calculated by equation (2) in Chapter 3.5.

As depicted in Fig. 5. 9a, the peaks of absorption and emission cross-section are located at 1660nm and 1875nm respectively. Compared with Tm^{3+} doped silica glass [20], the emission cross-section peak of in-house developed Tm Germanate glass is higher, around $7.06\times10^{-25}m^2$, which is comparable with those of Tm Germanate glasses in[122][49].i.e. $5.95\times10^{-25}m^2$ and $7\times10^{-25}m^2$.Furthermore, the gain coefficient form the $^3F_4 \rightarrow {}^3H_6$ transition could be calculated by equation (3) in Chapter 3.5.

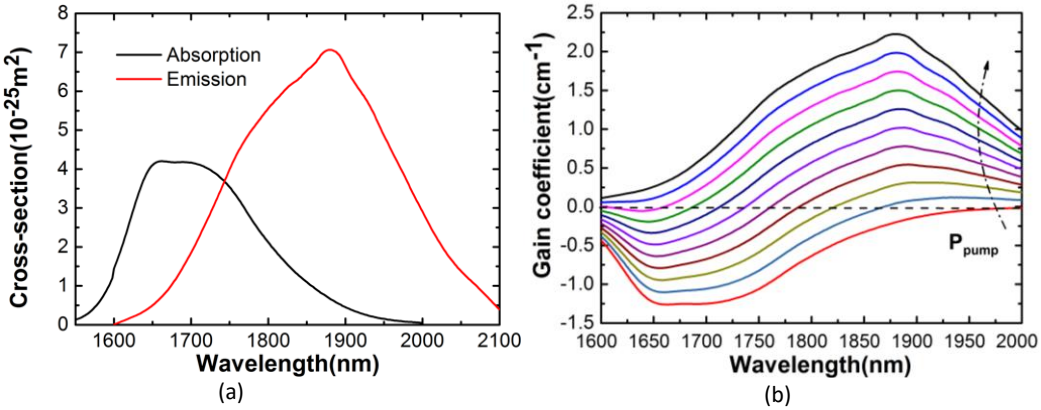

Figure 5. 9(a) Absorption and emission cross sections (b) the calculated gain coefficient of the core glass for different population fractions in level $^3F_4$.

As shown in Fig. 5. 9b, ideally, fluorescence of Thulium germanate glass covering from 1600nm to 2000nm and beyond. The calculated gain coefficient of core glass is also shown for population fraction *p* in level $^3F_4$ ranging from 0 to 1 with a step of 0.1. Note that *p* is expected to be higher than 0.1 to have a positive gain in the wavelength range from 1893 to 2050 nm, indicating that a low pumping threshold will be required for 2.0 μm laser operation in the Tm^{3+} doped germanate fiber. Furthermore, the maximum gain coefficient reaches 2.11cm^{-1}at 1878nm, which is larger than that of Tm^{3+}-doped silicate glass(1.5 cm^{-1}), showing promising applications for efficient 2.0 μm fiber lasers[128]. Considering the quasi-three-level behavior of Tm^{3+} dopant in the transition from $^3F_4 \rightarrow {}^3H_6$, it is difficult to achieve amplification and lasing in short wavelength region below 1700nm because of reabsorption. On the other hand, gain saturation effect resulted from amplified spontaneous emission (ASE) in the region from 1800-1900nm, limiting the emission at longer wavelength beyond 2050nm.

5.2.3 Effective mode area of Tm germanate glass fiber

Given the Sellmeier coefficient of refractive index in Tm germanate glass and the waveguide structure of the in-house developed Tm germanate glass fiber, we are able to calculate the mode effective area (A_{eff}) using the finite element model (COMSOL Multiphysics) to calculate the electric field of fundamental mode propagation along the fiber. As shown in Fig. 5. 10, the effective mode area increases from 368μm^2 to 397μm^2 in the wavelength region from 1900nm to 2050nm, corresponding to an effective mode diameter increment from 19.18μm to 19.92μm, and the simulation result also shows that Tm germanate fiber only supports fundamental mode with electric field shown in the inset of Fig. 5. 10, meanwhile the single-mode feature of Tm germanate fiber is verified by the V-number, decreasing from 2.3 down to 2.15 in the

wavelength region from 1900nm to 2050nm , smaller than single-mode cut-off V-number value of 2.405.

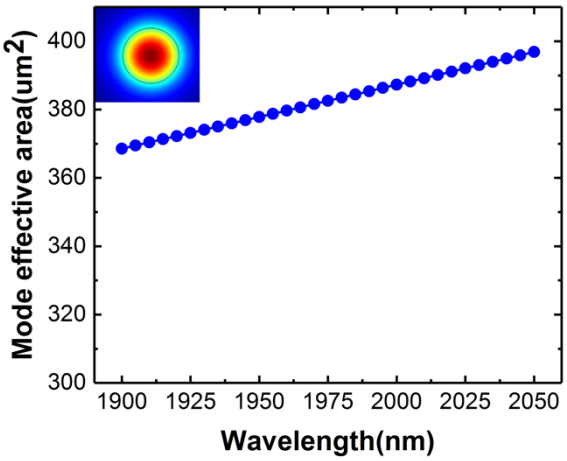

Figure 5. 10 The calculated effective mode area versus wavelength at 2μm waveband

5.2.4 Fiber laser performances

With fiber characterized as above, the lasing efficiency is tested. As shown in Fig.5. 11, the fiber laser cavity was implemented using a 14.1 cm long section of as-drawn Tm^{3+} doped germanate fiber. The cavity feedback incorporated a high reflectivity FBG centered at 1952 nm and a Sagnac loop mirror as an output coupler. The cavity was in-band pumped using a 1565nm fiber laser with the pump beam coupled into the doped fiber through a broadband WDM operating at 1550/1850 nm wavelength. Importantly the silica and in house germanate fibers used to construct the cavity were fusion spliced together to allow the construction of a monolithic all-fiber cavity. However, the splicing loss between Tm^{3+}-doped germanate fiber and single mode silica fiber (SMF28) is high because of the difference in melting temperature and core size mismatch. With optimization of the splicing parameters of fusion splicer (FujikuraFSM-45PM), the splicing loss is decreased. And the measured loss was in the range of 1.5-2.5dB, even if using the same splicing recipe, which is probably due to the varying cleaving angle. The splicing losses of two splicing samples (SMF-TGF-SMF) with respective TGF length of 1.3cm and 12.2cm are measured by 1300 nm ASE source, as shown in Fig.5.12a, the total average splicing losses for two samples are 3dB and 5dB respectively from 1300nm to 1350nm, and the high loss around 1250nm originates from the absorption transition from level 3H6 to level 3H5. Moreover, the spectral oscillation as shown in Fig. 5. 12a is from the interference between LP01 and LP11 modes guided around 1300nm for TDF, which is not an issue at 2μm waveband for TGF only supporting LP01 mode. Despite the relatively high intra-

cavity losses, the laser slope efficiency was measured to be 8.75 % with lasing spectrum shown in inset of Fig. 5.12 b. Considering the 2 dB splicing loss we estimate an "effective" slope efficiency value of 16.17 % regarding to real absorbed pump power, which is very promising considering the large potential for improvements spanning material synthesis, through to fiber and laser cavity design.

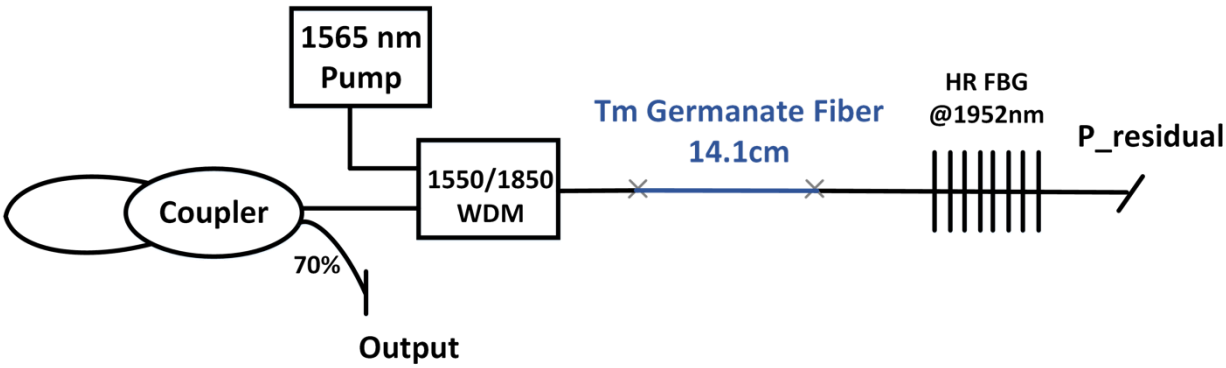

Figure 5. 11 Schematic diagram of all fiber Tm doped Germanate glass fiber laser

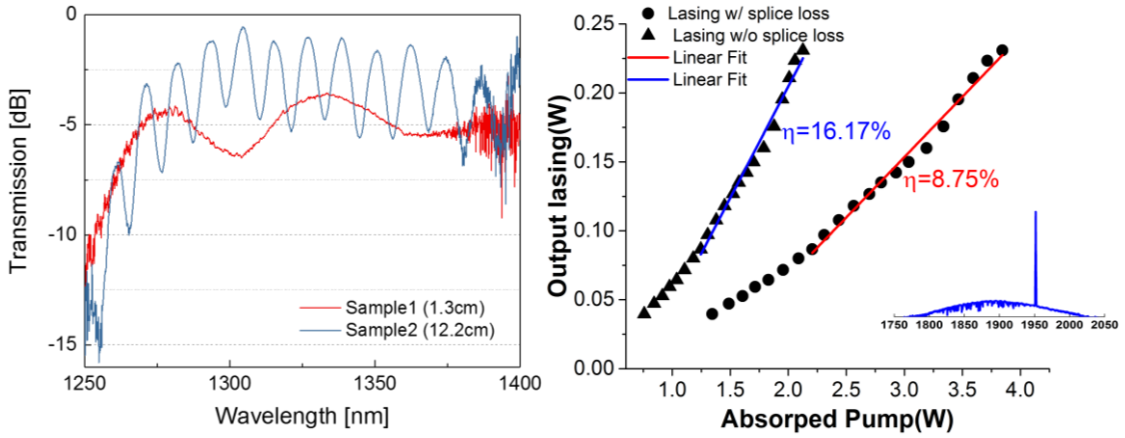

Figure 5. 12 (a) The total splicing loss with configuration SMF-Tm Germanate glass fiber-SMF; (b) Laser output power as a function of the absorbed pump power with a length of 14.1cm fiber

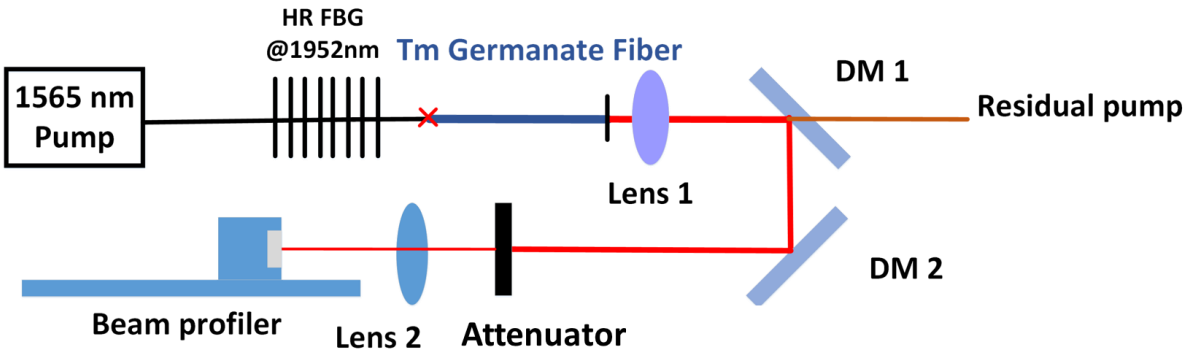

Figure 5. 13 Schematic diagram of experimental set-up for highly Thulium doped Germanate fiber laser

Because of the non-negligible splicing loss between Tm germanate fiber and SMF and the insertion loss in WDM, we propose the experimental scheme as shown in Fig. 5. 13, i.e., one-end core-pumping configuration coupled through high reflectivity fiber Bragg grating FBG instead of WDM. An in-house built Erbium-ytterbium co-doped fiber laser performed as pump power. The laser cavity was implemented using a 21cm long in-house fabricated Tm^{3+} -doped germinate glass fiber. One end of Tm^{3+} -doped germinate glass fiber was fusion spliced with the SMF pigtail of a high reflectivity FBG centered at 1952nm with a FWHM of 0.12 nm, and the other end facet of Tm^{3+} -doped germinate glass fiber was perpendicularly cleaved with a Fresnel reflection of approximately 5%, which functioned as partially reflective mirror of the laser cavity. Given that the FBG is wavelength selective, the 1565nm pump was coupled through the FBG without introducing additional passive component loss. Collimated light after aspheric lens with focal length of 15mm was splitted into residual pump and output signal by 45° dichroic mirror with high reflectivity at 2μm and high transmission at 1565nm. An additional dichroic mirror was used to filter the signal output beam. The output characteristics of laser and residual pump were measured using a thermal power meter (Ophir 3A-FS) and a Yokogawa OSA (AQ6375) with a resolution of 0.1nm.

Since the FBG is wavelength selective at 1952nm with narrow bandwidth, lasing efficiency could be maximized with the optimization of Tm^{3+} -doped germanate glass fiber length. When fiber length is ~21cm, the ASE peak was around 1952nm. As shown in Fig. 5. 14, the threshold pump power was around 0.3 W, and the fiber laser yielded a maximum output power of 1.52W with a slope efficiency of 38.7% regarding to the launched pump power. Considering the residual pump power and 1 dB splicing loss between Tm^{3+} -doped germanate glass fiber and SMF resulting from mismatch of mode field diameter, the effective slope efficiency regarding to absorbed pump was estimated to be 55.9%, marking the highest slope efficiency and highest

laser above 1.5W for Tm^{3+}-doped germinate glass fiber incorporating core-pumping scheme. It could also be seen that the OSNR of laser output was higher than 55 dB and the 3 dB bandwidth of laser lines was< 0.2nm.

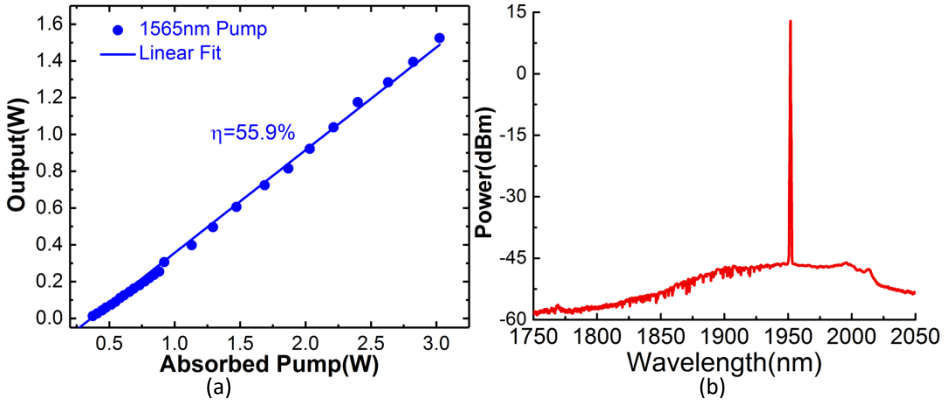

Figure 5. 14. (a) The laser output power versus absorbed pump power; (b) the lasing spectrum at 1952nm for 21.1 cm TGF.

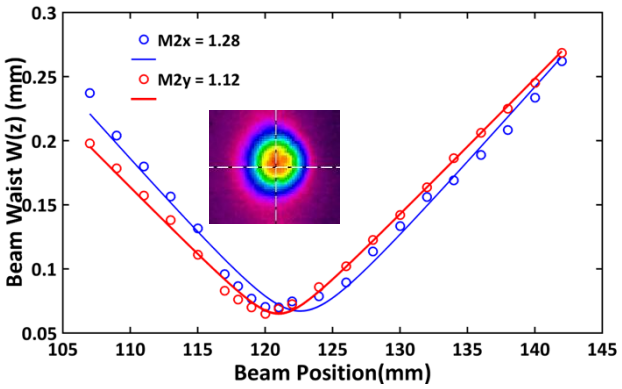

Figure 5. 15 Measured beam quality of the output beam, and the far field beam profile is shown in inset

To confirm its beam quality of the house-drawn fiber, the M^2 factor was measured. When laser output power was 1 W with the launched pump power of 3.01W, an attenuator was included after DM2 to attenuate the signal power to 50 mW before reaching the beam profiler from NanoScan (NS2s-Pyro/9/5-STD) and beam-profiling camera (Pyrocam iii) when measuring beam propagation factor M^2 and far field beam profile respectively. The M^2 factor was measured by focusing the laser beam with a 100 mm aspheric lens and by moving the beam profiler through the focus. The M^2 factor was determined by performing a hyperbolic fitting to the square of beam width along two perpendicular direction, i.e. M^2_x =1.28 and M^2_y=1.12. Such values confirm that the fabricated Tm^{3+} doped germanate LMA fiber operates as a single mode fiber dominantly.

Lasing wavelength (nm)	Doped level	Core diameter (μm)	λ_{Pump} (nm)	Output power (mW)	Slope efficiency	Reference
1950	($7.6*10^{20}$ /cm^3)	9.2	1568	160	17%	[49]
1950	2.8wt% ($4.5*10^{20}$ /cm^3)	8.6	1568	206	34.8%	[29]
1935	1wt%	~10	1560	318	21%	[129]
1740-2017	2 wt %	7	805	50	35%	[30]
1950	2.8 wt%	Not available	1568	102.5	24.7%	[130]
1950	5wt% ($7.6*10^{20}$ /cm^3)	Not available	1610	617	42.2%	[131]
1952	**($3*10^{20}$ /cm^3)**	**20**	**1565 nm**	**1500**	**55.9%**	**Our result**

Table 5. Summary of cw fiber laser based on TGFs, all the slope efficiencies in the table above are w.r.t. absorbed pump power for the in-band core-pumping scheme.

For comparison, the works based on Tm germanate glass fiber are summarized in table 5. All the works based on single-cladding Tm germanate glass fiber are demonstrated using core-pump configuration by in-band fiber pumping or 805nm LD pumping with low output power. However, one prominent advantage for Tm germanate glass fiber is very highly Tm^{3+}-doped, which could be 10 times higher than silica glass fiber without significant clustering. On the other hand, the cross-relaxation will be facilitated with the increment of Tm doping concentration, particularly when pumped at around 790 nm, which promotes higher lasing efficiency through the one-for-two effect. With a commercially available high power 790 nm laser, cladding pumping scheme will be the choice to get high power at 2 μm waveband for Tm

germanate glass fiber. Therefore, in the following section of this chapter, we will study the double-cladding Tm germanate glass fiber.

5.3 Double-clad Tm germanate glass fiber (TGF)

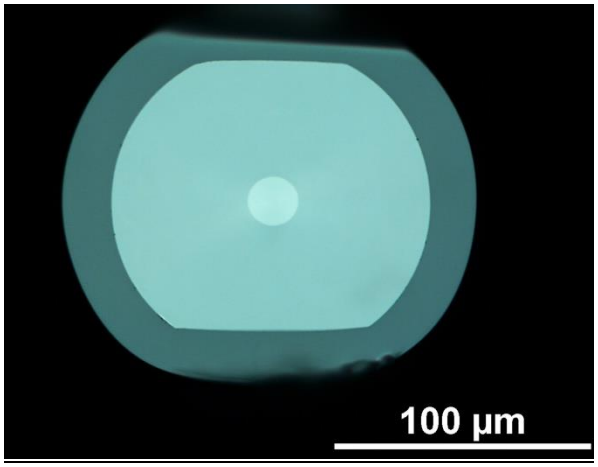

Figure 5. 16 Transmission micrograph of double-cladding germanate glass fiber

The core glass and inner cladding glass of the prepared double cladding Tm germanate glass fiber follow the same composition and fabrication procedure as the single-cladding Tm germanate glass fiber, i.e. Ge_01 as core glass and Ge_02 as inner-cladding glass. And the inner cladding is polished to obtain the double D-shape for cladding pump scheme. During fabrication, the outer cladding glass is crystallized to have a robust fiber structure. Together with the prepared core/inner cladding germanate glass, first trial D-shape double-cladding Tm germanate glass fiber is fabricated, with the cross-section view shown in Fig. 5. 16. Based on the same lasing scheme shown in Fig. 5. 13, lasing performance of double-cladding TGF core-pumped by 1565 nm fiber laser was tested with a slope efficiency of 40% regarding to the absorbed pump power, which is smaller than 55.9% of single cladding Tm germanate glass fiber as shown in Fig. 5. 14(a). As abovementioned, the core/inner-cladding glasses of double-cladding TGF are made of the same core/cladding compositions of the single-cladding TGF, therefore, we would like to explore the reason why the slope efficiency is decreased in the double-cladding TGF. A 980nm LD is used as pump source, which is coupled into the core of single-cladding or double–cladding TGF, the near field from the other end of fiber is measured by camera (Xeva XC-130). For the single-cladding TGF, fundamental mode as depicted in Fig. 5. 17(a) and LP11 modes as depicted in Fig. 5. 17(b) and (c) could be extracted separately by adjusting coupling into core of TGF. However, for the double cladding TGF, only distorted mode as shown in Fig. 5. 17(d) was able to be extracted, which seems to indicate refractive index variation resulting from unbalanced mechanical stress between crystallized outer-cladding and double D-shape inner-cladding. Therefore, the overlap amongst pump mode, lasing mode and doping distribution for double-cladding TGF is decreased as compare with the single-cladding TGF, resulting in a smaller lasing slope efficiency. Moreover, as shown in Fig. 5.17, all the

mode profiles are slightly elliptical even though the core area shown in Fig. 5. 16 is circular, verifying the slight difference of M^2_x and M^2_y measured in section 5.2.

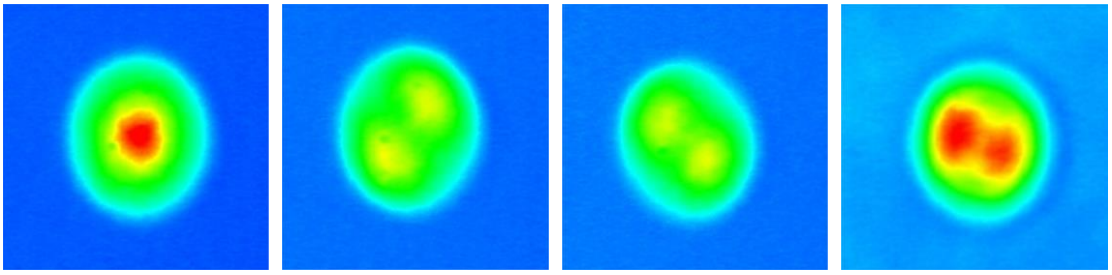

(a) (b) (c) (d)

Figure 5. 2(a) the extracted fundamental mode and (b), (c) the LP11 modes from single-clad TGF; (d) The extracted distorted mode from double-cladding TGF.

5.3.1 Tunable double-cladding TGF amplifier

Silica-based TDFAs is successfully demonstrated spanning from 1650nm to 2050nm[77][132], and the application of TDFA is demonstrated in 2 µm optical communication system[133]. Considering the capability of high Tm^{3+}-doping concentration in germanate glass, an ultra-short fiber amplifier could be an interesting application with the TGF. Even with the disturbed mode profile guided in our fabricated first generation double-cladding TGF, it is still valuable to explore its amplification in the 2 µm waveband. As illustrated in Fig. 5. 18, the schematic of our experimental setup included the in-house tunable laser source spanning from 1750 nm to 2000 nm with output power above 100 mW. A variable optical attenuator was utilized to obtain small signal (-20 dBm) and saturated signal (0 dBm) as input seed after tunable laser source. An isolator was used to suppress the unwanted feedback into the tunable laser source. We used a 21 cm double-cladding TGF in the experimental setup as shown in Fig 5. 18, which was core-pumped by 1565nm fiber laser with power of 800 mW. WDM couplers were used to combine and split the signal and pump at the input and output ends respectively. The output characteristics of laser and residual pump were measured using a thermal power meter (Ophir 3A-FS) and a Yokogawa optical OSA (AQ6375) with a resolution of 0.5 nm.

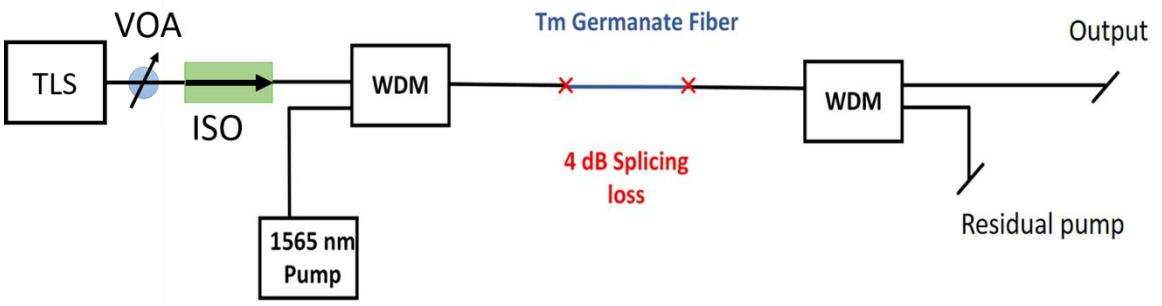

Figure 5. 18. The experimental setup of TDFA pumped by 1565nm fiber laser incorporating 21cm double clad germanate glass fiber. TLS: tunable laser source; VOA: variable optical attenuator; ISO: isolator; WDM: 1550/2000nm wavelength division multiplexer.

As shown in Fig. 5. 19(a), the average splicing loss of SMF-TGF-SMF is estimated to be 4 dB, . Then the estimated coupled pump power is around 500 mW. The external small signal gain and saturated signal gain are shown in Fig. 5.19b. The external gain peak of small signal and saturated signal both located at 1930 nm with the gain value of 12 dB and 10 dB respectively, and the 8 dB gain bandwidths for small signal and saturated signal are 100 nm and 75 nm respectively. Fig. 5. 19(c) and 19(d) show the amplified small signal and saturated signal spectra. For small signal spectra, the in-band OSNR across the amplified wavelength region varies from 30 dB to 35 dB. And the amplified saturated signal has a 45-50 dB OSNR. With the 4 dB splicing loss included, the gross gain of the small signal and saturated signal will be improved 4 dB thoroughly from 1880nm and 2000nm. On the other hand, the disturbed mode profile as shown in Fig. 5. 17(d) indicates that the gain coefficient of double-cladding TGF will decrease because of deteriorated spatial overlap between mode profile and doping distribution, thus making gain value decrease.

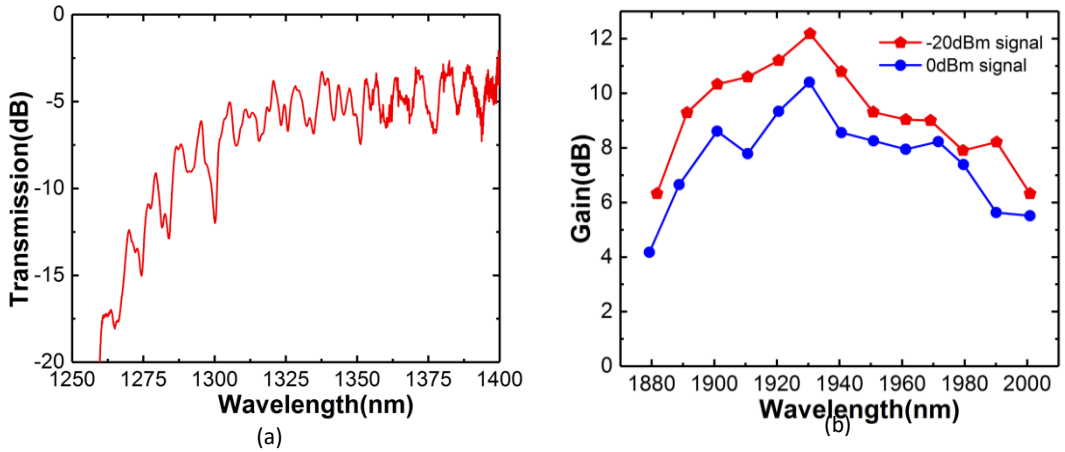

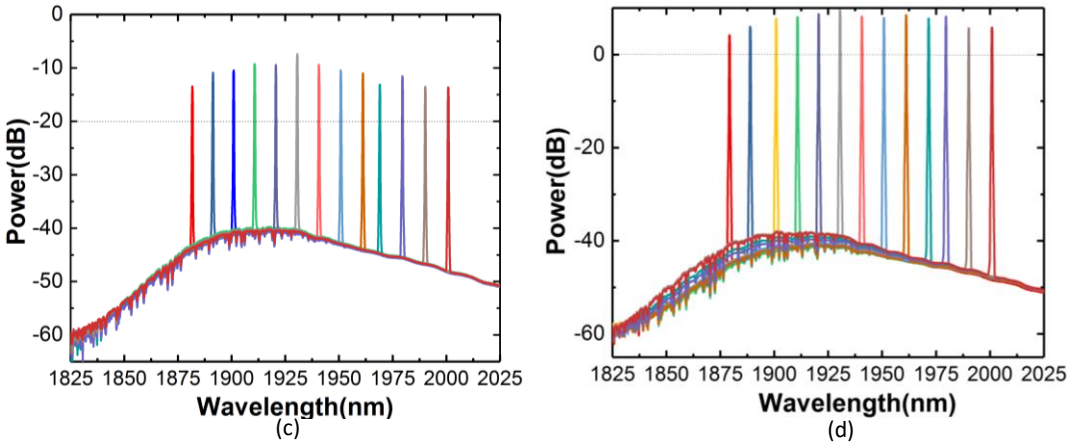

Figure 5. 19(a) The total splicing loss of SMF-TGF-SMF measured by ASE source with central wavelength at 1300n. (b) Gain performance of TDFAs for small signal and saturated signal spanning from 1880nm to 2000nm. (c) and (d) are the output spectra for small signal (-20dBm) and saturated signal (0dBm) respectively, measured with 0.5nm spectral resolution.

5.3.2 Master-oscillator power amplifier

Recently, ultrashort laser pulses at 2μm have attracted incremental interest in many application such as surgical operation, remote sensing and LIDAR. Compared to the achievement of ultra-short pulse in the wavelengths of 1 μm and 1.55 μm, the pulse energy of 2 μm fiber lasers still remain at a low level in mode-locked fiber laser regimes because the available Tm^{3+}-doped fibers still locates at the anomalous dispersion at 2 μm. Due to pulse breaking issue in conventional soliton in high power regime, researchers have contributed to build dissipative soliton by laser cavity dispersion management, thus giving an overall normal dispersion cavity even though the gain medium of Tm-doped fibers exhibit an anomalous dispersion. Based on this mentioned strategy, dispersion compensating fibers are employed to realize normal dispersion in laser cavity, however, the energy level of dissipative soliton at 2μm is still comparable to conventional soliton. However, Huang et al demonstrated with simulation and experiment that a dissipative soliton with higher energy was possible by shortening gain fiber length, which help separately control dispersion and nonlinearity [134]. Fortunately, the heavily TGF possesses a much higher gain coefficient with high Tm^{3+}-doping concentration compared with silica-based fiber. Therefore Tm^{3+}-doped TGF will be an alternative approach to achieving high energy dissipative soliton.

On the other hand, driven by the requirement of high power fiber laser, MOPAs are progressed to-date to achieve high power based on multi-stage amplification scheme. Usually, a MOPA system includes master oscillator, preamplifiers and main power amplifier. For main

power amplifier, LMA active fibers are employed with cladding pump scheme. In this section, we build a picosecond all-fiber MOPA system incorporating our in-house fabricated LMA (20 μm core) double-clad TGF as the gain fiber of power amplifier. The schematic setup of the fiber MOPA system is shown in Fig. 5. 20. Firstly, a SESAM passively mode-locked Tm^{3+}-doped fiber laser with a repetition rate of 13.5MHz and pulse duration of 38 ps constructs master oscillator for the MOPA system as a seed source. The output power of seed source is 3 mW, corresponding to an energy value of 0.22 nJ. In addition, three 2μm isolators were used to ensure the unidirectional operation avoiding the damage from backward reflection light. Before preamplifier, a 30 m dispersion compensating fiber (DCF38, Thorlabs) was used as a pulse stretcher to reduce the peak power of seed source. At the first stage of preamplifier, 1560 nm fiber laser was coupled into the core of the 0.6 m single mode Tm^{3+}-doped fiber (OFS TmDF200 5/125μm) through 1550/2000 WDM with low insertion loss. The output power after the first stage preamplifier is 102 mW. At the second stage of preamplifier, 1.8 m double-clad Tm^{3+}-doped fiber (Nufern PM-TDF-10/130μm-HE) was used as gain fiber with a cladding absorption of 4.7dB/m at 793nm. Moreover, cladding pump stripper (CPS) was used to strip out the residual pump, and we obtained an amplified pulse with power of 1W. Finally, at the main power amplifier stage, we incorporated the in-house TGF with 21 cm length. The cladding absorption of Tm^{3+} double-clad TGF is 407 dB/m at 793nm with background loss of 2 dB/m in the inner cladding. One end of Tm^{3+}-doped double-clad TGF is fusion spliced to the pigtail of (2+1) ×1 combiner with a splice loss of 2dB, and the other end of double-clad TGF is angle-cleaved. The collimated laser output power after 100 mm aspheric lens is measured from the reflection end of dichroic mirror (800nmHT/2000nmHR) using a thermal power meter (Ophir 3A-FS). And the laser pulse was monitored by the 2×2 5/95 coupler, where the spectrum was measured using Yokogawa optical OSA (AQ6375) with a resolution of 0.5nm. The pulse width of laser output after the power amplifier is 57 ps measured by autocorrelator (APE pulse check), and the maximum output power is 3.7 W at the pump power of 14 W, corresponding to the energy of $0.27\mu J$ and peak power of 47.37 kW. As shown in Fig. 5. 21(b), by increasing the pump power from 2W to 14W, the output power increases from 1.15W to 3.7W with a slope efficiency of 21.6%. Comparing the spectra of dissipative soliton seed source and output laser after power amplifier as depicted in Fig. 5. 21(a), there is still no mode instability sideband. And the OSNR of seed source and output laser both kept at around 20dB.

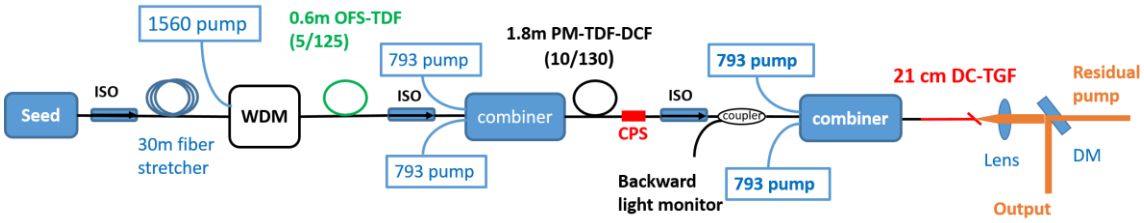

Figure 5. 20 Experimental setup of a pulse-MOPA system incorporating double-clad TGF. ISO: isolator; WDM: wavelength division multiplexer; CPS: cladding pump stripper; DM: dichroic mirror

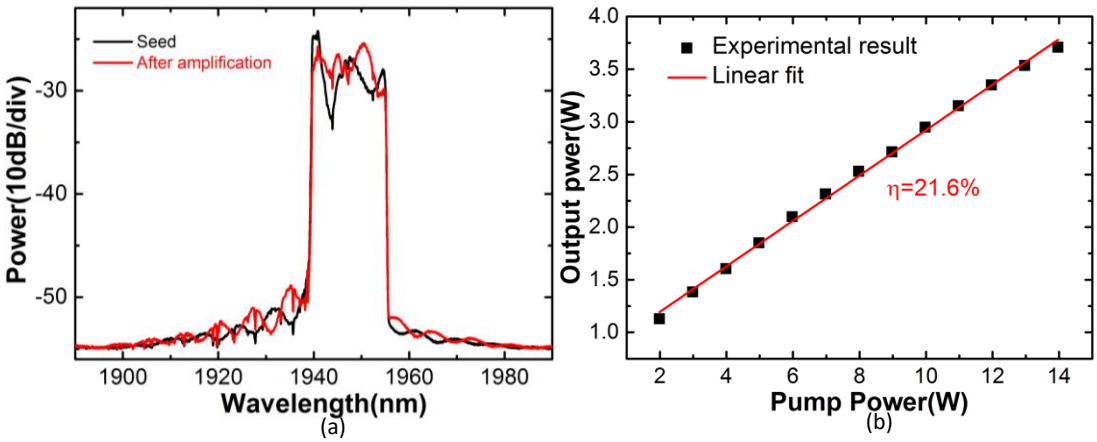

Figure 5. 21(a) the spectra of seed source and laser output after MOPA system. (b) The output power of MOPA system versus the launched pump power.

Chapter 6 Conclusion and Future works

The work in this thesis comprise fiber lasers and optical fiber amplifiers mainly based on two in-house fabricated TDFs, i.e., lowly Tm^{3+}-doped germanosilicate fiber (or namely Tm/Ge co-doped fiber) and Tm^{3+}-doped germanate glass fiber. Given the difference of glass composition and Tm^{3+}-doping concentration, the aforementioned two Tm^{3+}-doped fibers have distinct performances yet are both promising in the applications of fiber lasers and fiber amplifiers.

6.1 Tm/Ge co-doped fiber based applications

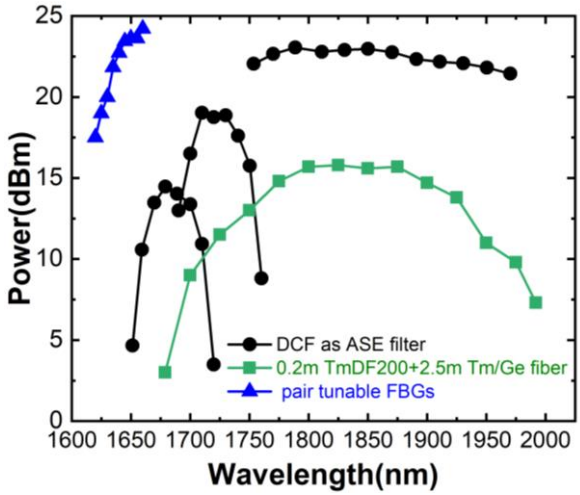

Figure 6. 1 Summary of output powers and wavelength coverages for different laser configurations incorporating Tm/Ge co-doped fiber, which are all included in this thesis

Due to the lowly Tm^{3+}-doping but highly germanium-doping concentration, Tm/Ge co-doped fiber exhibit a blue-shifted absorption and emission cross-section, assisting lasing and amplification in short wavelength region (<1700nm). In Chapter 4, various tunable TDFLs in CW regime are demonstrated in different laser configurations with the combined lasing wavelength covering from 1620nm to 1992nm as illustrated in Fig. 6. 1. The lasing wavelength of TDFL could be tuned down to 1620nm, to my best knowledge, this is to-date the shortest lasing wavelength by silica-based TDFs. Meanwhile, the wavelength of 1620nm is the L-band edge of silica-based EDFA. Moreover, the operational wavelength of tellurite-based EDFA could reach the wavelength of 1634nm. On the other hand, the state-of-the-art TDFAs could cover the wave band from 1650nm to 2050nm. Considering the blue-shifted emission feature of the in-house fabricated Tm/Ge co-doped fiber, therefore, I have built a Tm/Ge co-doped fiber amplifier with the operational wavelength from 1628nm to 1655nm, exhibiting a small signal gain of 17.2 dB at 1655nm. As shown in Fig. 6. 2, I have summarized the performances of the Tm/Ge co-doped fiber amplifier and the state-of-the-art EDFA as well as TDFA with

respect to gain and NF. In pulse fiber laser regime, by using a chirped FBG based band-pass filter with bandwidth of 20nm at 1650nm, I have demonstrated a to-date the shortest wavelength mode-locked TDFL at 1650nm waveband operated as soliton and noise-like pulse, showing as a great potential in OTC and deep-issue multiphoton imaging [8].

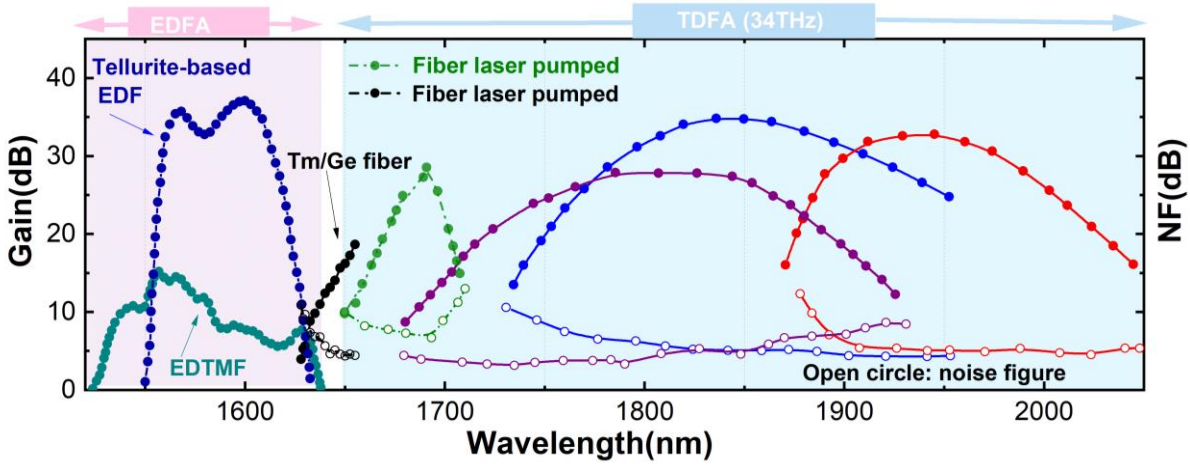

Figure 6. 2 summary of the gain and NF performance of TDFA incorporating the Tm/Ge co-doped fiber and TDFAs in [77] [132]as well as EDFAs from literatures, including [135]. Particularly, EDTMF refers to Erbium-doped tellurite based microstructure fiber (purple dotted line)[15].

Based on Tm/Ge co-doped fiber, it is exciting that the operational wavelength of TDFA have been pushed below 1650nm with short wavelength limit down to 1628nm, in addition, shortest wavelength operations of tunable TDFLs and mode-locked TDFL in soliton and noise-like pulse regimes have been reported. In order to improve the lasing efficiency and TDFA gain performance below 1.7μm, particularly at wavelength < 1650nm, potential design strategies could be implemented as follows: first, Tm^{3+}-doping and germanium-doping concentration in silica glass could be optimized with better performance below 1.7μm. Secondly, distributed long wavelength ASE filter is promising for efficient lasing below 1.7μm, such as co-dopant based ASE filter by doping terbium in cladding region and waveguide based ASE filtering (eg.,W-type fiber), therefore, efficient lasing and improved TDFA gain at short wavelength below 1.7μm or even 1650nm is realizable core-pumped by laser diodes. Particularly, 790nm laser diode pumping is a proper option due to its much higher pump absorption than that of 1.55μm band, thus short gain fiber is needed to minimize reabsorption. Moreover, higher 790nm pump power could be realized using two 790nm laser diodes by polarization beam combiner. On the other hand, with the improvement of passive devices with lower insertion loss, noise figure could be lowered. Therefore, efficient TDFL and TDFA with higher gain, lower noise below 1.7μm or even 1650nm can surely be envisaged.

6.2 Tm^{3+}-doped germanate glass fiber (TGF) based applications

By using the in-house fabricated LMA TGF with novel multi-oxide composition ($61GeO_2$-$15PbO$-$10ZnO$-$3ZnF_2$-$6Na_2O$-$4Nb_2O_5$-$1GdF_2$), I have demonstrated a 1.5 W TDFL at 1952nm when core-pumped at 1565nm. For this CW fiber laser at 1952nm, a high slope efficiency of 55.9% with respect to absorbed pump power and nearly diffraction-limited beam quality have been achieved. In addition to the promising performance of single clad LMA TGF, a D-shape double-clad LMA TGF have been proposed to explore the capability of high power pulse fiber laser at 2μm. Based on the fabricated double-clad TGF, a TGF based amplifier spanning from 1880nm to 2000nm has been demonstrated with peak gain of 13dB and 10dB at 1930nm for small signal and saturated signal respectively. Furthermore, with dissipative soliton as seed, I have also reported a pulse-MOPA fiber system incorporating double-clad LMA TGF as main amplifier. As a result, the output power of pulse is 3.7W, corresponding to peak power of 47.37kW with pulse duration 57ps.

Regarding to the fabricated TGF, the lasing performance could be further improved by using optimized fiber length of TGF used in the setup shown in Fig. 5. 13, based on the model in[45], numerical modelling could be conducted using RP fiber power to verify the experimental result. It can be seen that, when pumping by 1565 nm, the simulated slope efficiency gets to be 58.5% making the simulation and experiment results in good agreement. In the same simulation model with pump power of 4W, lasing output is investigated with respect to fiber length as depicted in Fig. 6. 3b. it shows that lasing is generated at the length of 5 cm, and it is obviously found that the maximum output power at 1952nm increases gradually when fiber length increases from 5cm to 40cm with maximum output power of 2.08W. Because of the quasi-three-level behavior between the level of $^3H_6$ and $^3F_4$, output power decreases as expected with fiber length increasing further. In addition, simulation shows that in the L-band from 1565nm to 1610nm with same pump power, pumping at longer wavelength will have a higher output power with higher slope efficiency; however, high power fiber laser beyond 1565nm is not available so far for demonstration. Therefore, cladding-pump by 793nm will an effective approach to achieve high output power with high slope efficiency considering the high Tm_2O_3 doping. And for the first generation D-shape double-clad TGF, despite that the mode profile is distorted as shown Fig. 5. 17d, a slope efficiency of 21.6% is achieved at the power amplifier stage regarding to the launched pumped power. To suppress mode profile distortion, a double-clad TGF with hexagonal cladding is proposed to improve laser and amplifier performance. Moreover, the multi-oxide glass composition of our prepared glass could be optimized to

achieve higher Tm_2O_3 doping concentration for ultra-short (a few cm) fiber devices so that the nonlinear effect could be mitigated further.

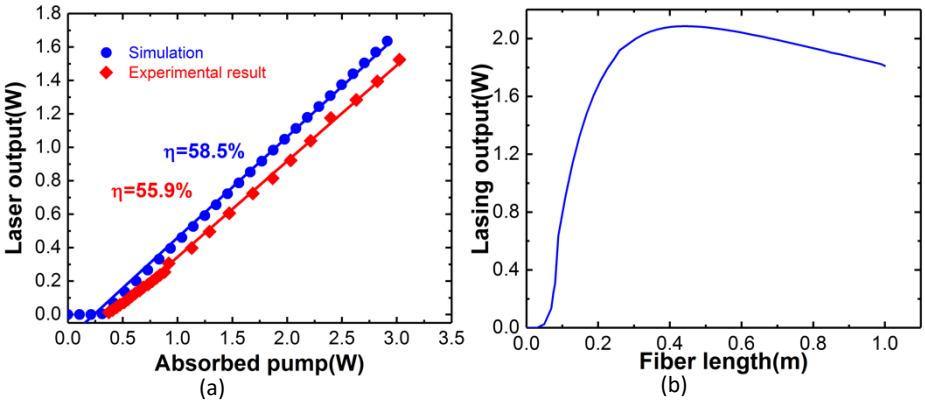

Figure 6. 3 (a) The laser output power at 1952nm versus absorbed pump power as well as the corresponding simulation result; (b) Simulation result of the maximum output power as a function of Tm3+ doped germanate fiber length from 0 to 1 m.

On the other hand, as described in[136][137] , the zero-material dispersion wavelength (ZDW) of germanate glass is located at 1734μm, amid the emission band of Tm^{3+}-doped fiber in the transition from level $^3F_4$ to level $^3H_6$. Compared with silica-based fibers with a 1300nm ZDW, germanate glass fibers will have a significantly red-shifted ZDW (>400nm). Moreover, a Tm^{3+}-doped fiber with normal dispersion at the emission band from level $^3F_4$ to level $^3H_6$, will obviously increase the pulse energy in ultrafast fiber laser[134]. Therefore, it is worthwhile to investigate the chromatic dispersion of the in-house fabricated TGF.

Conference paper

1. S. Chen, S. Yoo, P. P. Shum, X. Li, M. Liu, Y. Ma, and Q. J. Wang, "1-μm periodical grating structure on stainless steel designed by high-power nanosecond pulsed fiber lasers," in *2015 Conference on Lasers and Electro-Optics Pacific Rim*, (Optical Society of America, 2015), paper 26P_86.
2. S. Chen *et al*., "Ultra-wideband Operation of a Tunable Thulium Fibre Laser offering Tunability from 1679–1992 nm," *2017 European Conference on Optical Communication (ECOC)*, Gothenburg, 2017, pp. 1-3. (**Short-listed for Best Student Paper Award**).
3. S. Chen, Y. Jung, S. U. Alam, S. Jain, M. Ibsen, R. Sidharthan, D. Ho, S. Yoo, and D. J. Richardson, "Ultra-short wavelength operation of a thulium doped fiber laser in the 1620-1660nm wavelength band," in *Optical Fiber Communication Conference*, OSA Technical Digest (online) (Optical Society of America, 2018), paper M2J.4. (**Finalist for Corning Outstanding Student Paper Competition**)
4. Shaoxiang Chen , Yongmin Jung, Shaiful Alam, Raghuraman Sidharthan, Daryl Ho, Seongwoo Yoo, David Richardson, Jae Daniel, "Ultra-short Wavelength Operation of Thulium-doped Fibre Amplifier in the 1628-1655nm Waveband", *2018 European Conference on Optical Communication (ECOC)*, Rome, 2018, Mo3E.1.
5. F. Ben Slimen, S. Chen, J. Lousteau, Y. Jung, S. Alam, N. White, D. Richardson, and F. Poletti, "Tm^{3+} Doped Germanate Large Mode Area Single Mode Fiber for 2 μm Lasers and Amplifiers," in *Advanced Photonics 2018 (BGPP, IPR, NP, NOMA, Sensors, Networks, SPPCom, SOF)*, OSA Technical Digest (online) (Optical Society of America, 2018), paper SoTu4H.2.
6. Yuhao Chen; Shaoxiang Chen, Seongwoo Yoo et al., "All-Fiber 2 μm Amplifier Using A Normal Dispersion Thulium Fiber", CLEO, 2019, (accepted)

Journal papers published and under procedure

1. Shaoxiang Chen et al., "The exploitation of a novel Thulium/Germanium co-doped silica fiber at short wavelength in laser and amplifier." (under procedure)
2. Zhengqi Ren, Shaoxiang Chen*, Seongwoo Yoo, Raghuraman Sidharthan, David J. Ricahrdson and Shaif-ul Alam,"Ultra-short wavelength thulium doped mode-locked fiber laser in both soliton and noise-like pulse regimes" (corresponding author, prepare to submit to Journal of Optics Express)
3. Fedia Ben Slimen*, Shaoxiang Chen*,Joris Lousteau, Yongmin Yung, Nick White ,Shaiful Alam , David Richardson , Francesco Poletti, "Tm^{3+} doped Germanate

Large Mode Area Single Mode Fiber for 2 um Laser", (co-corresponding author, prepare to submit to Journal of Optical Material Express)

4. Meng Liu, Shaoxiang Chen, Betty Meng Zhang, Xiaohui Li, Perry Ping Shum, Qijie Wang, Xueping Cheng, "Pulse Shape Tuning for 1064 nm Nanosecond MOPA Fibre Laser", Procedia Engineering, Volume 140, 2016, Pages 123-126.

Reference

[1] H. Takara *et al.*, "1.01-Pb/s (12 SDM/222 WDM/456 Gb/s) Crosstalk-managed Transmission with 91.4-b/s/Hz Aggregate Spectral Efficiency," *ECOC Th3.C.1*, 2012.

[2] J. R. Williams and R. M. Percival, "Highly efficient 1.064 μm upconversion pumped 1.47 μm thulium doped fluoride fibre amplifier," *Electron. Lett.*, vol. 30, no. 20, pp. 1684–1685, 1994.

[3] S. Aozasa, H. Masuda, and M. Shimizu, "S-Band thulium-doped fiber amplifier employing high thulium concentration doping technique," *J. Light. Technol.*, vol. 24, no. 10, pp. 3842–3848, 2006.

[4] S. S. Yam and J. Kim, "Ground State Absorption in Thulium-Doped Fiber Amplifier : Experiment and Modeling," *Ieee J. Sel. Top. Quantum Electron.*, vol. 12, no. 4, pp. 797–803, 2006.

[5] A. H. M. Husein and F. I. El-Nahal, "Optimizing the thulium doped fiber amplifier (TDFA) gain and noise figure for S-band 16 × 10 Gb/s WDM systems," *Optik (Stuttg).*, vol. 124, no. 19, pp. 4052–4057, 2013.

[6] M. N. Petrovich *et al.*, "Demonstration of amplified data transmission at 2 μm in a low-loss wide bandwidth hollow core photonic bandgap fiber," *Opt. Express*, vol. 21, no. 23, p. 28559, 2013.

[7] M. Yamanaka, H. Kawagoe, and N. Nishizawa, "High power supercontinuum generation by high-repetition-rate ultrashort pulse fiber laser for ultrahigh resolution OCT in 1600 nm spectral band," vol. 254, no. 1991, p. 52501, 2015.

[8] P. Cadroas *et al.*, "All-fiber femtosecond laser providing 9 nJ, 50 MHz pulses at 1650 nm for three-photon microscopy," *J. Opt. (United Kingdom)*, vol. 19, no. 6, 2017.

[9] N. G. Horton *et al.*, "In vivo three-photon microscopy of subcortical structures within an intact mouse brain," *Nat. Photonics*, vol. 7, no. 3, pp. 205–209, 2013.

[10] S. K. Varshney, M. P. Singh, and R. K. Sinha, "Propagation characteristics of photonic crystal fibers," *J. Opt. Commun.*, vol. 24, no. 5, pp. 192–198, 2003.

[11] S. D. Emami, M. M. Dashtabi, H. J. Lee, A. S. Arabanian, and H. A. A. Rashid, "1700 Nm and 1800 Nm Band Tunable Thulium Doped Mode-Locked Fiber Lasers," *Sci. Rep.*, vol. 7, no. 1, pp. 1–8, 2017.

[12] Z. Li *et al.*, “90 Nm Gain Extension Towards 1.7 Mm for Diode-Pumped Silica-Based Thulium-Doped Fiber Amplifiers,” *Eur. Conf. Opt. Commun. ECOC*, pp. 7–9, 2014.

[13] N. Sugimoto, K. Ochiai, and S. Ohara, “Highly efficient and short length Lanthanum co-doped Bi2O3 -based EDF for extended L-band amplification,” *OAA, Opt. Soc. Am. PD5-3*, 2002.

[14] A. J. G. Ellison *et al.*, “Extending the L-band to 1620 nm using MCS fiber,” *Conf. Opt. Fiber Commun. Tech. Dig. Ser.*, vol. 54, p. TuA2/1-TuA2/3, 2001.

[15] Z. Jia, H. Li, X. Meng, L. Liu, G. Qin, and W. Qin, “Broadband amplification and highly efficient lasing in erbium-doped tellurite microstructured fibers,” *Opt. Lett.*, vol. 38, no. 7, pp. 1049–1051, 2013.

[16] P. Honzatko, Y. Baravets, I. Kasik, and O. Podrazky, “Wideband thulium–holmium-doped fiber source with combined forward and backward amplified spontaneous emission at 1600–2300 nm spectral band,” *Opt. Lett.*, vol. 39, no. 12, p. 3650, 2014.

[17] G. Xue, B. Zhang, K. Yin, W. Yang, and J. Hou, “Ultra-wideband all-fiber tunable Tm/Ho-co-doped laser at 2 μm,” *Opt. Express*, vol. 22, no. 21, p. 25976, 2014.

[18] M. Yamada, H. Ono, and J. Ono, “1.7 um band optical fiber amplifier,” *Opt. Fiber Commun. Conf.*, p. Tu2D.3, 2014.

[19] K. Ota *et al.*, “Tm3+–Tb3+-doped tunable fibre ring laser for 1700 nm wavelength region,” *Electron. Lett.*, vol. 49, no. 20, pp. 1287–1288, 2013.

[20] S. D. Agger and J. H. Povlsen, “Emission and absorption cross section of thulium doped silica fibers,” *Opt. Express*, vol. 14, no. 1, p. 50, 2006.

[21] C. Romano, R. E. Tench, J.-M. Delavaux, and Y. Jaouën, “Characterization of the 3F4 – 3H6 Transition in Thulium-doped Silica Fibres and Simulation of a 2μm Single Clad Amplifier,” *Ecoc*, no. 3, p. P1.SC1.2, 2017.

[22] J. M. O. Daniel, N. Simakov, M. Tokurakawa, M. Ibsen, and W. A. Clarkson, “Ultra-short wavelength operation of a thulium fibre laser in the 1660–1750 nm wavelength band,” *Opt. Express*, vol. 23, no. 14, p. 18269, 2015.

[23] I. Mingareev, F. Weirauch, A. Olowinsky, L. Shah, P. Kadwani, and M. Richardson, “Welding of polymers using a 2 μm thulium fiber laser,” *Opt. Laser Technol.*, vol. 44, no. 7, pp. 2095–2099, 2012.

[24] J. P. Cariou, B. Augere, and M. Valla, “Laser source requirements for coherent lidars based on fiber technology,” *Comptes Rendus Phys.*, vol. 7, no. 2, pp. 213–223, 2006.

[25] Y. Yatsenko and A. Mavritsky, “D-scan measurement of nonlinear refractive index in fibers heavily doped with GeO2,” *Opt. Lett.*, vol. 32, no. 22, pp. 3257–3259, 2007.

[26] J. Wu, Z. Yao, J. Zong, and S. Jiang, “Highly efficient high-power thulium-doped germanate glass fiber laser,” *Opt. Lett.*, vol. 32, no. 6, p. 638, 2007.

[27] C. Yang *et al.*, “Short all Tm-doped germanate glass fiber MOPA single-frequency laser at 1.95 μm,” *Opt. Express*, vol. 24, no. 10, p. 10956, 2016.

[28] K. Li, G. Zhang, and L. Hu, “Watt-level ∼ 2 μm laser output in Tm 3þ -doped tungsten tellurite glass double-cladding fiber,” *Opt. Lett.*, vol. 35, no. 24, pp. 4136–4138, 2010.

[29] X. He *et al.*, “1.95um kHz-linewidth single-frequency fiber laser using self-developed heavily Tm-doped germanate glass fiber,” *Opt. Express*, vol. 21, no. 18, pp. 875–877, 2013.

[30] J. Geng, J. Wu, S. Jiang, and J. Yu, “Efficient operation of diode-pumped single-frequency thulium-doped fiber lasers near 2 μm,” *Opt. Lett.*, vol. 32, no. 4, p. 355, 2007.

[31] Y. Jeong *et al.*, “Erbium : ytterbium co-doped large-core fiber laser with 297 W continuous-wave output power,” *IEEE J. Sel. Top. Quantum Electron.*, vol. 13, no. 3, pp. 1–24, 2007.

[32] H. Lin, Y. Feng, Y. Feng, P. Barua, J. K. Sahu, and J. Nilsson, “656 W Er-doped, Yb-free large-core fiber laser,” *Opt. Lett.*, vol. 43, no. 13, pp. 3080–3083, Jul. 2018.

[33] N. Simakov, A. Hemming, W. A. Clarkson, J. Haub, and A. Carter, “A cladding-pumped, tunable holmium doped fiber laser,” *Opt. Express*, vol. 21, no. 23, p. 28415, 2013.

[34] P. Peterka, I. Kasik, A. Dhar, B. Dussardier, and W. Blanc, “Theoretical modeling of fiber laser at 810 nm based on thulium-doped silica fibers with enhanced 3H4 level lifetime.,” *Opt. Express*, vol. 19, no. 3, pp. 2773–2781, 2011.

[35] A. Sincore, J. D. Bradford, J. Cook, L. Shah, and M. C. Richardson, “High Average Power Thulium-Doped Silica Fiber Lasers: Review of Systems and Concepts,” *IEEE J. Sel. Top. Quantum Electron.*, vol. 24, no. 3, pp. 1–8, 2018.

[36] P. Scaling *et al.*, “Tm-Doped Fiber Lasers : Fundamentals and Tm-Doped Fiber Lasers : Fundamentals and Power Scaling,” vol. 15, no. November 2016, pp. 85–92, 2009.

[37] S. D. Jackson, “Towards high-power mid-infrared emission from a fibre laser,” *Nat. Photonics*, vol. 6, no. 7, pp. 423–431, 2012.

[38] D. Y. Shen, J. K. Sahu, and W. A. Clarkson, “High-power widely tunable Tm:fibre lasers pumped by an Er,Yb co-doped fibre laser at 1.6 μm,” *Opt. Express*, vol. 14, no. 13, p. 6084, 2006.

[39] S. D. Jackson, “Cross relaxation and energy transfer upconversion processes relevant to the functioning of 2 μm Tm3+-doped silica fibre lasers,” *Opt. Commun.*, vol. 230, no. 1–3, pp. 197–203, 2004.

[40] R. A. Hayward, W. A. Clarkson, P. W. Turner, J. Nilsson, A. B. Grudinin, and D. C. Hanna, “Efficient cladding-pumped Tm-doped silica fibre laser with high power singlemode output at 2 [micro sign]m,” *Electron. Lett.*, vol. 36, no. 8, p. 711, 2000.

[41] P. C. Shardlow, D. Jain, R. Parker, J. Sahu, and W. A. Clarkson, “Optimising Tm-Doped Silica Fibres for High Lasing Efficiency,” vol. 2707, p. 2707, 2015.

[42] W. L. Barnes and J. E. Townsend, “Highly tunable and efficient diode pumped operation of Tm 3+ doped fibre lasers,” *Electron. Lett.*, vol. 26, no. 11, pp. 746–747, 1990.

[43] B. M. Walsh, “Review of Tm and Ho materials; spectroscopy and lasers,” *Laser Phys.*, vol. 19, no. 4, p. 855, 2009.

[44] S. D. Jackson, “The spectroscopic and energy transfer characteristics of the rare earth ions used for silicate glass fibre lasers operating in the shortwave infrared,” *Laser Photonics Rev.*, vol. 3, no. 5, pp. 466–482, 2009.

[45] S. D. Jackson and T. A. King, “Theoretical modeling of Tm-doped silica fiber lasers,” *J. Light. Technol.*, vol. 17, no. 5, pp. 948–956, 1999.

[46] G. Turri, V. Sudesh, M. Richardson, M. Bass, A. Toncelli, and M. Tonelli, “Temperature-dependent spectroscopic properties of Tm3+ in germanate, silica, and phosphate glasses: A comparative study,” *J. Appl. Phys.*, vol. 103, no. 9, 2008.

[47] B. M. Walsh and N. P. Barnes, “Comparison of Tm: ZBLAN and Tm: Silica fiber

lasers; Spectroscopy and tunable pulsed laser operation around 1.9 μm," *Appl. Phys. B Lasers Opt.*, vol. 78, no. 3–4, pp. 325–333, 2004.

[48] P. Moulton, "High power Tm: silica fiber lasers: current status, prospects and challenges (Invited)," *Eur. Conf. Lasers Electro-Optics*, p. 2000, 2011.

[49] X. Wen *et al.*, "Highly Tm 3+ doped germanate glass and its single mode fiber for 2.0 I 1/4m laser," *Sci. Rep.*, vol. 6, no. December 2015, pp. 2–11, 2016.

[50] D. A. Simpson and G. Baxter, "Spectroscopy of Thulium Doped Silica Glass," *PhD thesis*, p. 44, 2007.

[51] W. Miniscalco, "Optical and Electronic Properties of Rare Earth Ions in Glasses," 2001.

[52] S. D. Jackson, "Cross relaxation and energy transfer upconversion processes relevant to the functioning of 2 μm Tm3+-doped silica fibre lasers," *Opt. Commun.*, vol. 230, no. 1–3, pp. 197–203, 2004.

[53] M. Engelbrecht, F. Haxsen, D. Wandt, and D. Kracht, "Wavelength resolved intracavity measurement of the cross sections of a Tm-doped fiber.," *Opt. Express*, vol. 16, no. 3, pp. 1610–1615, 2008.

[54] X. Zou and H. Toratani, "Spectroscopic properties and energy transfers in Tm3+ singly- and doubly-doped glasses," *J. Non. Cryst. Solids*, vol. 195, no. 1–2, pp. 113–124, 1996.

[55] Z. Li, S. U. Alam, Y. Jung, A. M. Heidt, and D. J. Richardson, "All-fiber, ultra-wideband tunable laser at 2 mum," *Opt Lett*, vol. 38, no. 22, pp. 4739–4742, 2013.

[56] A. K. Ngo, "Laser welding of urinary tissues, ex vivo, using a tunable Thulium fiber laser," *Proc. SPIE*, vol. 6078, no. February 2006, p. 60781B–60781B–8, 2006.

[57] F. Hanson, P. Poirier, D. Haddock, D. Kichura, and M. Lasher, "Laser propagation at 1.56 μm and 3.60 μm in maritime environments," *Appl. Opt.*, vol. 48, no. 21, pp. 4149–4157, 2009.

[58] P. Sprangle, A. Ting, J. Peñano, R. Fischer, and B. Hafizi, "Incoherent combining and atmospheric propagation of high-power fiber lasers for directed-energy applications," *IEEE J. Quantum Electron.*, vol. 45, no. 2, pp. 138–148, 2009.

[59] S. O. Antipov *et al.*, "Holmium fibre laser emitting at 2.21 μm," *Quantum Electron.*,

vol. 43, no. 7, pp. 603–604, 2013.

[60] D. Creeden *et al.*, “Mid-infrared ZnGeP_2 parametric oscillator directly pumped by a pulsed 2 μm Tm-doped fiber laser,” *Opt. Lett.*, vol. 33, no. 4, p. 315, 2008.

[61] W. A. Clarkson, N. P. Barnes, P. W. Turner, J. Nilsson, and D. C. Hanna, “High-power cladding-pumped Tm-doped silica fiber laser with wavelength tuning from 1860 to 2090 nm,” *Opt. Lett.*, vol. 27, no. 22, p. 1989, 2002.

[62] K. Yin, B. Zhang, G. Xue, L. Li, and J. Hou, “High-power all-fiber wavelength-tunable thulium doped fiber laser at 2 μm,” *Opt. Express*, vol. 22, no. 17, p. 19947, 2014.

[63] J. Li *et al.*, “Wide wavelength selectable all-fiber thulium doped fiber laser between 1925 nm and 2200 nm,” *Opt. Express*, vol. 22, no. 5, p. 5387, 2014.

[64] H. Sakata, M. Ichikawa, and H. Nakagami, “Tunable Tm-doped fiber ring laser operating at 1.9 μm band using force-induced fiber grating as wavelength tuner.,” *Appl. Opt.*, vol. 50, no. 3, pp. 291–5, 2011.

[65] V. V. Alexander *et al.*, “Photothermolysis of sebaceous glands in human skin ex vivo with a 1,708 nm Raman fiber laser and contact cooling,” *Lasers Surg. Med.*, vol. 43, no. 6, pp. 470–480, 2011.

[66] V. M. Paramonov *et al.*, “Continuous-wave bismuth fibre laser tunable from 1.65 to 1.8 μm,” *Quantum Electron.*, vol. 47, no. 12, pp. 8–11, 2017.

[67] S. P. Chong *et al.*, “Noninvasive, in vivo imaging of subcortical mouse brain regions with 1.7 μm optical coherence tomography,” *Opt. Lett.*, vol. 40, no. 21, p. 4911, 2015.

[68] C. Crotti *et al.*, “Wavelength optimization in femtosecond laser corneal surgery,” *Investig. Ophthalmol. Vis. Sci.*, vol. 54, no. 5, pp. 3340–3349, 2013.

[69] X. Xiao *et al.*, “3 W narrow-linewidth ultra-short wavelength operation near 1707 nm in thulium-doped silica fiber laser with bidirectional pumping,” *Appl. Phys. B Lasers Opt.*, vol. 123, no. 4, pp. 1–6, 2017.

[70] L. Qian, D. Fortusini, S. D. Benjamin, G. Qi, P. V Kelkar, and V. L. da Silva, “Gain-flattened, extended L-band (1570-1620 nm), high power, low noise erbium-doped fiber amplifiers,” in *Optical Fiber Communication Conference and Exhibit*, 2002, pp. 459–461.

[71] B. O. Guan, H. Y. Tam, S. Member, S. Y. Liu, P. K. a Wai, and N. Sugimoto, "Ultrawide-Band La-Codoped Bi 2 O 3 -Based EDFA for," vol. 15, no. 11, pp. 1525–1527, 2003.

[72] Y. Ohishi, A. Mori, M. Yamada, H. Ono, Y. Nishida, and K. Oikawa, "Gain characteristics of tellurite-based erbium-doped fiber amplifiers for 15-μm broadband amplification," *Opt. Lett.*, vol. 23, no. 4, p. 274, 1998.

[73] M. R. Oermann, H. Ebendorff-Heidepriem, D. J. Ottaway, D. G. Lancaster, P. J. Veitch, and T. M. Monro, "Extruded microstructured fiber lasers," *IEEE Photonics Technol. Lett.*, vol. 24, no. 7, pp. 578–580, 2012.

[74] S. D. Le, F. Saliou, and P. Chanclou, "Beyond 90-km reach of a 16 × 2.5 Gb/s C/L-band dense wavelength-division multiplexing metropolitan network based on self-seeded reflective semiconductor optical amplifiers," *Fiber Integr. Opt.*, vol. 33, pp. 337–346, 2014.

[75] L. Gasca, "From O to L: The Future of Optical-Wavelength Bands," *Broadband Prop.*, no. June, pp. 83–85, 2008.

[76] T. Kasamatsu, Y. Yano, and T. Ono, "1.49- m-Band Gain-Shifted Thulium-Doped Fiber Amplifier for WDM Transmission Systems," *J. Light. Technol.*, vol. 20, no. 10, pp. 1826–1838, 2002.

[77] Z. Li *et al.*, "Exploiting the short wavelength gain of silica-based thulium-doped fiber amplifiers," *Opt. Lett.*, vol. 41, no. 10, p. 2197, 2016.

[78] J. Wang, S. Liang, Q. Kang, Y. Jung, S. Alam, and D. J. Richardson, "Broadband silica-based thulium doped fiber amplifier employing multi-wavelength pumping," *Opt. Express*, vol. 24, no. 20, p. 23001, 2016.

[79] Y. Jung *et al.*, "Silica-Based Thulium Doped Fiber Amplifiers for Wavelengths beyond the L-band," *Opt. Fiber Commun. Conf.*, p. M3D.5, 2016.

[80] Z. Li, J. M. O. Daniel, A. M. Heidt, Y. Jung, S. U. Alam, and D. J. Richardson, "Over 300 nm Wideband Operation of Thulium-doped Fiber Amplifiers at 2 μm," vol. 1, no. 1 m, pp. 10–12, 2000.

[81] M. N. Petrovich *et al.*, "First Demonstration of 2μm Data Transmission in a Low-Loss Hollow Core Photonic Bandgap Fiber," *Eur. Conf. Exhib. Opt. Commun.*, no. 1, p. Th.3.A.5, 2012.

[82] H. Zhang *et al.*, “100 Gbit/s WDM transmission at 2 μm: transmission studies in both low-loss hollow core photonic bandgap fiber and solid core fiber,” *Opt. Express*, vol. 23, no. 4, p. 4946, 2015.

[83] H. Zhang *et al.*, “Dense WDM transmission at 2 μ m enabled by an arrayed waveguide grating,” *Opt. Lett.*, vol. 40, no. 14, pp. 3308–3311, 2015.

[84] E. Jaunart, P. Crahay, P. Megret, J. C. Froidure, M. Lamquin, and M. Blondel, “Analysis of numerical methods efficiency for EDFA modelling,” in *Electrotechnical Conference, 1994. Proceedings., 7th Mediterranean*, 1994, pp. 145–148 vol.1.

[85] C. R. Giles and E. Desurvire, “Modeling erbium-doped fiber amplifiers,” *J. Light. Technol.*, vol. 9, no. 2, pp. 271–283, 1991.

[86] Q. Kang *et al.*, “Modal Gain Control in a Multimode Erbium Doped Fiber Amplifier Incorporating Ring Doping,” vol. 20, no. 19, pp. 17–19, 2012.

[87] Y. Tang and J. Xu, “in Tm 3 + -doped fiber lasers,” vol. 27, no. 2, pp. 179–186, 2010.

[88] G. Yu, J. Chang, Q. Wang, X. Zhang, Z. Liu, and Q. Huang, “A theoretical model of thulium-doped silica fiber’s ASE in the 1900 nm waveband,” *Optoelectron. Lett.*, vol. 6, no. 1, pp. 45–47, Jan. 2010.

[89] Khamis M. and Ennser K., “Theoretical Model of a Thulium-doped Fiber Amplifier Pumped at 1570 nm and 793 nm in the Presence of Cross Relaxation,” *J. Light. Technol.*, vol. PP, no. 99, 2016.

[90] Q. Kang, “Modelling of Multimode Erbium-doped Fibre Amplifiers for Mode-division Multiplexed Transmission Systems,” *PhD thesis, Chapter 2.12 , Chapter 2.13*, 2012.

[91] Z. Li, “Thulium-Doped Fiber Sources for Novel Applications,” no. November, 2015.

[92] F. Ben Slimen, “Caract´erisation des verres luminescents pr´epar´es par la m´ethode sol-gel. Optique,” *PhD thesis*, pp. 39–44, 2016.

[93] C. C. Santos *et al.*, “Spectroscopic properties of Er3+-doped lead phosphate glasses for photonic application,” *J. Phys. D. Appl. Phys.*, vol. 43, no. 2, 2010.

[94] R. E. Tench and M. Shimizu, “Fluorescence-based measurement of g*(λ) for erbium-doped fluoride fiber amplifiers,” *J. Light. Technol.*, vol. 15, no. 8, pp. 1559–1564, 1997.

[95] C. Guo, D. Shen, J. Long, and F. Wang, “High-power and widely tunable Tm-doped

fiber laser at 2 μm," *Chin. Opt. Lett.*, vol. 10, no. 9, p. 91406, Sep. 2012.

[96] Z. Liu *et al.*, "High-Capacity Directly Modulated Optical Transmitter for 2-μm Spectral Region," *J. Light. Technol.*, vol. 33, no. 7, pp. 1373–1379, Apr. 2015.

[97] U. Sharma, E. W. Chang, and S. H. Yun, "Long-wavelength optical coherence tomography at 1.7 μm for enhanced imaging depth," *Opt Express*, vol. 16, no. 24, pp. 19712–19723, 2008.

[98] M. Yamanaka, T. Teranishi, H. Kawagoe, and N. Nishizawa, "Optical coherence microscopy in 1700 nm spectral band for high-resolution label-free deep-tissue imaging," *Sci. Rep.*, vol. 6, no. August, pp. 1–8, 2016.

[99] L.-C. Cheng, N. G. Horton, K. Wang, S.-J. Chen, and C. Xu, "Measurements of multiphoton action cross sections for multiphoton microscopy," *Biomed. Opt. Express*, vol. 5, no. 10, p. 3427, 2014.

[100] C. Li *et al.*, "High-power widely tunable all-fiber thulium-assisted optical parametric oscillator at SWIR band," *Opt. Lett.*, vol. 41, no. 22, p. 5258, 2016.

[101] C. Li, X. Wei, S. Tan, N. Chen, J. Kang, and K. K. Y. Wong, "Short wavelength mode-locked thulium-doped fiber laser based on nonlinear polarization rotation," vol. 2, pp. 1–2, 2017.

[102] T. Noronen, O. Okhotnikov, and R. Gumenyuk, "Electronically tunable thulium-holmium mode-locked fiber laser for the 1700-1800 nm wavelength band," *Opt. Express*, vol. 24, no. 13, p. 14703, 2016.

[103] A. J. Harris and P. F. Castle, "Bend Loss Measurements on High Numerical Wavelength and Bend Radius," *J. Light. Technol.*, vol. LT-4, no. 1, pp. 34–40, 1986.

[104] H. Umezawa *et al.*, "Very-large-mode-area singlle mode multicore fiber," *Opt. Lett.*, vol. 34, no. 18, pp. 26–28, 2007.

[105] M. R. Mokhtar *et al.*, "Fibre Bragg grating compression-tuned over 110 nm," *Electron. Lett.*, vol. 39, no. 6, p. 509, 2003.

[106] J. Yang, H. Zhong, S. Zhang, and D. Fan, "Theoretical Characterization of the Ultra-Broadband Gain Spectra at ~ 1600-2100 nm from Thulium-Doped Fiber Amplifiers," *IEEE Photonics J.*, vol. 8, no. 6, 2016.

[107] T. S. McComb *et al.*, "High-power widely tunable thulium fiber lasers," *Appl. Opt.*,

vol. 49, no. 32, p. 6236, 2010.

[108] M. a Solodyankin *et al.*, "Mode-locked 1.93 microm thulium fiber laser with a carbon nanotube absorber.," *Opt. Lett.*, vol. 33, no. 12, pp. 1336–1338, 2008.

[109] S. Chen *et al.*, "Ultra-short wavelength operation of a thulium doped fiber laser in the 1620-1660nm wavelength band," *Opt. Fiber Commun. Conf.*, vol. 1, p. M2J.4, 2018.

[110] S. Liu *et al.*, "Noise-like pulse generation from a thulium-doped fiber laser using nonlinear polarization rotation with different net anomalous dispersion," *Photonics Res.*, vol. 4, no. 6, p. 318, 2016.

[111] M. Horowitz, Y. Barad, and Y. Silberberg, "Noise-like pulses with a broadband spectrum generated from an erbium-doped fiber laser," *Opt. Lett.*, vol. 22, no. 11, pp. 799–801, 1997.

[112] G. Sobon, J. Sotor, T. Martynkien, and K. M. Abramski, "Ultra-broadband dissipative soliton and noise-like pulse generation from a normal dispersion mode-locked Tm-doped all-fiber laser," *Opt. Express*, vol. 24, no. 6, p. 6156, 2016.

[113] J. Li *et al.*, "All-fiber passively mode-locked Tm-doped NOLM-based oscillator operating at 2-μm in both soliton and noisy-pulse regimes," *Opt. Express*, vol. 22, no. 7, p. 7875, 2014.

[114] N. J. Doran and D. Wood, "Nonlinear-optical loop mirror," *Opt. Lett.*, vol. 13, no. 1, p. 56, 1988.

[115] L. E. Nelson, D. J. Jones, K. Tamura, H. A. Haus, and E. P. Ippen, "Ultrashort-pulse fiber ring lasers," *Appl. Phys. B*, vol. 65, no. 2, pp. 277–294, 1997.

[116] Q. Wang, T. Chen, B. Zhang, A. P. Heberle, and K. P. Chen, "All-fiber passively mode-locked thulium-doped fiber ring oscillator operated at solitary and noiselike modes," *Opt. Lett.*, vol. 36, no. 19, p. 3750, 2011.

[117] X. He *et al.*, "60nm Bandwidth, 17nJ Noiselike Pulse Generation from a Thulium-Doped Fiber Ring Laser," *Appl. Phys. Express*, vol. 6, p. 112702, 2013.

[118] J. U. Kang, "Broadband quasi-stationary pulses in mode-locked fiber ring laser," *Opt. Commun.*, vol. 182, no. 4, pp. 433–436, 2000.

[119] L. M. Zhao, D. Y. Tang, J. Wu, X. Q. Fu, and S. C. Wen, "Noise-like pulse in a gain-guided soliton fiber laser.," *Opt. Express*, vol. 15, no. 5, pp. 2145–2150, 2007.

[120] L. M. Zhao and D. Y. Tang, “Generation of 15-nJ bunched noise-like pulses with 93-nm bandwidth in an erbium-doped fiber ring laser,” *Appl. Phys. B Lasers Opt.*, vol. 83, no. 4, pp. 553–557, 2006.

[121] B. M. Walsh, “Review of Tm and Ho materials; spectroscopy and lasers,” *Laser Phys.*, vol. 19, no. 4, pp. 855–866, 2009.

[122] K. Han, P. Zhang, S. Wang, Y. Guo, D. Zhou, and F. Yu, “Optical characterization of Tm^{3+} doped Bi2O3-GeO2-Ga2O3 glasses in absence and presence of BaF2,” *Sci. Rep.*, vol. 6, no. July, pp. 1–9, 2016.

[123] L. Pearson, J. W. Kim, Z. Zhang, M. Ibsen, J. K. Sahu, and W. A. Clarkson, “High-power linearly-polarized single-frequency thulium-doped fiber master-oscillator power-amplifier,” Opt. Express 18,1607–1612, 2010.

[124] X. Wen *et al.*, “Highly Tm3+ doped germanate glass and its single mode fiber for 2.0 μm laser,” *Sci. Rep.*, vol. 6, no. October 2015, p. 20344, 2016.

[125] R. Xu, L. Xu, L. Hu, and J. Zhang, “Structural Origin and Laser Performance of Thulium-Doped Germanate Glasses,” pp. 14163–14167, 2011.

[126] H. T. Munasinghe *et al.*, “Lead-germanate glasses and fibers: a practical alternative to tellurite for nonlinear fiber applications,” *Opt. Mater. Express*, vol. 3, no. 9, p. 1488, 2013.

[127] S. Yu, Z. Yang, and S. Xu, “Judd-Ofelt and laser parameterization of Tm3+-doped barium gallo-germanate glass fabricated with efficient dehydration methods,” *Opt. Mater. (Amst).*, vol. 31, no. 11, pp. 1723–1728, 2009.

[128] Ming Li etal., “Investigation on Tm3+-doped silicate glass for 1.8μm emission.”, Journal of Luminescence 132, 183-1835, 2012.

[129] D. Y. Shen, Z. Zhang, A. J. Boyland, J. K. Sahu, W. A. Clarkson, and M. Ibsen, “Thulium-Doped Distributed-Feedback Fiber Laser with > 0 . 3 W Output at 1935 nm,” *America (NY).*, pp. 5–7, 1935.

[130] Q. Yang *et al.*, “A Single-Frequency Linearly Polarized Fiber Laser Using a Newly Developed Heavily Tm3+-Doped Germanate Glass Fiber at 1.95 μm,” *Chinese Phys. Lett.*, vol. 32, no. 9, pp. 5–9, 2015.

[131] X. I. G. Uan *et al.*, “Fiber Laser At 1950 Nm,” vol. 26, no. 6, pp. 10956–10961, 2018.

[132] J. Wang, S. Liang, Q. Kang, Y. Jung, S. Alam, and D. J. Richardson, “Broadband silica-based thulium doped fiber amplifier employing multi-wavelength pumping,” *Opt. Express*, vol. 24, no. 20, pp. 23001–23008, 2016.

[133] M. N. Petrovich *et al.*, “Demonstration of amplified data transmission at 2 μm in a low-loss wide bandwidth hollow core photonic bandgap fiber,” *Opt. Express*, vol. 21, no. 23, p. 28559, 2013.

[134] C. Huang, C. Wang, W. Shang, N. Yang, Y. Tang, and J. Xu, “Developing high energy dissipative soliton fiber lasers at 2 micron,” *Sci. Rep.*, vol. 5, pp. 1–7, 2015.

[135] M. Kakui and S. Ishikawa, “Long-wavelength-band optical amplifiers employing silica-based erbium doped fibers designed for wavelength division multiplexing systems and networks,” *IEICE Trans. Electron.*, vol. E83–C, no. 6, pp. 799–815, 2000.

[136] S. Sakaguchi, S. Todoroki, and N. Rigout, “Refractive index dispersion in ternary germanate glasses,” *Jpn. J. Appl. Phys.*, vol. 34, no. 10, pp. 5615–5620, 1995.

[137] T. Hosaka, S. Sudo, and K. Okamoto, “Dispersion of pure GeO_2 glass core and f-doped GeO_2 glass cladding single-mode optical fibre,” *Electron. Lett.*, vol. 23, no. 1, pp. 24–26, 1987.